ANALYSIS OF COUPLED LINES IN MICROWAVE PRINTED CIRCUIT ELEMENTS

A THESIS SUBMITTED TO
THE GRADUATE SCHOOL OF NATURAL AND APPLIED SCIENCES
OF
MIDDLE EAST TECHNICAL UNIVERSITY

BY

ŞEFİKA ÖZKAL PİROĞLU

IN PARTIAL FULFILLMENT OF THE REQUIREMENTS
FOR
THE DEGREE OF MASTER OF SCIENCE
IN
ELECTRICAL AND ELECTRONICS ENGINEERING

DECEMBER 2007

Approval of the thesis:

ANALYSIS OF COUPLED LINES IN MICROWAVE PRINTED CIRCUIT ELEMENTS

submitted by **ŞEFİKA ÖZKAL PİROĞLU** in partial fulfillment of the requirements for the degree of **Master of Science in Electrical and Electronics Engineering, Middle East Technical University** by,

Prof. Dr. Canan ÖZGEN
Dean, Graduate School of **Natural and Applied Sciences** _____

Prof. Dr. İsmet ERKMEN
Head of Department, **Electrical and Electronics Engineering** _____

Prof. Dr. Gülbin DURAL
Supervisor, **Electrical and Electronics Engineering, METU** _____

Examining Committee Members:

Prof. Dr. Canan TOKER
Electrical and Electronics Engineering, METU _____

Prof. Dr. Gülbin DURAL
Electrical and Electronics Engineering, METU _____

Prof. Dr. Mustafa KUZUOĞLU
Electrical and Electronics Engineering, METU _____

Assoc. Prof. Dr. Şimşek DEMİR
Electrical and Electronics Engineering, METU _____

Ahmet MUTLU
Senior Engineer, ASELSAN _____

Date: _____

I hereby declare that all information in this document has been obtained and presented in accordance with academic rules and ethical conduct. I also declare that, as required by these rules and conduct, I have fully cited and referenced all material and results that are not original to this work.

Name, Last name :

Signature :

To My Family

ABSTRACT

ANALYSIS OF COUPLED LINES IN MICROWAVE PRINTED CIRCUIT ELEMENTS

Piroğlu, Şefika Özkal

M.S., Department of Electrical and Electronics Engineering

Supervisor: Prof. Dr. Gülbin Dural

December 2007, 100 Pages

Full wave analysis of microstrip lines at microwave frequencies is performed by using method of moments in conjunction with closed-form spatial domain Green's functions. The Green's functions are in general Sommerfeld-type integrals which are computationally expensive. To improve the efficiency of the technique, Green's functions are approximated by their closed-forms.

Microstrip lines are excited by arbitrarily located current sources and are terminated by complex loads at both ends. Current distributions over microstrip lines are represented by rooftop basis functions. At first step, the current distribution over a single microstrip line is calculated. Next, the calculation of the current distributions over coupled microstrip lines is performed. The technique is then, applied to directional couplers. Using the current distributions obtained by the analysis, the scattering parameters of the structures are evaluated by using Prony's method. The results are compared with the ones gathered by using simulation software tools, CNL/2™ and Agilent Advanced Design System™ (ADS).

Keywords: Method of Moments, Green's Functions, Microstrip Lines, Coupled Microstrip Lines, Directional Couplers.

ÖZ

MİKRODALGA BASKI DEVRE ELEMANLARINDA ETKİLEŞİMLİ HATLARIN İNCELENMESİ

Piroğlu, Şefika Özkal

Yüksek Lisans, Elektrik ve Elektronik Mühendisliği Bölümü

Tez Yöneticisi : Prof. Dr. Gülbin Dural

Aralık 2007, 100 Sayfa

Mikroşerit hatların, mikrodalga frekanslarındaki tam dalga analizlerinde, Moment metodu ile birlikte gerçek uzaydaki kapalı form Green fonksiyonları kullanılmıştır. Genel olarak Green fonksiyonları, Sommerfeld tipi integrallerden oluşmaktadır ve hesaplanmaları zaman alıcı ve zordur. Tekniğin verimini artırabilmek için, kapalı form Green fonksiyonları kullanılmıştır.

Mikroşerit hatlar, üzerindeki keyfi olarak seçilmiş noktalara yerleştirilmiş olan akım kaynaklarından beslenmiştir ve hatların her biri iki ucundan kompleks yüklerle sonlandırılmıştır. Mikroşerit hatlar üzerindeki akım dağılımı, çatı taban fonksiyonları ile ifade edilmiştir. İlk aşamada, tek bir mikroşerit hat üzerindeki akım dağılımı hesaplanmıştır. Sonra, kuplajlanmış mikroşerit hatlar üzerindeki akım dağılımları hesaplanmıştır. Son olarak, teknik yönlü bağlayıcılara uygulanmıştır. Analizlerin sonucunda elde edilen akım dağılımları ile Prony metodu kullanılarak, örnek yapıların s-parametreleri bulunmuştur. Bulunan s-parametreleri, CNL/2™ ve Agilent Advanced Design System™ (ADS) simulasyon yazılımlarından elde edilen s-parametreleri ile karşılaştırılmıştır.

Anahtar Kelimeler: Moment Metodu, Green Fonksiyonları, Mikroşerit Hatlar, Kuplajlanmış Mikroşerit Hatlar, Yönlü Bağlayıcılar.

ACKNOWLEDGEMENTS

I would like to express my sincere gratitude to my supervisor Prof. Dr. Gülbin Dural for all her attention and support during my graduate study and, of course, for her valuable guidance and most importantly for her patience and trust.

My special thanks are due to Prof. Dr. Canan Toker for his helpful discussions, criticism and suggestions. I am grateful to him for sharing his valuable time with me.

I would also like to thank Prof. Dr. İrşadi Aksun for his valuable guidance and for sending me 2-D Quasi-static Modeling Tool and necessary data for my thesis.

I am indebted to ASELSAN Inc. for providing the facilities for the completion of the thesis.

I would also like to thank my parents, Rabia Özkal and Mehmet Özkal, for believing in my work and for sacrifices that they have made for me. I feel very lucky to have my wonderful sisters, Şule and Fatma. Moreover, I would like to thank to my best friend Funda for her love and support.

Finally, I would like to express my sincere appreciation to my dear husband, Ahmet Münir Piroğlu. Through my study, his love, friendship and encouragements never let me be alone. Without his support and understanding, I would never have finished the thesis.

TABLE OF CONTENTS

LIST OF FIGURES

FIGURES

LIST OF TABLES

TABLES

CHAPTER 1

INTRODUCTION

Printed structures in multilayer planar media which can be manufactured using printed circuit board technology have found widespread areas of applications since the mid 1970's. They are generally used in the design of microstrip antennas and monolithic microwave integrated circuits (MMIC).

Satellite, airborne communications and electronic warfare (EW) systems are some areas where printed structures are used. Microstrip line-based filters, impedance transformers, hybrids, couplers, power dividers/combiners, delay lines, etc. and antennas are some example applications of printed structures. The reason for such a wide range of applications is the numerous advantages of printed structures. The main advantage of printed structures is their ease of construction and relatively low cost. Next, they are low profile and lightweight structures. Moreover, printed structures can be wrapped easily; it is possible to adapt the structures according to the requirements of the body where it will be placed. However, there are also some disadvantages of using printed structures as antennas. One of them is the radiated power which is quite small compared to other radiating structures because of the small distance between the patch and the ground plane. The small radiated power also leads to low efficiency.

To analyze the microstrip structures, various methods are used which can be divided into two main groups as quasi-static approach and full wave analysis. Quasi-static approach assumes the nature of mode of propagation as pure transverse electromagnetic (TEM) wave and according to this approach, the microstrip characteristics are calculated from the electrostatic capacitance of the structure. This method is not accurate at higher frequencies. Full wave analysis takes into account hybrid nature of the mode of the propagation. The techniques used in full wave analysis are more rigorous and analytically complex. In this study, full wave analysis of the printed structures using the Method of Moments

(MoM) which has been successfully applied to a wide variety of electromagnetic problems is experienced and e^{jwt} type time dependence is assumed throughout the study. The integral equations are transformed into a matrix equation by approximating the unknown functions representing them in terms of known basis functions and then applying boundary conditions and they are tested using testing functions. The Finite Difference Time Domain (FDTD) method and the Finite Element method are other numerical methods which are used in computational electromagnetics. To apply these methods, the microstrip geometry should be modeled by three dimensional meshing including the surrounding volume around the structure. Because it is not possible to model infinite space, these two methods are not preferred in this study.

MoM is applied to different printed structures in conjunction with closed-form Green's functions in the spatial domain because using closed-form Green's functions in the analysis of microstrip geometry by MoM improves computational efficiency significantly. By using this approximate solution, the current distribution on a microstrip structure is achieved. Once the current distribution of a structure is known, then all other parameters can be obtained. Because the conventional spatial domain Green's functions and spectral domain Green's functions include slowly convergent integrals, closed-form Green's function is used. The details of the conventional approaches are given in chapter 2.

In this study, first a single microstrip line is analyzed using MoM and closed-form Green's functions. The formulation of the physical problem is introduced and the current distribution on the line is calculated. Then, the same approach is applied to a coupled microstrip line. As a last application, the analysis of the directional couplers is performed.

Chapter 2 starts with a brief introduction of the MoM. Types of basis and testing functions are represented and the importance of the choice of the basis and testing functions are pointed out. After that, the Green's functions are introduced. The conventional spatial domain and spectral Green's functions formulation for printed structures using MoM are derived and the disadvantages of these two approaches are mentioned in printed structure analysis. Finally, closed-form Green's functions in spatial domain are derived and computational efficiency of using this approach is emphasized.

Chapter 3 starts with the definition of the structure of a single microstrip line. The derivation of the formulas required to solve the problem is represented. In the analysis, the Galerkin's Method of Moments is used in which the basis and testing functions are chosen to be the same. The basis functions used in our applications are rooftop functions. Each final equation is an inner product term which is a 4-dimensional integral. Two of the integrals are from the definition of the inner product and two of them are from the closed-form Green's functions. Choosing the basis functions as rooftops, the two of the integrals which are called as convolution integral over testing and basis functions can be carried out analytically. Details of the convolution integrals are represented in appendix A. By the transmission line approach, the complex loads at the edge of the line are related to the other basis functions and the actual MoM matrix elements are constructed. Derivation of the load equations are given in detail in appendix B. Once the current distribution over a single microstrip line is found then using Prony's method, the incident and reflected wave coefficients are found. The current distributions of structures with different load terminations are presented in this chapter.

In chapter 4, the technique described above is applied to parallel coupled microstrip lines. Effects of spacing between the lines, horizontal shift and the width of lines on current distribution are presented for open-circuited parallel coupled lines. To relate the loads at the edge of the lines to the other basis functions, the Maxwellian capacitance and inductance values are required in this part of the study. Those values are obtained using a software program named RLGC - 2D Quasi-static Modeling Tool™. Next, 7dB, 10dB, 15dB and 20dB directional coupler structures are analyzed and the s-parameters of the structures are found. These values are then, compared with the ones obtained by using simulation programs, CNL/2™ and Agilent Advanced Design System - ADS™.

The conclusions of this study are in presented in chapter 5.

CHAPTER 2

ANALYSIS OF PRINTED STRUCTURES USING MOM

In this chapter, a brief description of the Method of Moments (MoM) formulation will be given for the solution of the Mixed Potential Integral Equations (MPIE). First, the basic information for the MoM will be introduced. Next, the Green's functions will be presented. The spatial domain and spectral domain MoM formulation in conjunction with the Green's functions will be detailed and the two approaches will be compared for their advantages and disadvantages. Finally, the closed-form Green's functions in spatial domain will be discussed. This approach eliminates the most important bottleneck of the spatial domain formulation of MoM.

2.1 The Method of Moments

MoM is a numerical technique which was first used in electromagnetic theory by R. F. Harrington in 1967 [1]. It is used to solve linear equations stated as

$$Lf(x) = g(x) \tag{II.1}$$

where L is a linear operator which may be a differential, integral, algebraic operator, f is the unknown function to be determined and g is the known function.

To solve (II.1), the unknown function f is approximated by a linear combination of a set of known functions $(f_1, f_2, ..., f_n)$ which are called as basis or expansion functions:

$$f(x) = \sum_{n=1}^{N} \alpha_n f_n(x) \tag{II.2}$$

where α_n's are the unknown coefficients to be determined, f_n are the basis functions and N is the number of basis functions. By substituting (II.2) into (II.1), the equation below is obtained.

$$L\left\{\sum_{n=1}^{N}\alpha_n f_n(x)\right\} = g(x) \tag{II.3}$$

Since L is a linear operator, (II.3) can be derived as

$$\sum_{n=1}^{N}\alpha_n L f_n(x) = g(x) \tag{II.4}$$

Then, residual or error function is defined as

$$R(x) = \left[\sum_{n=1}^{N}\alpha_n L f_n(x)\right] - g(x) \tag{II.5}$$

where the aim is to make R(x) arbitrarily small [2]. To achieve this, another set of functions $(w_1, w_2, ..., w_m)$ are used. These functions are called as weighting or testing functions. Once the inner product of $R(x)$ with each w_m is equated to zero, the following expression is gathered:

$$\sum_{n=1}^{N}\alpha_n \langle w_m, L f_n(x)\rangle = \langle w_m, g(x)\rangle \quad for \quad m = 1,2,...,N \tag{II.6}$$

The inner product of functions u and v can be defined as

$$\langle u, v\rangle = \int_{\Omega} u v^* d\Omega \tag{II.7}$$

where * denotes complex conjugate and the integration is performed over Ω. The inner product satisfies the following conditions:

$$\begin{aligned}
&\langle u, v\rangle = \langle v, u\rangle \\
&\langle \alpha u + \beta v, h\rangle = \alpha\langle u, h\rangle + \beta\langle v, h\rangle \quad \alpha \text{ and } \beta \text{ are scalars.} \\
&\langle f^*, f\rangle > 0 \quad if \quad f \neq 0 \\
&\langle f^*, f\rangle = 0 \quad if \quad f = 0
\end{aligned} \tag{II.8}$$

The set of equations (II.6) can be written in matrix form as

$$[I_{mn}][\alpha_n] = [g_m] \tag{II.9}$$

where

$$[I_{mn}] = \begin{bmatrix} \langle w_1, Lf_1 \rangle & \langle w_1, Lf_2 \rangle & \text{.....} & \langle w_1, Lf_n \rangle \\ \langle w_2, Lf_1 \rangle & \langle w_2, Lf_2 \rangle & \text{.....} & \langle w_2, Lf_n \rangle \\ \text{.....} & \text{.....} & \text{.....} & \text{.....} \\ \langle w_m, Lf_1 \rangle & \langle w_m, Lf_2 \rangle & \text{.....} & \langle w_m, Lf_n \rangle \end{bmatrix} \tag{II.10}$$

$$[\alpha_n] = \begin{bmatrix} \alpha_1 \\ \alpha_2 \\ . \\ \alpha_n \end{bmatrix} \quad \text{and} \quad [g_m] = \begin{bmatrix} \langle w_1, g \rangle \\ \langle w_2, g \rangle \\ . \\ \langle w_m, g \rangle \end{bmatrix} \tag{II.11}$$

I matrix is called 'the MoM matrix' and g matrix is called 'the excitation matrix'. If the MoM matrix is nonsingular its inverse exists. Then, the unknown coefficients of the basis functions can be represented as

$$[\alpha_n] = [I_{nm}]^{-1}[g_m] \tag{II.12}$$

The first step of applying MoM is derivation of the appropriate equation describing the physical problem. The next step is choosing appropriate basis and testing functions. According to the chosen basis and testing functions, the unknown function will be approximated. Then the matrix elements can be manipulated and solved [3]. In order to find the unknown coefficients α_n's, iterative matrix inverse technique can be used or direct inverse of I matrix can be calculated.

The basis and weighting functions are chosen according to the geometry of the problem, the physical characteristics of the fields, the accuracy needed and the available basis and weighting functions.

2.1.1 Choice of the Basis Functions

There are two types of basis functions: 'Entire Domain Basis Functions' and 'Sub-Domain Basis Functions'.

2.1.1.1 Entire Domain Basis Functions

If each basis function is defined and nonzero over the entire domain $x \in [a, b]$, then the basis functions are called 'Entire Domain Basis Functions'.

Sine, cosine functions and Chebyshew polynomials are examples of ‘Entire Domain Basis Functions’.

2.1.1.2 Sub-Domain Basis Functions

In defining the basis functions, the domain can also be divided into sub-domains and each basis function can be zero over a majority of the-sub domains. Such basis functions are called ‘Sub-domain Basis Functions’. As an example, if the region $[a,b]$ is divided into N sub-domains as shown in figure 1, $f_n(x)$ can be represented as below:

$$f(x) = \sum_{n=1}^{N} \alpha_n f_n(x) = \begin{cases} \alpha_1 f_1(x) & x \in \Delta x_1 \\ \alpha_2 f_2(x) & x \in \Delta x_2 \\ . & \\ . & \\ \alpha_N f_N(x) & x \in \Delta x_N \end{cases} \qquad \text{(II.13)}$$

In many applications of MoM, ‘Sub-domain Basis Functions’ are used because by using ‘Sub-domain Basis Functions’, the integration range becomes smaller when compared to ‘Entire Domain Basis Functions’. However, wisely chosen ‘Entire Domain Basis Functions’ leads to more accurate results with smaller matrix size compared to a sub-domain type formulation.

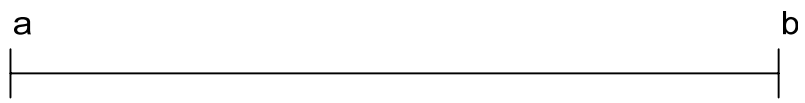

Figure 1 Example Domain Representation of Entire Domain Basis Function.

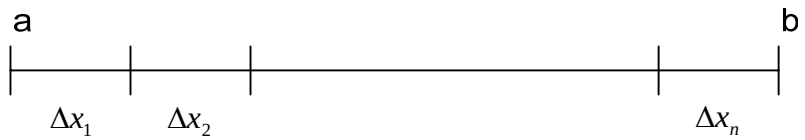

Figure 2 Example Domain Representation of Sub-domain Basis Function.

Pulse or piecewise constant functions, piecewise linear or triangular functions, piecewise sinusoidal functions are some of types of the ‘Sub-domain Basis Functions’.

2.1.2 Choice of the Weighting Functions

In this section, different methods which use different weighting functions are given and their advantages and disadvantages are discussed.

2.1.2.1 Point Matching or Collocation Method

In point matching or collocation method weighting functions are chosen to be Dirac delta functions. If $[a,b]$ represents the spatial domain over which f (unknown function) is defined,

$$w_m(x) = \delta(x - x_m) \quad for \quad m = 1,2,..., N \tag{II.14}$$

where w_m ‘s are chosen points in $[a,b]$. Then,

$$\langle w_m, R \rangle = \int_a^b R(x)\delta(x - x_m)dx = 0 \tag{II.15}$$

(II.15) indicates that residual function is made zero for the N points chosen over $[a,b]$. This method is the simplest one but the chosen points which are called as ‘collocation points’ may not be suitable points and the results may not be accurate enough.

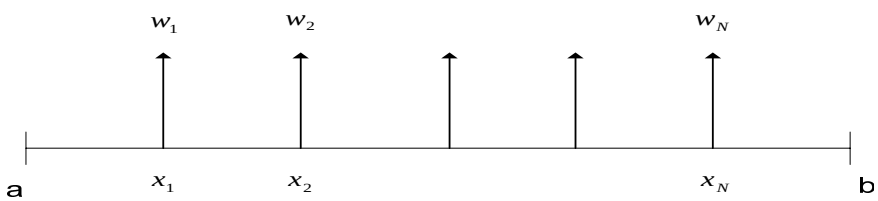

Figure 3 Dirac Delta Function

2.1.2.2 Subsectional Collocation Method

In this method $[a,b]$ is divided into N sub-domains Ω_m, such that they are piecewise disjoint. This method is a smooth version of point matching.

$$w_m(x) = \begin{cases} 1 & x \in \Omega_m \\ 0 & elsewhere \end{cases} \quad \text{and} \quad \int_{\Omega_m} R(x)dx = 0 \quad m = 1,2,3,\ldots,N \qquad \text{(II.16)}$$

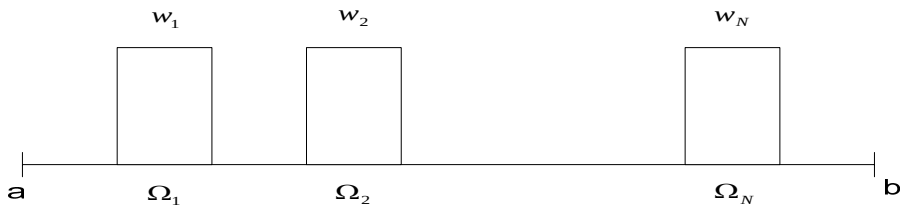

Figure 4 Sub-domains Weighting Function

(II.16) indicates that residual function is made zero over different sub-domains Ω_m of Ω. Hence, when this method is used, the results can be more accurate than point matching or collocation method. However, since the method include one-dimensional integration it is complicated than point matching or collocation method.

2.1.2.3 Galerkin's Method

In this method, the weighting functions are chosen to be identical to the basis function as

$$w_m = f_m \quad m = 1,2,\ldots,N \qquad \text{(II.17)}$$

Using Galerkin's method, symmetric matrix is gathered, which reduces the computation time of a problem, as it is enough to find one row or one column of the matrix to fill the entire matrix. However, the integration becomes more complex when compared to point matching or subsectional collocation method.

2.1.2.4 Method of Least Squares

In this method, weighting function is chosen as

$$w_m = Lf_m \qquad \text{(II.18)}$$

and final equation becomes

$$\sum_{n=1}^{N} \alpha_n \langle Lf_m(x), Lf_n(x) \rangle = \langle Lf_m(x), g(x) \rangle \quad for \quad m = 1,2,..., N \tag{II.19}$$

Although this method may give better results when compared to other methods described above, it is the most complicated one.

2.2 Analysis of Planar Printed Structures Using MoM

In this section, first Green's functions are introduced. Next, conventional spatial domain MoM formulation and spectral domain MoM formulation are described. Finally, spatial domain closed-form Green's function is given in detail.

2.2.1 Green's Function

The Green's function of a wave equation is the solution of the wave equation for a point source. Because a general source is a linear superposition of point source and wave equation is linear, as the solution of the wave equation for a point source is known, the solution for a general source can also be found using linear superposition [4].

As an example, to solve a scalar wave equation (II.20) in volume V where V is represented in figure 5,

$$(\nabla^2 + k^2)\varphi(\bar{r}) = s(\bar{r}) \tag{II.20}$$

first the Green's function in the same V can be found. The Green's function is the solution of the equation below:

$$(\nabla^2 + k^2)g(\bar{r}, \bar{r}') = -\delta(\bar{r} - \bar{r}') \tag{II.21}$$

Because the general source can be obtained as

$$s(\bar{r}) = \int d\bar{r}' s(\bar{r}')\delta(\bar{r} - \bar{r}') \tag{II.22}$$

using the principle of linear superposition, the solution of the scalar wave equation (II.20) can be found as

$$\varphi(r) = -\int_V d\bar{r}' g(\bar{r}, \bar{r}') s(\bar{r}') \tag{II.23}$$

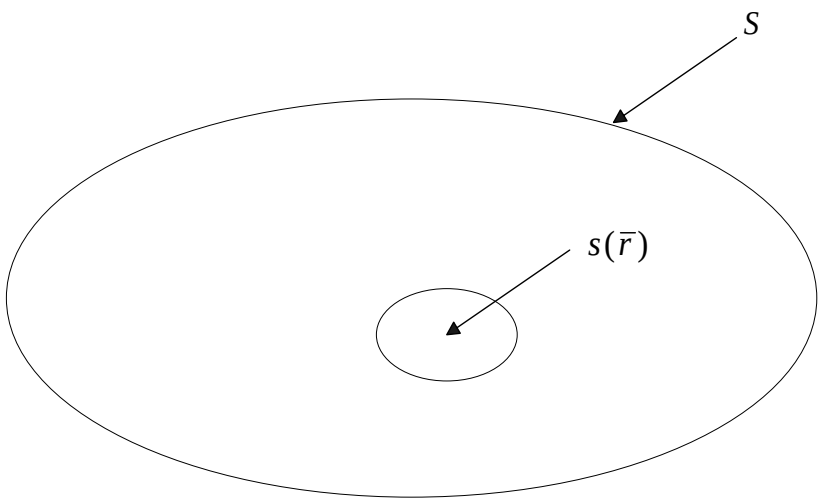

Figure 5 The Radiation of a Source $s(\bar{r})$ in a Volume V [4].

In general,

$$g(\bar{r},\bar{r}') = \frac{e^{ik|\bar{r}-\bar{r}'|}}{4\pi\,|\,\bar{r}-\bar{r}'\,|} \tag{II.24}$$

and the solution of (II.20), from equation (II.24), is then determined as

$$\varphi(\bar{r}) = -\int_V d\bar{r}'\,\frac{e^{ik|\bar{r}-\bar{r}'|}}{4\pi\,|\,\bar{r}-\bar{r}'\,|}s(\bar{r}') \tag{II.25}$$

2.2.2 Spatial Domain MoM Formulation

This formulation is based on the spatial domain Green's functions for the vector and scalar potentials which are represented by Sommerfeld integrals. Spatial domain Green's functions are used in the solution of the mixed potential integral equation (MPIE) by the MoM. A general microstrip structure is shown in figure 6, where it is assumed that the substrate layer extends to infinity in the transverse directions where d denotes the thickness of the substrate and ε_r denotes the permittivity of the substrate. Although the formulation of Green's functions presented herein is for a single layered structure, it can be extended to analyze multilayered structures [5]. Moreover, in this study, the formulation is based on the electric type currents, but it can also be adapted to analyze other types of structures involving magnetic type currents. One of the studies based on magnetic type currents is [6].

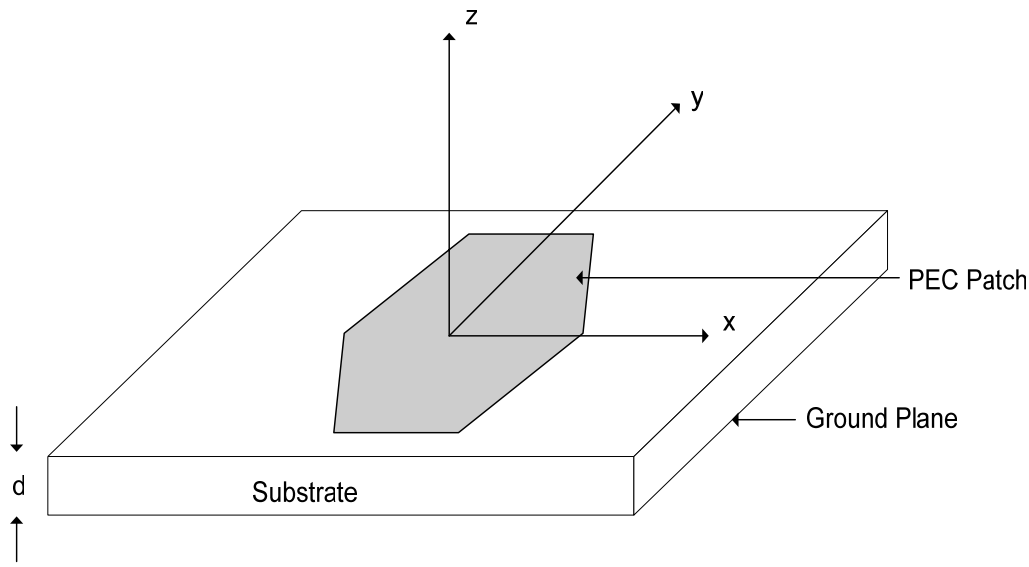

Figure 6 A General Microstrip Structure [5].

For the analysis of the microstrip structures, an integral equation in terms of the induced currents which occur on the conducting surfaces should be obtained. This can be done by expressing the electric field in terms of scalar and vector potentials, A and ϕ, respectively [7].

$$\mathbf{E} = -jw\mathbf{A} - \nabla\phi \tag{II.26}$$

The vector and scalar potentials can be written in terms of induced surface current density $\mathbf{J}$ and the Green's functions for the vector and scalar potentials as

$$\mathbf{A} = \overline{\mathbf{G}}^{A} * \mathbf{J} \tag{II.27}$$

$$\phi = G_q * (-\frac{1}{jw}\nabla.\mathbf{J}) \tag{II.28}$$

where $\overline{\mathbf{G}}^{A}$ is the dyadic Green's function of the vector potential, G_q is the Green's function of the scalar potential, $\mathbf{J}$ is the surface current density and * implies the convolution integral [7]. The potentials and fields of horizontal electric dipole (HED) on a microstrip structure gives the Green's functions $\overline{\mathbf{G}}^{A}$ and G_q. By substituting (II.27) and (II.28) into (II.26) and using the condition that the tangential electric field on the perfect electric conductors (PEC) (at $z = 0$) should be zero, the following integral equations are obtained:

$$E_x = -jwG_{xx}^A * J_x + \frac{1}{jw}\frac{\partial}{\partial x}\left[G_q * \nabla.\mathbf{J}\right] \tag{II.29}$$

$$E_y = -jwG_{yy}^A * J_y + \frac{1}{jw}\frac{\partial}{\partial y}\left[G_q * \nabla.\mathbf{J}\right] \tag{II.30}$$

where E_x and E_y are the x and y components of the electric field due to the source current, $\mathbf{J_s}$, respectively [7].

To find the surface current density of the PEC patch by MoM method, first the current density is expanded as a linear combination of basis functions where N is the number of basis functions and A_n and B_n are the unknown coefficients of the basis functions, J_{xn} and J_{yn}.

$$J_x = \sum_{n=1}^{N} A_n J_{xn}(x, y) \tag{II.31}$$

$$J_y = \sum_{n=1}^{N} B_n J_{yn}(x, y) \tag{II.32}$$

After substituting (II.31) and (II.32) into (II.29) and (II.30), respectively, the resulting expression is tested by the testing functions, T_{xm} and T_{ym}, using a suitable inner product form as:

$$\sum_n A_n \left\{ \left\langle T_{xm}, G_{xx}^A * J_{xn} \right\rangle + \frac{1}{w^2}\left\langle T_{xm}, \frac{\partial}{\partial x}\left[G_q * \frac{\partial}{\partial x} J_{xn} \right] \right\rangle \right\} + \sum_n B_n \left\{ \frac{1}{w^2}\left\langle T_{xm}, \frac{\partial}{\partial x}\left[G_q * \frac{\partial}{\partial y} J_{yn} \right] \right\rangle \right\} = 0 \tag{II.33}$$

$$\sum_n B_n \left\{ \left\langle T_{ym}, G_{yy}^A * J_{yn} \right\rangle + \frac{1}{w^2}\left\langle T_{ym}, \frac{\partial}{\partial y}\left[G_q * \frac{\partial}{\partial y} J_{yn} \right] \right\rangle \right\} + \sum_n A_n \left\{ \frac{1}{w^2}\left\langle T_{ym}, \frac{\partial}{\partial y}\left[G_q * \frac{\partial}{\partial x} J_{xn} \right] \right\rangle \right\} = 0 \tag{II.34}$$

The inner product terms in (II.33) and (II.34) are five dimensional integral equations. The inner product itself involves two integrations. Moreover, convolution itself results in two more integration. The last integration comes from

the Green's function which involves an improper integral over an infinite domain. As an example, one of the integral forms of the inner product terms is represented below:

$$\left\langle T_{ym,} G_{yy}^{A} * J_{yn} \right\rangle = \iint_{D(T)} dxdy T_{ym}(x,y) \iint_{D(B)} dx'dy' G_{yy}^{A}(x-x', y-y') J_{yn}(x', y') \tag{II.35}$$

where $D(T)$ and $D(B)$ are the domain of the testing and basis functions, respectively and

$$G_{yy}^{A}(\rho) = \frac{1}{4\pi} \int_{-\infty}^{+\infty} dk_{\rho} k_{\rho} H_{o}^{(2)}(k_{\rho}\rho) \tilde{G}_{yy}^{A}(\rho) \tag{II.36}$$

where $k_{\rho}^{2} = k_{x}^{2} + k_{y}^{2}$, ρ is the variable in cylindrical coordinate system, G and $\tilde{G}$ are the Green's functions in the spatial and spectral domains, respectively and $H_{o}^{(2)}$ is the Hankel function of the second kind. In this study, Green's functions are represented as G_{st}^{A} which gives s-component of the potential existing at the point $\mathbf{r}$ created by a t-directed HED located at the point $\mathbf{r}'$.

The inner product terms in (II.33) and (II.34) involve convolution integrals that can not be evaluated analytically because $G_{q} \sim O(1/r)$ as $r \to 0$, where r is the distance between the source and observation points. This means that Green's functions may involve singularity of the first order. If the basis functions are chosen as a set of piecewise differentiable functions, using the convergence analysis described in [7], it can be proven that Green's functions satisfy the convergence conditions. Convolution analysis of the inner product terms and the proper choice of the basis and testing functions are detailed in [8] and [9]. Then, by using integration by parts, the inner product terms involving differentiation in (II.33) and (II.34) can be simplified [7]. An example of this can be represented as:

$$\left\langle T_{xm}, \frac{\partial}{\partial x}\left[G_{q} * \frac{\partial}{\partial x} J_{xn} \right] \right\rangle = -\left\langle \frac{\partial}{\partial x} T_{xm}, G_{q} * \frac{\partial}{\partial x} J_{xn} \right\rangle \tag{II.37}$$

The order of the integrals can also be changed as below:

$$\left\langle T_{xm}, \frac{\partial}{\partial x}\left[G_q * \frac{\partial}{\partial x} J_{xn} \right] \right\rangle =$$

$$-\iint dxdyG_q(x,y)\iint dx'dy' \frac{\partial}{\partial x'} T_{x'm}(x',y') \frac{\partial}{\partial x'} B_{x'm}(x'-x, y'-y)$$

(II.38)

where the inner double integral is a correlation function integral which can be evaluated analytically [7]. Then, the inner product terms are reduced to two-dimensional integrals over a finite domain. However, these integrals involve the spatial domain Green's functions which can be obtained by the integration of the spectral domain Green's functions as shown in (II.36). As the kernel of the transformation is the Bessel function of the first kind and the function to be transferred is the spectral domain Green's function, the integrand is an oscillatory and slow-converging function. Hence, the calculation of the spatial domain Green's function is very difficult for spatial domain MoM application. To eliminate this problem, closed-form Green's functions method is used as described in Section 2.3.

In the next section, the spectral domain MoM formulation will be analyzed to understand its advantageous and disadvantageous when compared to spatial domain MoM formulation.

2.2.3 Spectral Domain MoM Formulation

Since the convolution integral in the spatial domain is represented by a multiplication in the spectral domain, (II.29) and (II.30) can be expressed as follows,

$$\tilde{E}_x(k_x,k_y) = \tilde{Z}_{xx}(k_x,k_y)\tilde{J}_x(k_x,k_y) + \tilde{Z}_{xy}(k_x,k_y)\tilde{J}_y(k_x,k_y) \qquad \text{(II.39)}$$

$$\tilde{E}_x(k_x,k_y) = \tilde{Z}_{xx}(k_x,k_y)\tilde{J}_x(k_x,k_y) + \tilde{Z}_{xy}(k_x,k_y)\tilde{J}_y(k_x,k_y) \qquad \text{(II.40)}$$

where ~ implies Fourier transforms and the electric field Green's functions Z_{ij} in the spectral domain are expressible in closed-forms [10]. To apply MoM, first Fourier transforms of the expanded current densities, (II.31) and (II.32), are substituted to (II.39) and (II.40). Next, testing with the Fourier transforms of the testing functions is performed. Then, the following equations are obtained:

$$\sum_n A_n \left\langle \tilde{T}_{xm}, \tilde{Z}_{xx} \tilde{J}_{xn} \right\rangle + \sum_n B_n \left\langle \tilde{T}_{xm}, \tilde{Z}_{xy} \tilde{J}_{yn} \right\rangle = 0 \tag{II.41}$$

$$\sum_n A_n \left\langle \tilde{T}_{ym}, \tilde{Z}_{yx} \tilde{J}_{xn} \right\rangle + \sum_n B_n \left\langle \tilde{T}_{ym}, \tilde{Z}_{yy} \tilde{J}_{yn} \right\rangle = 0 \tag{II.42}$$

where the inner products are defined over the infinite domain. As an example, one of the inner products can be expressed as below:

$$\left\langle \tilde{T}_{ym}, \tilde{Z}_{yx} \tilde{J}_{xn} \right\rangle = \iint_{-\infty}^{\infty} dk_x dk_y \tilde{T}_{ym}^{*}(k_x, k_y) \tilde{Z}_{yx}(k_x, k_y) \tilde{J}_{xn}(k_x, k_y) \tag{II.43}$$

Spectral domain MoM application can be more efficient than the spatial domain approach because the integral dimension is reduced to two. However, this approach is usually applied in conjunction with an acceleration technique as it is still time consuming. Acceleration techniques are employed by subtracting the asymptotic part of the Green's function from its original form. The contribution of the asymptotic part is then calculated either analytically or in a numerically efficient manner [5]. In spite of the usage of acceleration techniques, the computation can be still expensive because of the oscillatory nature of the integrands, especially for the self terms for which the observation segment coincides with the source segment. Hence, as a more efficient technique, the spatial domain MoM formulation in conjunction with the closed-from Green's functions is found in the analysis of printed structures.

2.3 Closed-form Green's Functions

As described in the previous section, if MoM is applied in the spectral domain then the inner products are defined over an infinite domain and the resulting integral equation consists of double integrals. This time consuming method can be replaced by applying MoM with the closed-form representations of the spatial domain Green's functions which results in two-dimensional integral equations in finite domains. This approach was first introduced in [12] for a one-layer planar medium where horizontal electric dipole (HED) over a thick substrate was backed by a ground plane. In this study, conventional spectral domain Green's functions are approximated as closed-form expressions using Prony's method. Then, this study is improved for a two-layer planar medium using both Prony's method and least-square Prony's method [13]. The approach is generalized for the sources of horizontal electric, magnetic, and vertical electric,

magnetic dipoles embedded in general, multilayer, planar media in [14]. In this study, the general closed-form Green's functions of the vector and scalar potentials of sources located in an arbitrary layer of a planar-layered medium are derived. In figure 7, a typical layered medium is shown. The sources in the figure 7 are embedded in region i and the observation point can be located in an arbitrary layer. The electric and magnetic properties (ε_r, μ_r) and the thicknesses of each layer d_i can have different values. The perfect electric or magnetic conducting planes and half space are considered as layers for the formulation. The steps of obtaining the general closed-form Green's functions can be summarized as below [14]:

1.) Derivation of the Green's functions in the spectral domain

a.) Green's functions are derived in the source layer,

b.) Green's functions in the observation layer are obtained using an iterative algorithm applied to each transverse electric (TE) and transverse magnetic (TM) component of the Green's functions in the source layer,

2.) Derivation of the spatial domain, closed-form Green's functions

a) Spectral Domain Green's functions, after having the surface wave poles and the direct terms extracted, are approximated in terms of complex exponentials obtained from the generalized pencil of function (GPOF) method [15],

b) Closed-form Green's functions are obtained analytically using the Sommerfeld identity for each complex exponential.

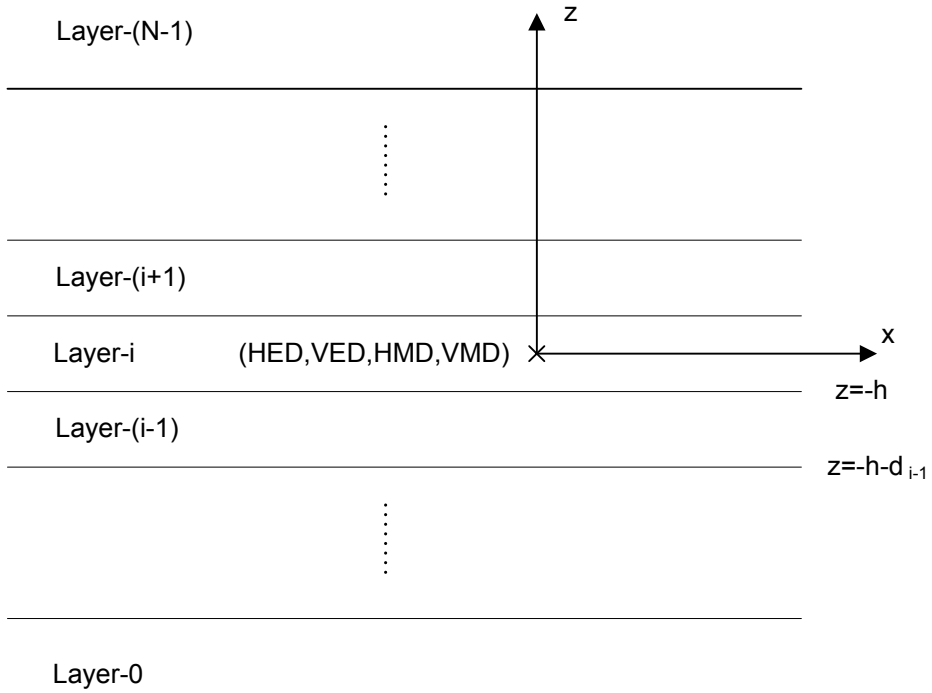

Figure 7 A Typical Layered Medium with Embedded Sources in Layer-i [14].

Derivation of the spectral domain Green's functions is performed for the scalar and vector potentials in detail in [14] using the similar methods described in [4] for obtaining the electric and magnetic field Green's functions.

As mentioned before in (II.36), the spatial domain Green's functions are expressed by the Sommerfeld integrals as:

$$G^{A,q}(\rho) = \frac{1}{4\pi} \int_{SIP} dk_\rho k_\rho H_o^{(2)}(k_\rho \rho) \tilde{G}^{A,q}(\rho) \qquad \text{(II.43)}$$

where SIP is the Sommerfeld integration path [11]. (II.43) can not be evaluated analytically except for a few special cases. However, if the spectral domain Green's function is approximated by exponentials, then (II.43) can be evaluated analytically using the well-known Sommerfeld identity:

$$\frac{e^{-jk_s r}}{r} = -\frac{j}{2} \int_{SIP} dk_\rho k_\rho H_o^{(2)}(k_\rho \rho) \frac{e^{-jk_z |z|}}{k_z} \qquad \text{(II.44)}$$

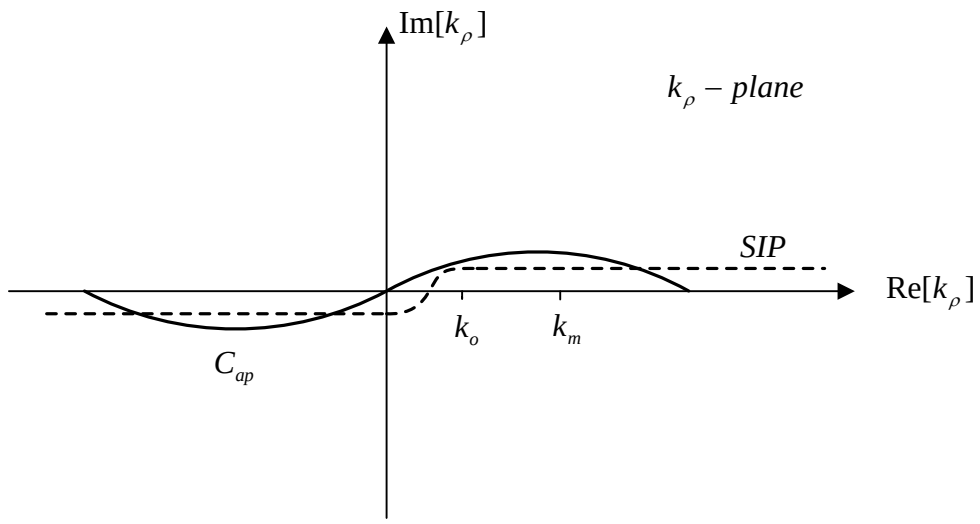

Figure 8 Definitions of the Sommerfeld Integration Path and Integration Path for One Level Approximation [16].

In [14], to derive the spatial domain Green's functions, instead of using Prony's method or least square Prony's method, the generalized pencil of function (GPOF) method is used for the approximation of the spectral domain Green's functions with the complex exponentials. Similar to the other two methods, the generalized pencil of function (GPOF) method requires uniform sampling of a complex valued-function along a real variable. The sampling could be along the k_ρ variable, which results in exponentials in terms of k_ρ. However, to use the Sommerfeld identity, the exponentials should be in terms of k_z. To obtain the required exponentials in terms of k_z, a deformed path on k_z plane was defined as a mapping of a real variable t onto the complex k_z plane as

$$k_z = k\left[-jt + (1 - \frac{t}{T_o})\right], \quad 0 \le t \le T_o \tag{II.45}$$

where k_z and k are defined in the source layer [14]. The integration path C_{ap} is shown in figure 8. The Green's functions are sampled uniformly on $t \in [0, T_o]$, which maps onto the path C_{ap} with $k_{\rho\max} = k[1 + T_o^2]^{1/2}$ in the k_ρ plane, and approximated in terms of exponentials of t which can easily be transformed into a form of exponentials of k_z. This scheme is called the one-level approximation

because the complex function to be approximated is sampled between zero and T_o and is assumed to be negligible beyond T_o [15].

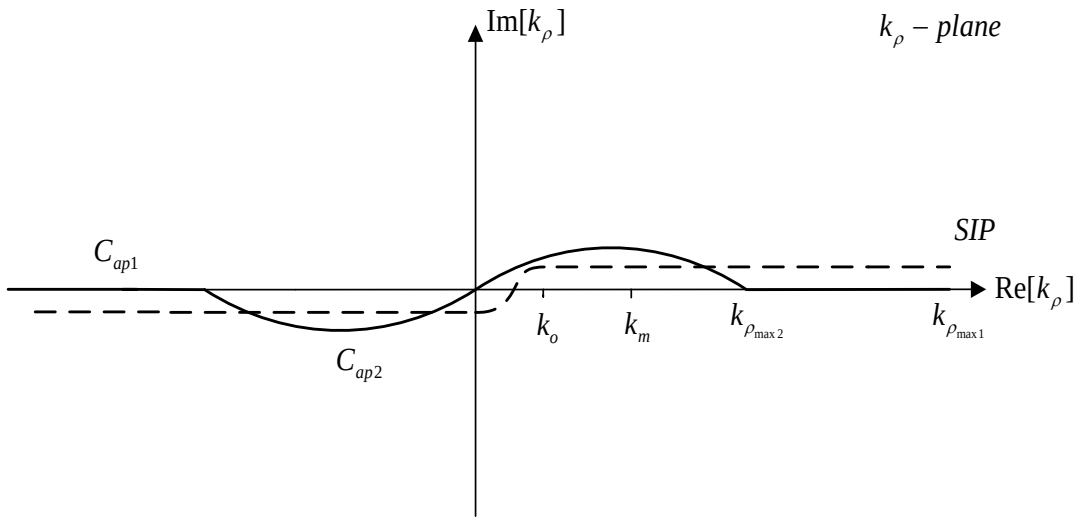

Figure 9 The Paths $C_{a\rho 1}$ and $C_{a\rho 2}$ Used in Two-Level Approximation [16].

The choice of the approximation parameters T_o and the number of samples are very important for the success of GPOF. The number of samples should be large enough to fit the abrupt changes that occur for small values of k_ρ and T_o must be large enough to capture the asymptotic behavior of the Green's function. However, this results in a redundant over-sampling at large values of k_ρ, where the Green's functions are, in general, slowly varying and well-behaved [7]. To circumvent this problem, two level approximations in conjunction with GPOF are introduced [16]. Using this approach, the first part of the approximation is performed along the path C_{ap1} while the second part is done along the path C_{ap2} as shown in figure 9. The asymptotic behavior of the approximated function is extracted in the first approximation. Then, in the second approximation, the fine features of the remaining function are captured by using small number of sampling points. Along C_{ap1} and C_{ap2}, two different functions are used to map the real variable t onto the complex variable k_z, which are as given in [7] can be represented as below:

$$C_{ap1} : k_z = -jk_s[T_{o2} + t], \quad 0 \le t \le T_{o1} \tag{II.46}$$

$$C_{ap2} : k_z = k_s[-jt + (1 - \frac{t}{T_{o2}})], \quad 0 \le t \le T_{o2} \tag{II.47}$$

Applying the two-level approximation, the spectral domain scalar Green's functions can be approximated as

$$\tilde{G} \cong \frac{1}{j2\varepsilon_i k_{zi}} \left[e^{-jk_{zi}|z|} + \sum_{n=1}^{N_1} a_{1n} e^{-\alpha_{1n} k_{zi}} + \sum_{n=1}^{N_2} a_{2n} e^{-\alpha_{2n} k_{zi}} \right] \tag{II.48}$$

where a_{1n} and α_{1n} are the coefficients and exponents obtained from the first part of the two-level approximation and a_{2n} and α_{2n} are from the second part of the two-level approximation. Then, to get the closed-form spatial domain Green's function, its spectral domain representation is substituted in the Sommerfeld identity (II.44) and the following spatial domain Green's function is obtained:

$$G \cong \frac{1}{4\pi\varepsilon_i} \left[\frac{e^{-jk_i r}}{r} + \sum_{n=1}^{N_1} a_{1n} \frac{e^{-jk_i r_{1n}}}{r_{1n}} + \sum_{n=1}^{N_2} a_{2n} \frac{e^{-jk_i r_{2n}}}{r_{2n}} \right] \tag{II.49}$$

where $r_{1n} = \sqrt{x^2 + y^2 - \alpha_{1n}^2}$ and $r_{2n} = \sqrt{x^2 + y^2 - \alpha_{2n}^2}$ are the complex distances and k_i is the wave number in the source layer. (II.48) and (II.49) are obtained by direct sampling of spectral domain Green's functions. Alternatively, the quasi-static terms and surface wave contributions of the spectral domain Green's functions can be extracted analytically first, and then, using GPOF, sampled Green's functions can be approximated by complex exponentials [17]. According to this approach, (II.48) and (II.49) turns to:

$$\tilde{G} \cong \frac{1}{j2\varepsilon_i k_{zi}} \left[\sum_{n=1}^{N_1} a_{1n} e^{-\alpha_{1n} k_{zi}} + \sum_{n=1}^{N_2} a_{2n} e^{-\alpha_{2n} k_{zi}} \right] \tag{II.50}$$

$$G \cong \frac{1}{4\pi\varepsilon_i} \left[\sum_{n=1}^{N_1} a_{1n} \frac{e^{-jk_i r_{1n}}}{r_{1n}} + \sum_{n=1}^{N_2} a_{2n} \frac{e^{-jk_i r_{2n}}}{r_{2n}} \right] \tag{II.51}$$

The above representation can be simplified as:

$$G \cong \sum_{m=1}^{N} a_m \frac{e^{-jk_i r_m}}{r_m} \tag{II.51}$$

where $r_m = \sqrt{\rho^2 - b_m^2}$ is the complex distance and k_i is the wave number of the region where the source is located. A computer program based on the formulation given in [14] produces the coefficients a_m and b_m's for a given layered medium with embedded sources. This program is used to provide those coefficients for different mediums as input to this study.

In figure 10, a 3-layer structure is represented. For this structure, the Green's function of the vector potential due to a HED, G_{xx}^A and G_x^q are obtained by using two-level approximation scheme at 1 GHz frequency. The magnitude and phase of G_{xx}^A with respect to $k_o\rho$ are given in figure 11 and figure 12 respectively. The magnitude and phase of G_x^q with respect to $k_o\rho$ are given in figure 13 and figure 14 respectively.

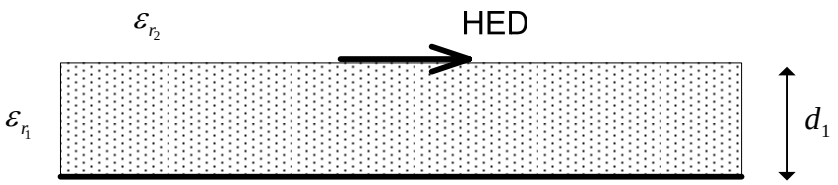

Figure 10 Geometry of a 3-layer Structure. Layer-0: PEC, Layer-2: Half Space. ($f = 1GHz$, $\varepsilon_{r_1} = 4$, $\varepsilon_{r2} = 1$, $d_1 = 0.02032\,cm$)

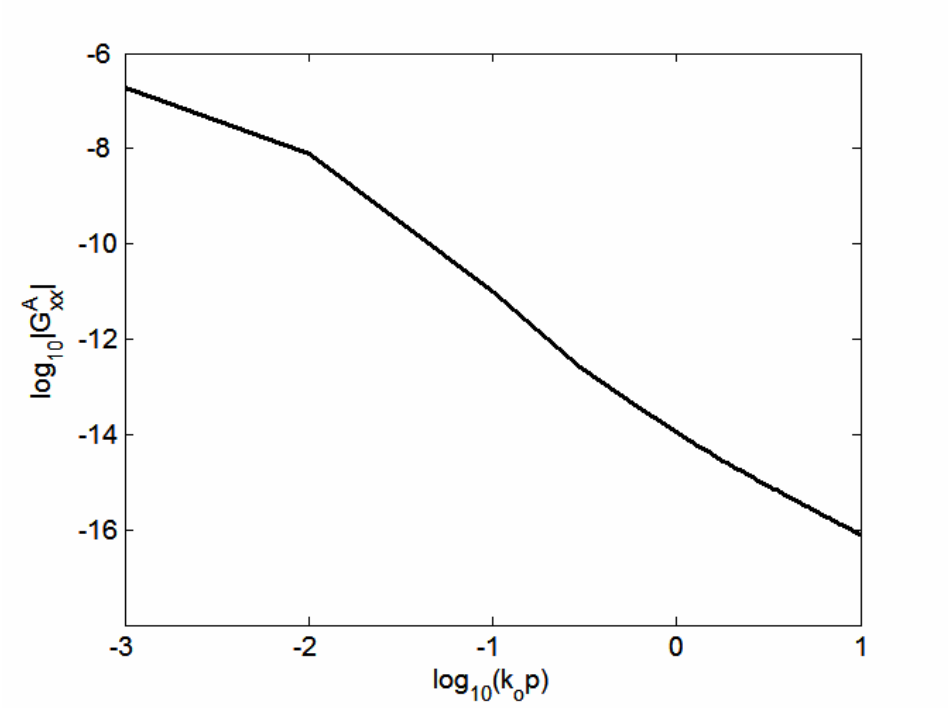

Figure 11 Magnitude of the Green's Function for the Vector Potential G_{xx}^{A}.

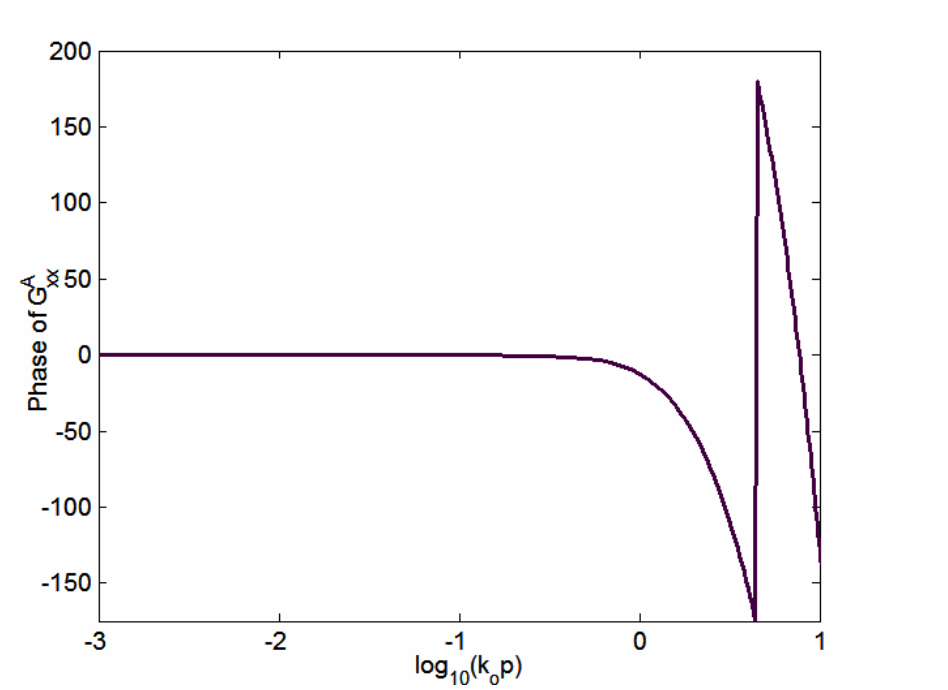

Figure 12 Phase of the Green's Function for the Vector Potential G_{xx}^{A}.

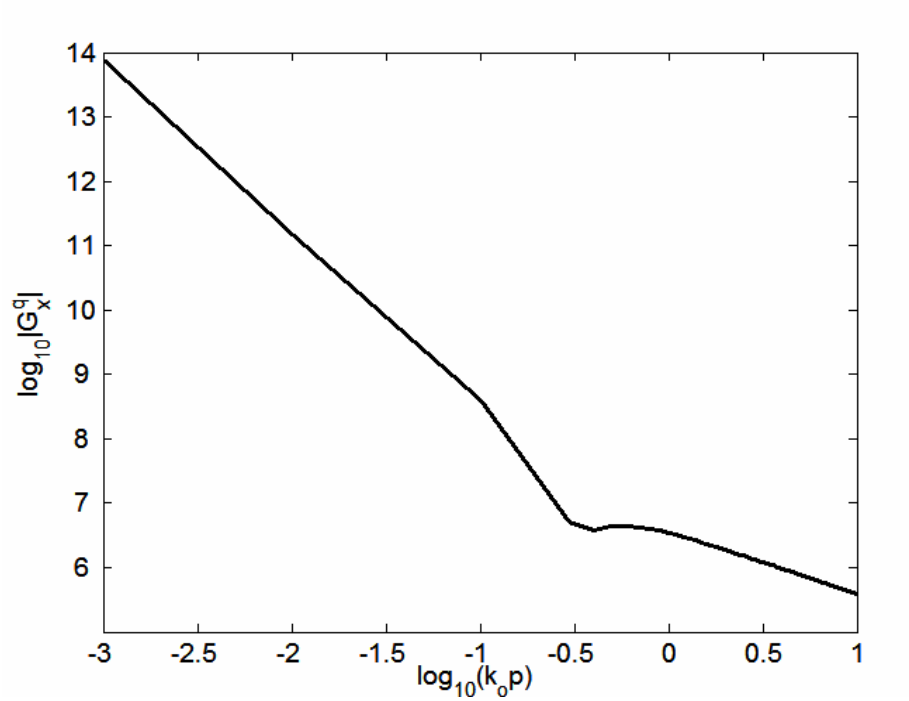

Figure 13 Magnitude of the Green's Function for the Scalar Potential G_x^q.

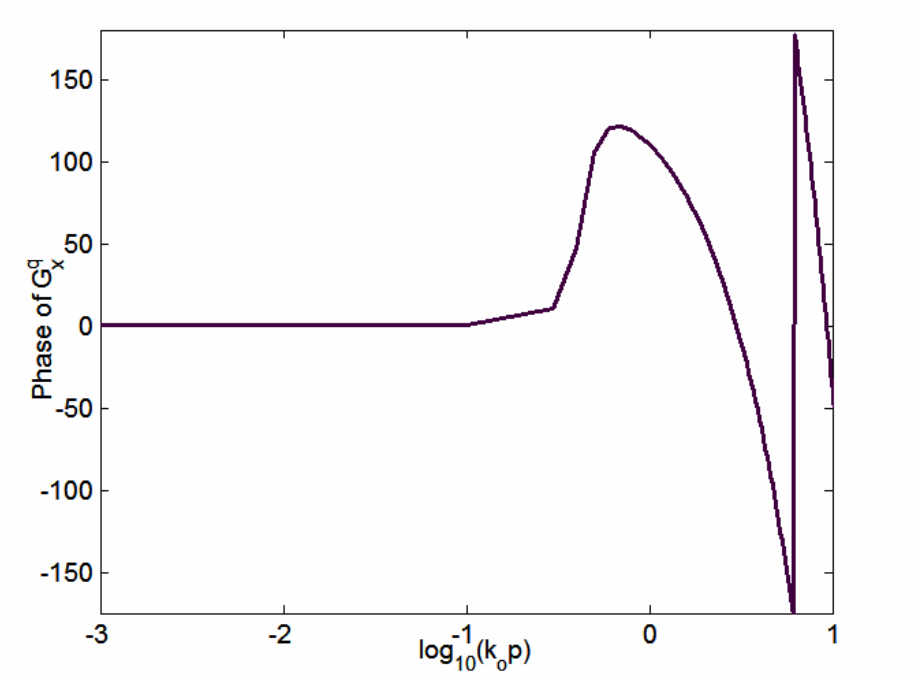

Figure 14 Phase of the Green's Function for the Scalar Potential G_x^q.

As mentioned before, to get the approximated Green's functions successfully, one should choose the correct approximation parameters in two-level approximation scheme. Because single-level approximation scheme requires much more number of samples, two-level approximation is better to use. However, two-level approximation scheme can also be extended to obtain multi-level approximation scheme.

Once the closed form Green's functions are obtained for a layer structure, then, these values can be used repeatedly, in the analysis of many microstrip geometries having the same layer structure. This is the most important advantage of using closed-form Green's functions.

In this chapter, first, a brief description of MoM formulation is introduced. Next, the Green's functions are presented. The spatial domain and spectral domain MoM formulation in conjunction with the Green's functions are detailed and the two approaches are compared for their advantages and disadvantages. Finally, the closed-form Green's function in spatial domain is discussed. In the next chapters, using MoM in conjunction with the closed-from Green's functions, analysis of microstrip lines will be achieved.

CHAPTER 3

CURRENT DISTRIBUTION ON PRINTED STRUCTURES: SINGLE LINE

In this chapter, the current distribution on a single microstrip line will be calculated using closed-form Green's function in the spatial domain in conjunction with Galerkin's Method of Moment. First, a single microstrip line will be analyzed: the structure will be defined, the derivation of the necessary formulas will be achieved, the computer program to calculate the current distributions will be discussed. Finally, the results will be presented according to different load termination of the microstrip lines.

3.1 Definition of the Structure and the Problem

A single microstrip line is a geometry which consists of a wide dielectric substrate, a ground plane located under the substrate, a single conductor trace placed over the dielectric substrate, is shown in figure 15.

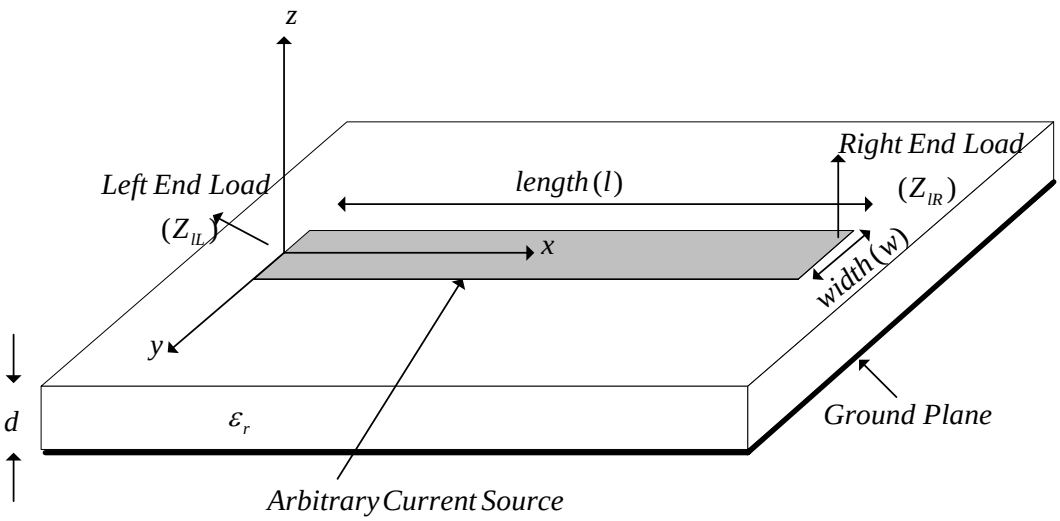

Figure 15 A Single Microstrip Line Geometry

The ends of the line are terminated with arbitrary loads Z_{IL} and Z_{IR}. The excitation point of the microstrip line is also arbitrary.

3.2 Derivation of Formulas

As indicated in (II.26), the electric field can be expressed in terms of scalar and vector potentials and the scalar and the vector potentials can be written in terms of induced surface current density as shown in (II.27) and (II.28). In this study, only the x-directed current density will be calculated because the line width of the microstrip structure is very small as compared to the wavelength. The y-directed current density is assumed to be uniform. Hence, (II.29) is used in the electric field representation of the microstrip line as:

$$E_x = -j\omega G_{xx}^A * J_x + \frac{1}{j\omega}\frac{\partial}{\partial x}[G_q * \frac{\partial}{\partial x} J_x] \qquad \text{(III.1)}$$

where the unknown function J_x can be approximated using a series of known basis functions as

$$J(x,y) = \sum_n I_n J_{xn}(x,y) + J_s(x,y) \qquad \text{(III.2)}$$

I_n are the unknown coefficients of the basis functions and J_s is the basis function for the source [18].

As mentioned before, since the tangential electric field on the microstrip line is zero, then using the testing function, the equation below is obtained:

$$\left\langle J_{xm}(x,y), E_x \right\rangle = 0 \tag{III.3}$$

The above formula can be rewritten substituting (III.1) and (III.2) as:

$$j\omega\left\langle J_{xm}(x,y), G_{xx}^{A} * J_s(x,y)\right\rangle - \frac{1}{j\omega}\left\langle J_{xm}(x,y), \frac{\partial}{\partial x}\left[G_q * \frac{\partial}{\partial x} J_s(x,y)\right]\right\rangle =$$
$$\sum_n I_n \left\{ -j\omega\left\langle J_{xm}(x,y), G_{xx}^{A} * J_{xn}(x,y)\right\rangle + \frac{1}{j\omega}\left\langle J_{xm}(x,y), \frac{\partial}{\partial x}\left[G_q * \frac{\partial}{\partial x} J_{xn}(x,y)\right]\right\rangle \right\}$$

(III.4)

As the basis functions in this study are chosen as rooftops which are piecewise differentiable functions, it is possible to use the integration by parts as described in [7] to change order of the integrals and by dividing both sides to $-j\omega$ then (III.4) can be rewritten as:

$$\sum_n I_n \left\{ \left\langle G_{xx}^{A}, J_{xm}(x,y) * J_{xn}(x,y)\right\rangle - \frac{1}{\omega^2}\left\langle G_q, \frac{\partial}{\partial x} J_{xm}(x,y) * \frac{\partial}{\partial x} J_{xn}(x,y)\right\rangle \right\} =$$
$$-\left\langle G_{xx}^{A}, J_{xm}(x,y) * J_s(x,y)\right\rangle + \frac{1}{\omega^2}\left\langle G_q, \frac{\partial}{\partial x} J_{xm}(x,y) * \frac{\partial}{\partial x} J_s(x,y)\right\rangle \tag{III.5}$$

One of the inner product terms of (III.5) is written in open form as:

$$\left\langle G_{xx}^{A}, J_{xm} * J_{xn}\right\rangle = \iint dudv G_{xx}^{A}(u,v) \iint dxdy J_{xm}(x-u, y-v) J_{xn}(x,y) \tag{III.6}$$

The double integration of basis and testing functions shown in the above equation represents the convolution of the basis and testing functions which can be carried out analytically. Then, (III.5) can be solved just by double integration. The details of the calculations of these convolution integrals are described in appendix A.

In this study, Galerkin's Method of Moments is used. Hence the basis functions $J_{xn}(x,y)$ and testing functions $J_{xm}(x,y)$ are chosen to be same. The load and source basis function representations are also chosen to be compatible with the rooftops [18]. In the subsections of this part, the exact representations of the basis functions and testing functions will be detailed.

3.2.1 Basis Functions

Basis functions are rooftops which are triangular in longitudinal direction and uniform in the transverse direction. The rooftop basis functions are shown in figure 16 (a). The mathematical representation of the rooftop basis functions is given below [18]:

$$J_{xn}(x,y)=\begin{cases}\frac{1}{wh_x}[(1-n)h_x+x] & (n-1)h_x \le x \le nh_x \quad , \quad |y| \le \frac{w}{2} \\ \frac{1}{wh_x}[(1+n)h_x-x] & nh_x \le x \le (n+1)h_x \quad , \quad |y| \le \frac{w}{2} \\ 0 & elsewhere \end{cases} \qquad \text{(III.7)}$$

3.2.2 Source Basis Function

Source basis function is also rooftop which is triangular in longitudinal direction and uniform in the transverse direction. The rooftop source basis function is shown in figure 16 (c). The mathematical representation of the rooftop source function is given below [18]:

$$J_s(x,y)=\begin{cases}\frac{1}{wh_x}[(a-1)h_x-x] & (a-1)h_x \le x \le ah_x \quad , \quad |y| \le \frac{w}{2} \\ \frac{1}{wh_x}[(a+1)h_x-x] & ah_x \le x \le (a+1)h_x \quad , \quad |y| \le \frac{w}{2} \\ 0 & elsewhere \end{cases} \qquad \text{(III.8)}$$

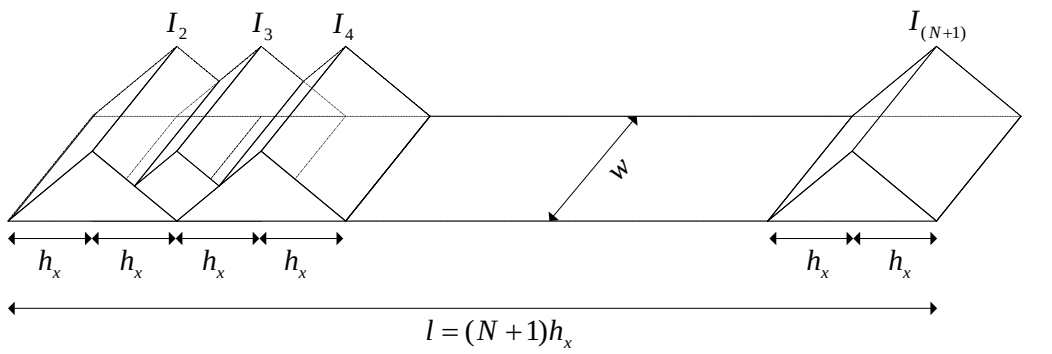

(a)

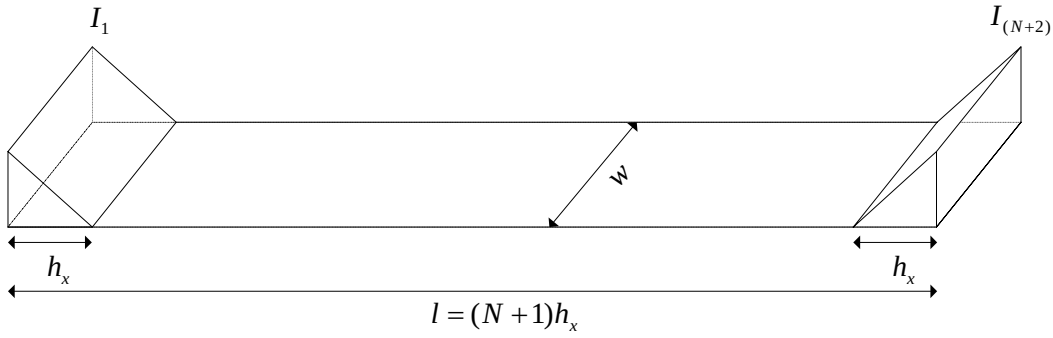

(b)

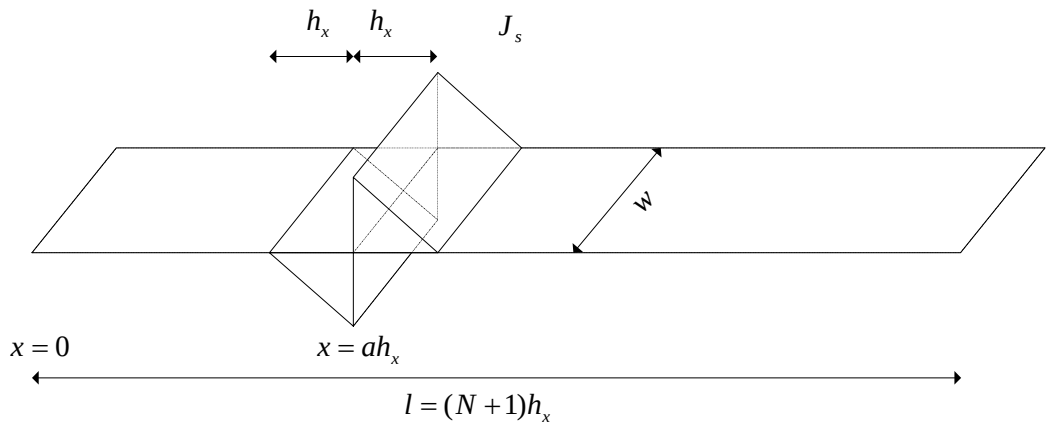

(c)

Figure 16 (a) Basis Functions, (b) Load Basis Functions, (c) Source Basis Function [3].

3.2.3 Load Basis Functions

Load basis functions are haft rooftops which are also triangular in longitudinal direction and uniform in the transverse direction. The model of the load basis functions at each terminal of the single microstrip line is shown in figure 16 (b). The mathematical representation of the rooftop load basis functions are given below [18]:

$$J_{lL}(x,y)=\begin{cases}-\dfrac{1}{wh_x}[x-h_x] & 0\le x\le h_x \quad , \quad |y|\le \dfrac{w}{2}\\ 0 & elsewhere\end{cases} \tag{III.9}$$

$$J_{lR}(x,y)=\begin{cases}\dfrac{1}{wh_x}[x-Nh_x] & Nh_x\le x\le (N+1)h_x \quad , \quad |y|\le \dfrac{w}{2}\\ 0 & elsewhere\end{cases} \tag{III.10}$$

where N is the number of basis functions.

The load basis functions at each end of the single microstrip line should be related to the rest of the basis functions. To do this, the boundary conditions at each load terminals are considered. The voltages at each end of the line can be expressed in terms of load impedances, the coefficients of the load basis functions and coefficients of the other basis functions as the voltage difference between the line and ground is the product of the line current and the load impedance [18]. Then, using transmission line analysis and finite differencing approach, the following equations are obtained:

$$I_1[1+j\beta h_x\frac{Z_{lL}}{Z_c}-\frac{\beta^2h_x^2}{2}]-I_2=0 \tag{III.11}$$

$$I_{N+1}+I_{N+2}[1+j\beta h_x\frac{Z_{lR}}{Z_c}-\frac{\beta^2h_x^2}{2}]=0 \tag{III.12}$$

where Z_{lL} is the load impedance of the left end of the line, Z_{lR} is the load impedance of the right end of the line, Z_c is the characteristic impedance of the line and β is the propagation constant. The derivation of (III.11) and (III.12) are given in appendix B. The characteristic impedance of the line, Z_c is found using approximate formulas [20], which is detailed in appendix C.

3.2.4 Singularity Extraction

As $r \to 0$, due to the direct term of the Green's functions given in (III.13), a singularity occurs.

$$G \cong \sum_{n=1}^{N} a_n \frac{e^{-jk\, r_n}}{r_n} \tag{III.13}$$

To remove the singularity, first double integration in (III.6) is performed by extracting the direct term from the total equation. Then, the direct term is expanded using Taylor series expansion. e^{-jkr} about $r = 0$ can be expressed as below:

$$e^{-jkr} = 1 + (-jkr) + \frac{(-jkr)^2}{2!} + \ldots \tag{III.14}$$

As (III.14) divided by r, the equation below is obtained:

$$\frac{e^{-jkr}}{r} = \frac{1}{r} + (-jk) + r\left[\frac{(-jk)^2}{2!} + \ldots\right] \tag{III.15}$$

Then, the second term of the right part of (III.15) can be added to the double integration. The source and observation points are at $z = 0$. As the first term of the right part of (III.15) is $1/r = 1/\sqrt{x^2 + y^2}$, this representation is used in the double integration as [3]:

$$\begin{aligned}\int_{y_1}^{y_2}\int_{x_1}^{x_2} \frac{1}{\sqrt{x^2+y^2}}\, dxdy = {} & y_2 \log[\frac{-x_1 + \sqrt{x_1^2 + y_2^2}}{-x_2 + \sqrt{x_2^2 + y_2^2}}] + y_1 \log[\frac{-x_2 + \sqrt{x_2^2 + y_1^2}}{-x_1 + \sqrt{x_1^2 + y_1^2}}] \\ & + x_2 \log[\frac{-y_1 + \sqrt{x_2^2 + y_1^2}}{-y_2 + \sqrt{x_2^2 + y_2^2}}] + x_1 \log[\frac{-y_2 + \sqrt{x_1^2 + y_2^2}}{-y_1 + \sqrt{x_1^2 + y_1^2}}]\end{aligned} \tag{III.16}$$

With the above equation, the effect of direct term is completely added to the analysis.

3.3 Software Implementation

The current distribution of a single line can be determined by solving (III.5) for basis function coefficients, I_n's. First, MoM matrix equation is constructed as:

$$Ax = b \tag{III.17}$$

where A is an N by N matrix and x and b are N by 1 matrices. The elements of these matrices are represented as:

$$A_{mn} = \left\langle G_{xx}^{A}, J_{xm}(x,y) * J_{xn}(x,y) \right\rangle - \frac{1}{\omega^2} \left\langle G_q, \frac{\partial}{\partial x} J_{xm}(x,y) * \frac{\partial}{\partial x} J_{xn}(x,y) \right\rangle,$$

$$x_n = I_n,$$

$$b_m = -\left\langle G_{xx}^{A}, J_{xm}(x,y) * J_s(x,y) \right\rangle + \frac{1}{\omega^2} \left\langle G_q, \frac{\partial}{\partial x} J_{xm}(x,y) * \frac{\partial}{\partial x} J_s(x,y) \right\rangle$$

(III.18)

where $m = 2, 3, ..., (N+1)$, $n = 2, 3, ..., (N+1)$ and N is the number of basis and testing functions over the microstrip line. The entries of matrices A and b require double integration which can be numerically approximated using Gaussian Quadrature which performs double integration of a complex function of two variables. The microstrip line is excited by a current source $J_s(x,y)$ from an arbitrary point of line.

Because basis and testing functions are chosen to be same, A matrix is symmetric. Hence, it is enough to calculate one of the row or column entries to determine the actual A matrix. This reduces the computation time considerably.

Next, A matrix is extended to A' matrix which is an $N+2$ by $N+2$ matrix to relate the effects of the terminal loads of microstrip line to the basis functions by using the load equations given in (III.11) and (III.12). Hence, the MoM matrix equation is updated as:

$$A'x' = b' \tag{III.19}$$

where x' and b' are $N+2$ by 1 matrices. These matrices are represented as:

$$A' = \begin{bmatrix} l1 & -1 & 0 & 0 & 0 & 0 \\ A_{21} & A_{22} & A_{23} & \cdots & A_{2(N+1)} & A_{2(N+2)} \\ A_{31} & A_{32} & A_{33} & \cdots & A_{3(N+1)} & A_{3(N+2)} \\ \vdots & \vdots & & & & \\ A_{(N+1)1} & A_{(N+1)2} & A_{(N+1)3} & \cdots & A_{(N+1)(N+1)} & A_{(N+1)(N+2)} \\ 0 & 0 & 0 & 0 & -1 & l2 \end{bmatrix} \tag{III.20}$$

$$x' = \begin{bmatrix} I_1 \\ I_2 \\ I_3 \\ \vdots \\ I_{(N+1)} \\ I_{(N+2)} \end{bmatrix} \text{ and } b' = \begin{bmatrix} 0 \\ b_2 \\ b_3 \\ \vdots \\ b_{(N+1)} \\ 0 \end{bmatrix} \qquad \text{(III.21)}$$

where $l1 = [1 + j\beta h_x \frac{Z_{lL}}{Z_c} - \frac{\beta^2 h_x^2}{2}]$ and $l2 = [1 + j\beta h_x \frac{Z_{lR}}{Z_c} - \frac{\beta^2 h_x^2}{2}]$. To find A_{m1} entries, the left end load basis function is used and similarly, to find $A_{m(N+2)}$ entries, the right end load basis function is used. The evaluation of the convolution integrals over load basis functions and testing functions are detailed in appendix A.1.

Finally, after filling matrices A' and b', the unknown current coefficients, I_n's are calculated taking the inverse of A' since $x' = (A')^{-1} b'$.

The program which performs all the above calculation is written in programming language MATLAB™.

3.4 Results

In this section, results of the analysis of a single microstrip line structure for different load terminations will be represented. The structure of the microstrip line is defined in figure 17.

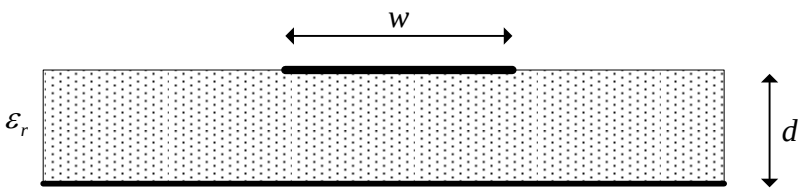

Figure 17 Single microstrip line

The parameters required for the analysis are given below as:

$f = 1\,GHz$
$\varepsilon_r = 4.0$
$d = 0.02032\ cm\ (8\ mils)$
$w = 0.08128\ cm\ (32\ mils)$
$l = 12\ cm$
$z_c = 32.035\,\Omega$

The amplitude and phase plots of closed-form spatial domain vector and scalar potentials of this structure were given in chapter 2. To find the current distribution over a single microstrip line, closed-form spatial domain vector and scalar potentials of the structure are used.

In figure 18, 19, 20 and 22, the amplitude of the current distribution over the line is represented for the matched load terminations at both ends of the line for different number of basis and excitation points. The phase of the current distribution over the line is also represented in figure 21 and 23.

In figure 24, 26 and 27, the amplitude of the current distribution over the line is represented for the open circuited terminations at both ends of the line for different number of basis and excitation points. The phase of the current distribution over the line is also represented in figure 25 and 28.

In figure 29, the amplitude of the current distribution over the line is represented for the short circuited terminations at both ends of the line. The phase of the current distribution over the line is also represented in figure 30.

Using the same procedure described in this chapter, current distribution can be evaluated for multilayered structures using the power of the closed-form Green's functions.

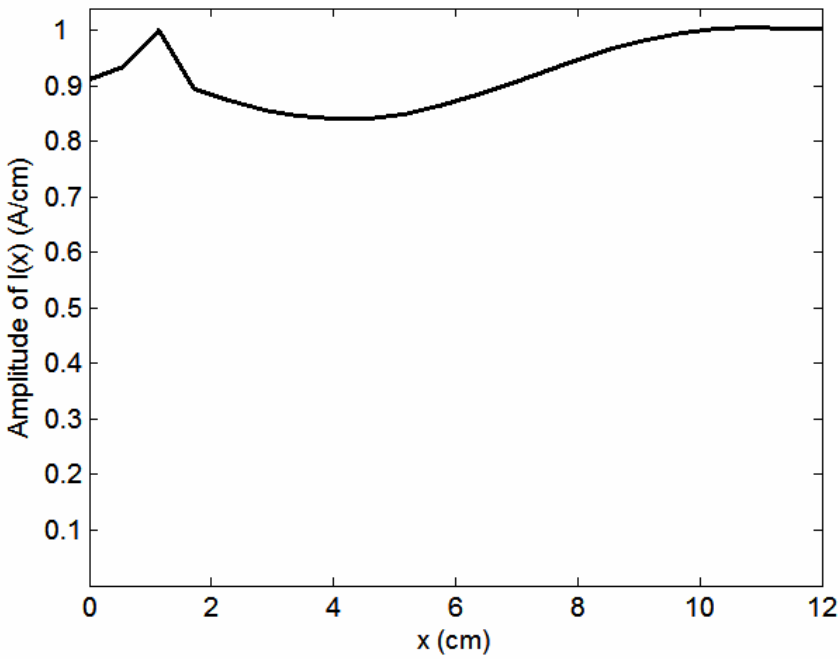

Figure 18 Matched load terminations, excited at x=1, number of basis=40.

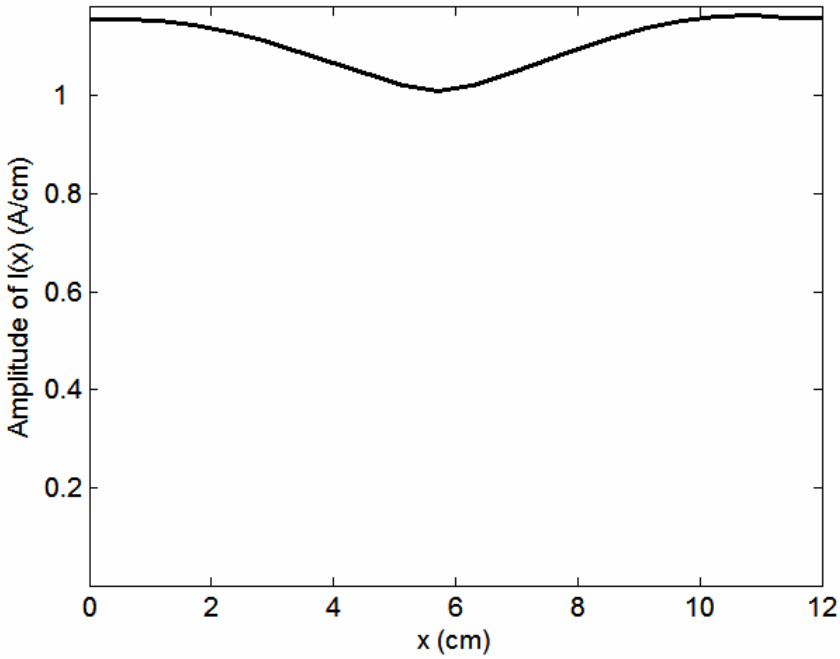

Figure 19 Matched load terminations, excited at x=6, number of basis=40.

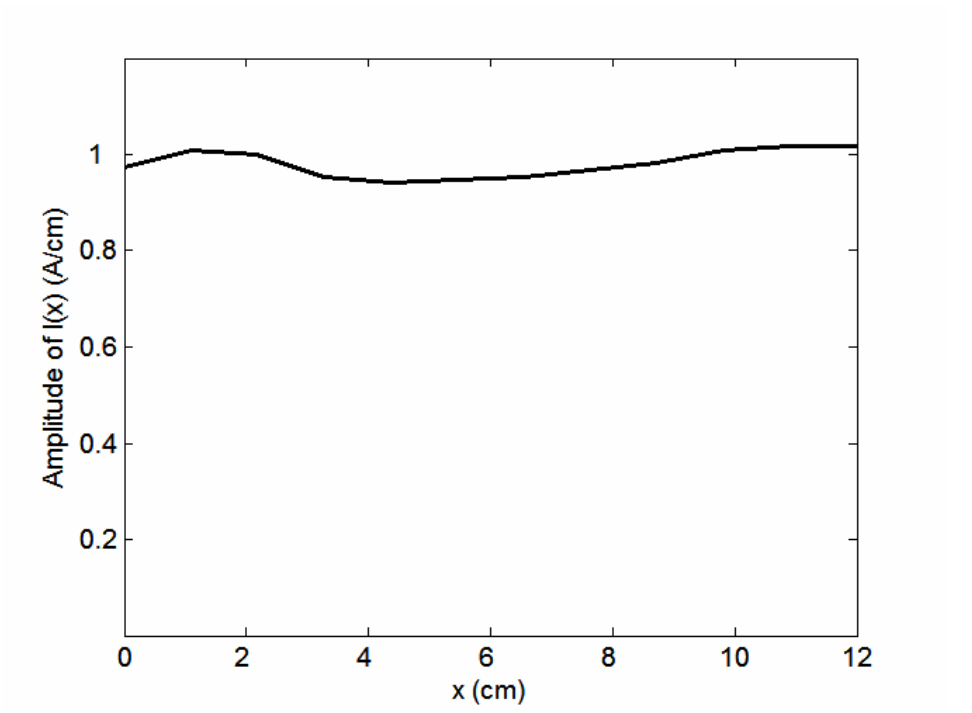

Figure 20 Matched load terminations, excited at x=1, number of basis=50.

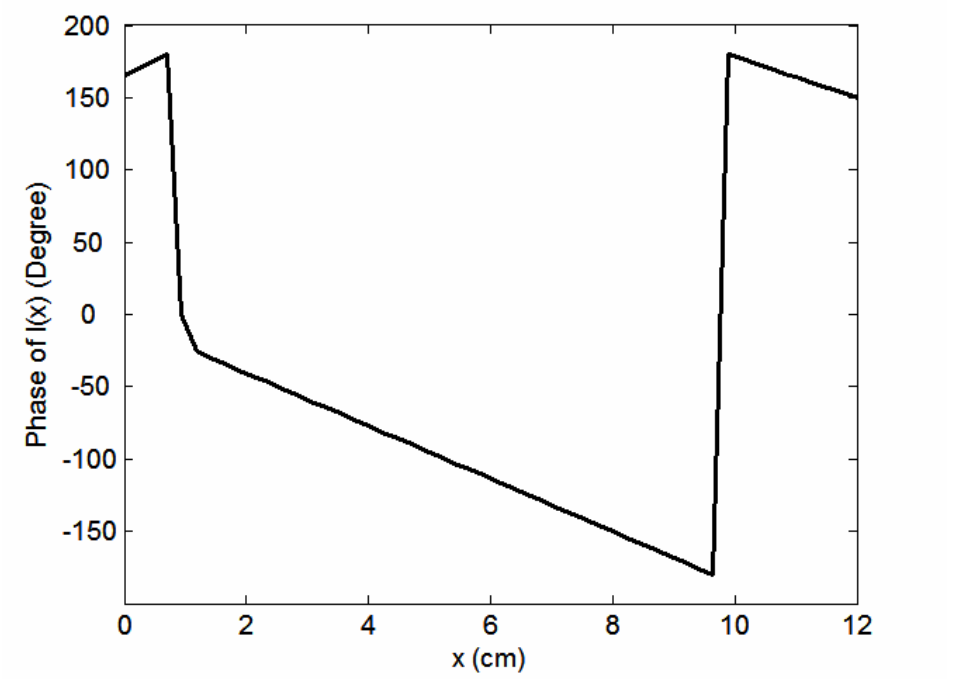

Figure 21 Matched load terminations, excited at x=1, number of basis=50.

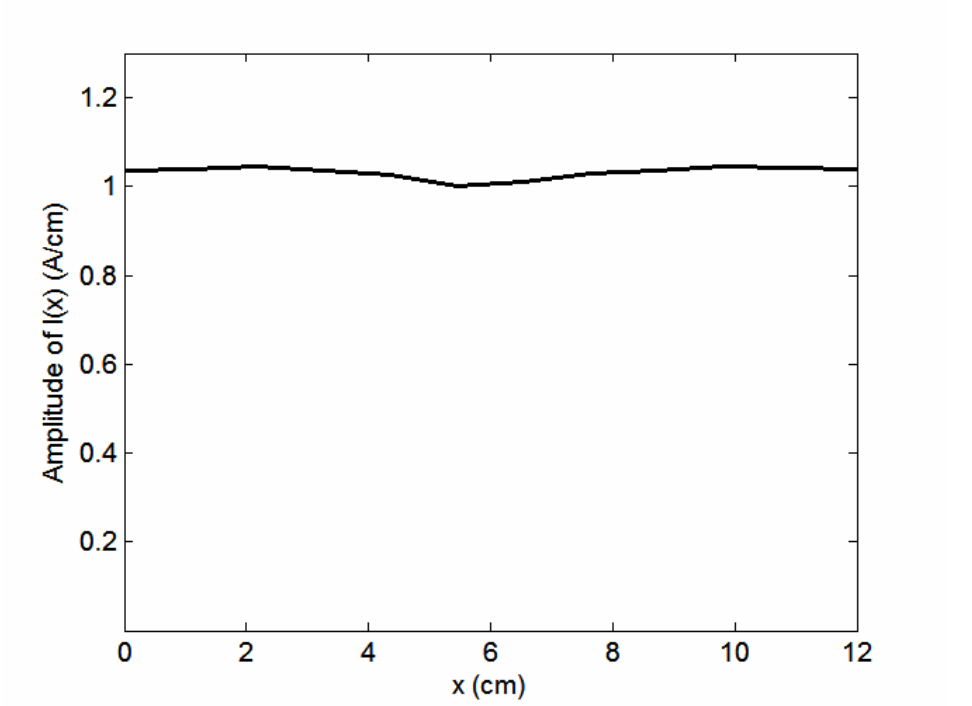

Figure 22 Matched load terminations, excited at x=6, number of basis=50.

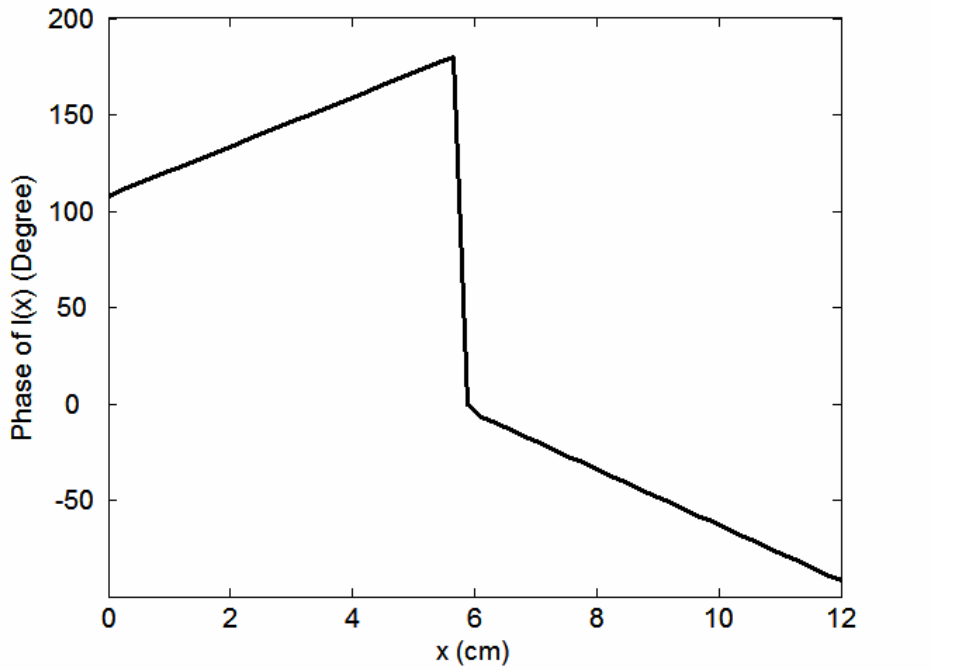

Figure 23 Matched load terminations, excited at x=6, number of basis=50.

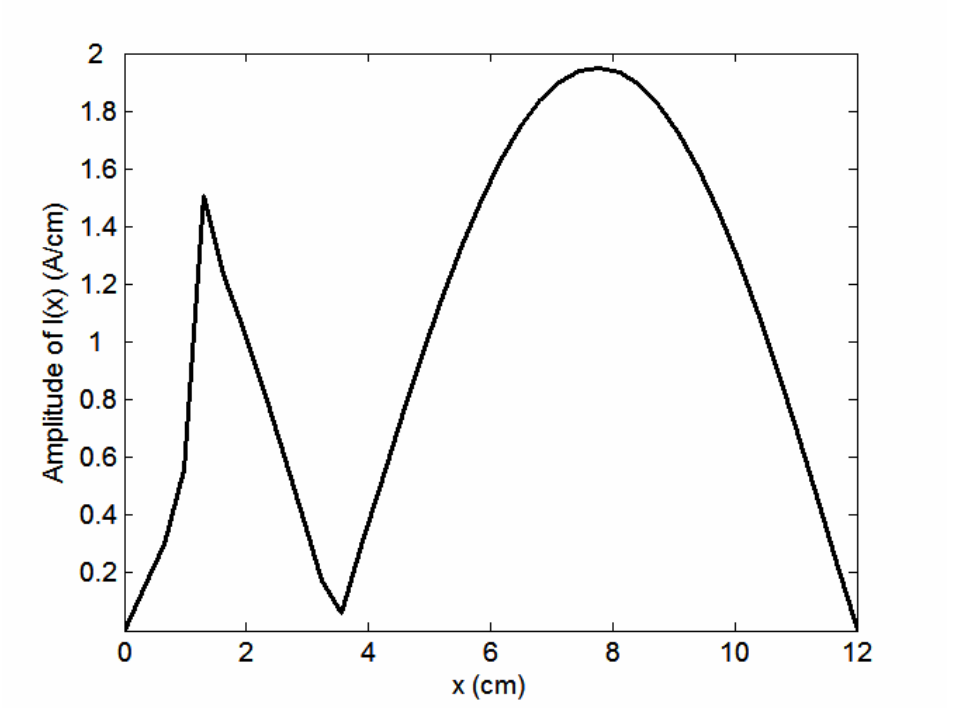

Figure 24 Open circuited terminations, excited at x=1, number of basis=40.

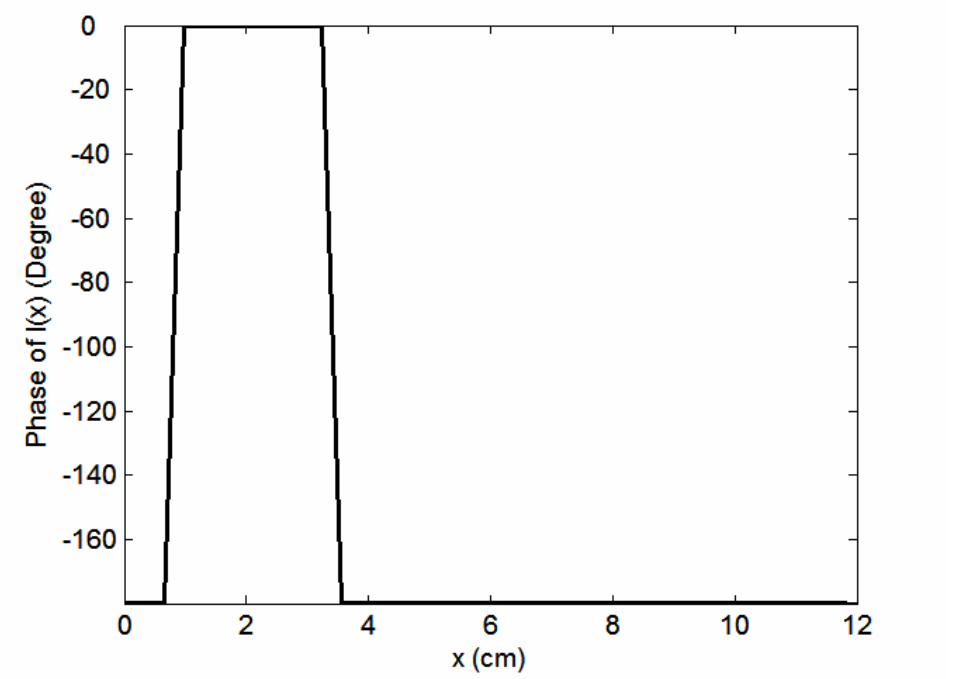

Figure 25 Open circuited terminations, excited at x=1, number of basis=40.

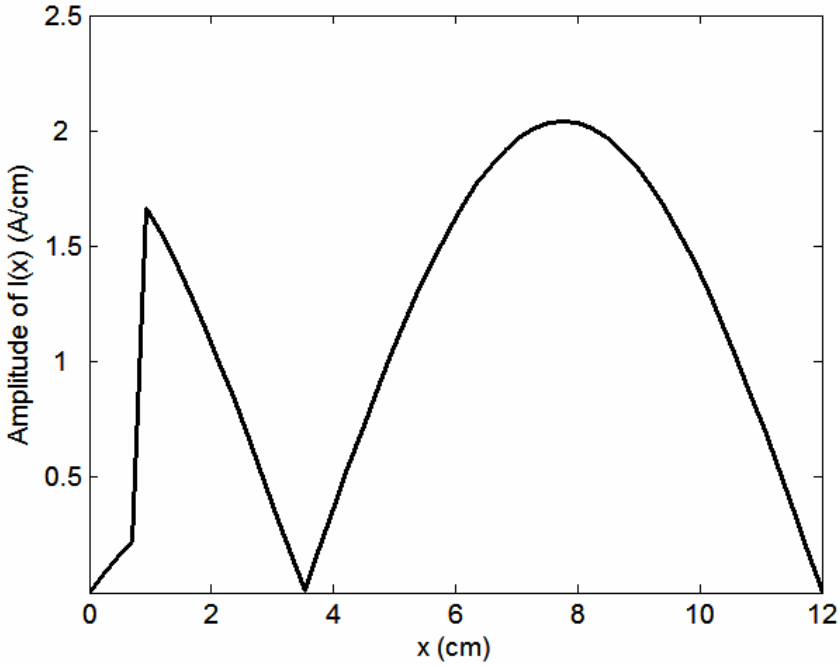

Figure 26 Open circuited terminations, excited at x=1, number of basis=50.

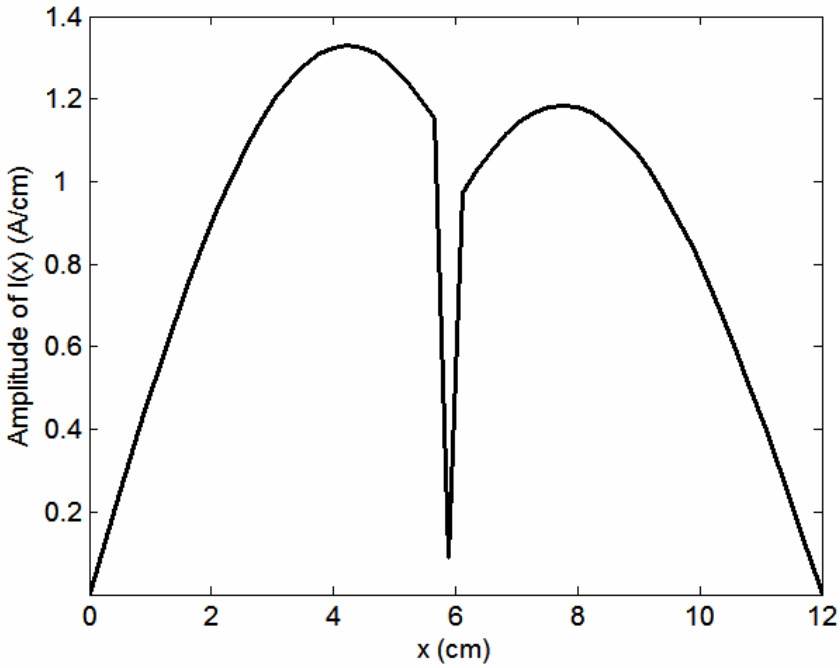

Figure 27 Open circuited terminations, excited at x=6, number of basis=50.

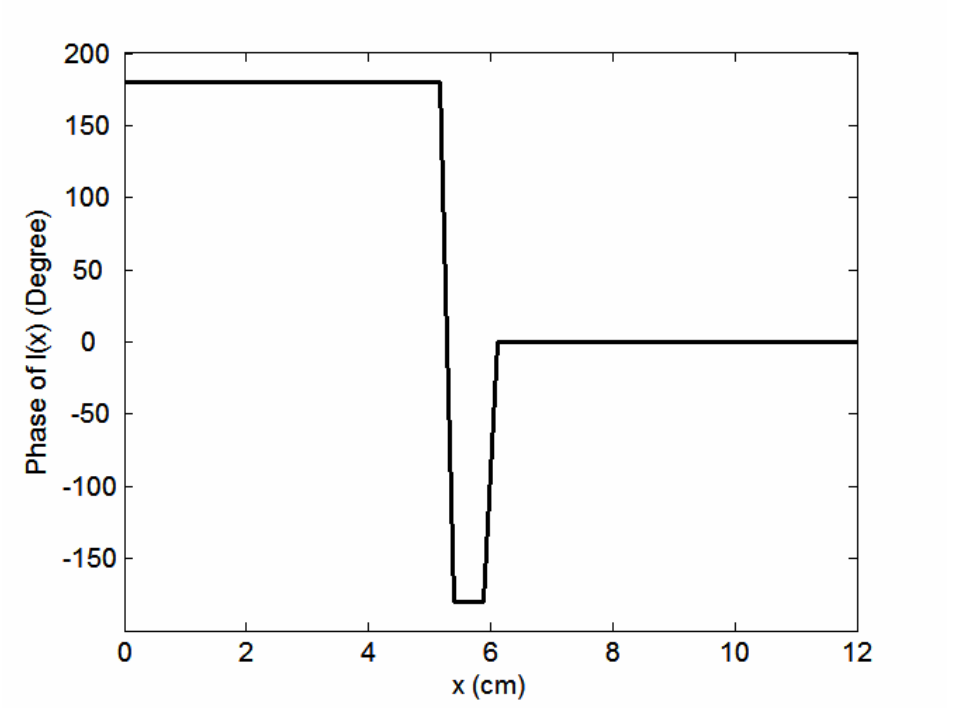

Figure 28 Open circuited terminations, excited at x=6, number of basis=50.

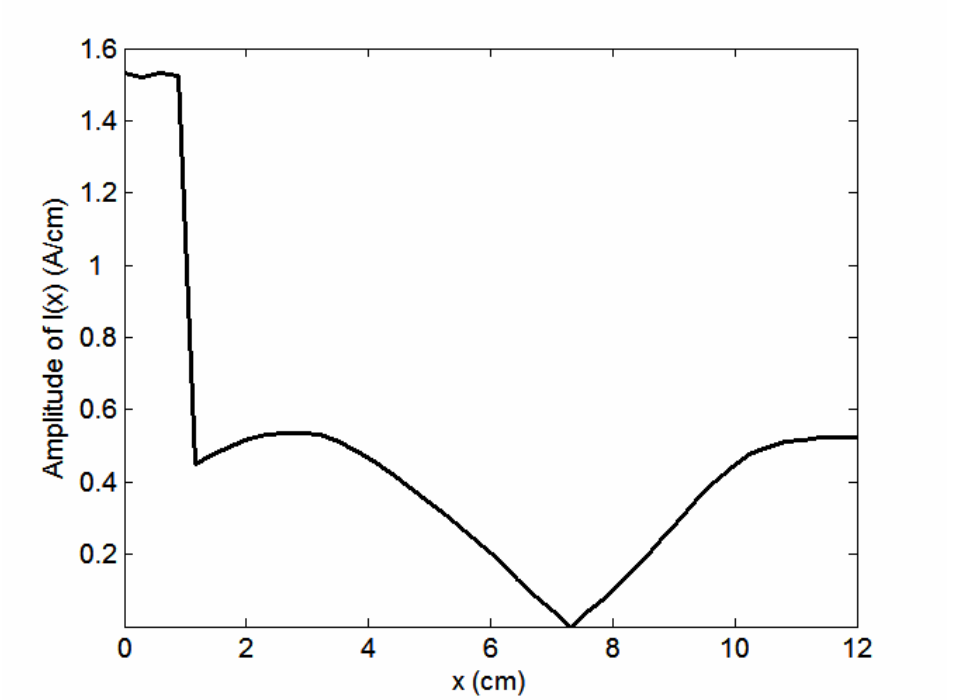

Figure 29 Short circuited terminations, excited at x=1, number of basis=40.

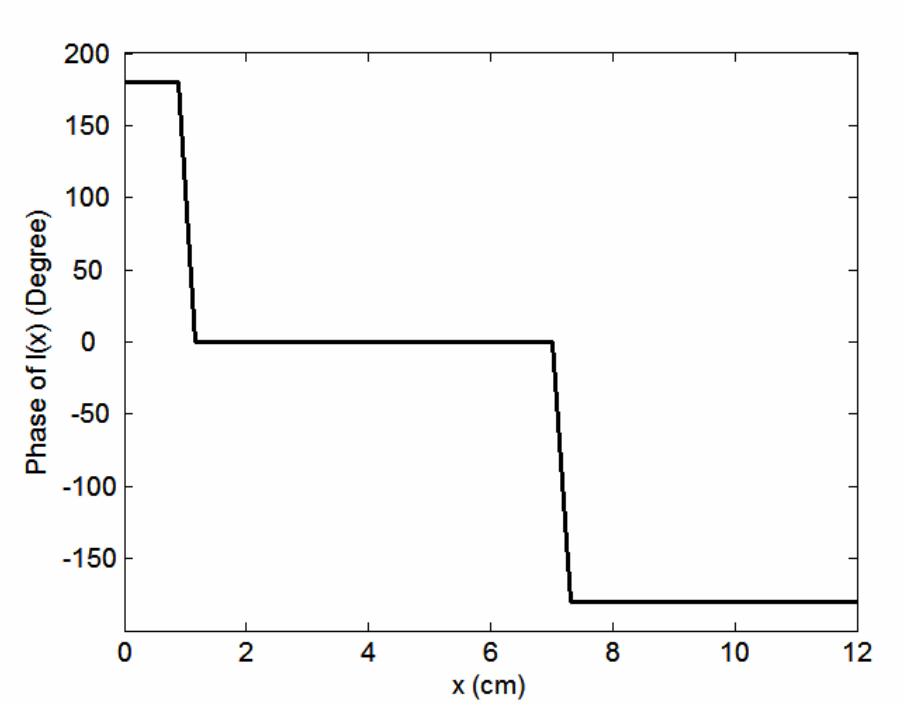

Figure 30 Short circuited terminations, excited at x=1, number of basis=40.

Once the current distribution over the line is evaluated, then using the sampled data, current distribution can be formulated by representing forward and backward propagating waves:

$$I(x) = I^{-}(x) + I^{+}(x)$$
$$I(x) = c_1 e^{\beta_1 x} + c_2 e^{\beta_2 x} \qquad \text{(III.22)}$$

where c_1 is the coefficient for the incident waves and c_2 is the coefficient for the reflected waves. This can be achieved using Prony's method [21], which is an approximating method for modeling sampled data as a linear combination of exponentials. The detailed information about Prony's method is given in appendix D. Once the coefficients of incident and reflected waves are found, one can found the reflection coefficient which is the ratio of the amplitudes of the forward and backward propagating waves:

$$\Gamma = \frac{c_2}{c_1} \qquad \text{(III.23)}$$

When number of basis is chosen as 40, excitation point at x=1 cm, for the open circuited terminations:

$$c_1 = 0.8004 + 0.9370i$$
$$c_2 = 0.8006 - 0.9370i$$
$$\beta_1 = 0.0429 - 0.3413i$$
$$\beta_2 = -0.0429 - 0.3413i$$

When number of basis is chosen as 40, excitation point at x=1 cm, for the short circuited terminations:

$$c_1 = 0.2481 + 0.1166i$$
$$c_2 = 0.2481 - 0.1166i$$
$$\beta_1 = 0.0251 + 0.3222i$$
$$\beta_2 = -0.0251 + 0.3222i$$

CHAPTER 4

CURRENT DISTRIBUTION ON PRINTED STRUCTURES: COUPLED LINES

In this chapter, the current distributions on parallel coupled microstrip lines will be calculated using closed-form Green's function in the spatial domain in conjunction with Galerkin's Method of Moment. First, parallel coupled microstrip lines will be analyzed: the structure will be defined, the derivation of the necessary formulas will be achieved, the computer program to calculate the current distributions will be discussed and the results will be presented according to open circuited terminations of the microstrip lines. Then using the same technique, parallel coupled microstrip lines designed as directional couplers will be analyzed and their s-parameters will be evaluated.

4.1 Definition of the Structure and the Problem

Adapting the procedure described in chapter 3, the structure consisting of two parallel microstrip lines is analyzed in this section. The geometry of coupled microstrip lines is drawn in figure 31.

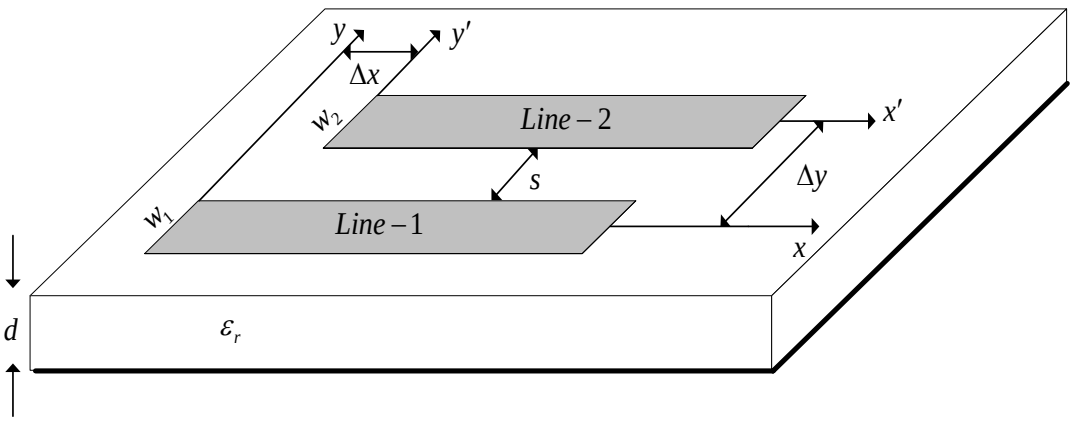

Figure 31 Geometry of Asymmetric Parallel Lines [18].

4.2 Derivation of Formulas

In this application, the current distributions are represented by a series of basis functions, expressing the distribution in two lines as:

$$J_x(x,y) = \sum_n I_{1n} J_{1xn}(x,y) + J_s(x,y) + \sum_n I_{2n} J_{2xn}(x,y) \qquad \text{(IV.1)}$$

where I_{1n} and I_{2n} are the unknown coefficients of the basis functions used on the active and passive lines, respectively and J_{1xn} and J_{2xn} are the basis functions of the active and passive lines, respectively. The expression given in (IV.1) is substituted in (III.1) and then the testing of the resulting equation is performed with testing functions J_{1xm} and J_{2xm}. Since $\overline{E}$ is zero on the lines:

$$\left\langle J_{1xm}, E_x \right\rangle = 0 \qquad \text{(IV.2.a)}$$

$$\left\langle J_{2xm}, E_x \right\rangle = 0 \qquad \text{(IV.2.b)}$$

The final equations of the coupled microstrip lines using (IV.2) are obtained as:

$$\begin{aligned} &\sum_n I_{1n} \left\{ \left\langle G_{xx}^A, J_{1xm} * J_{1xn} \right\rangle - \frac{1}{\omega^2} \left\langle G_q, \frac{d}{dx} J_{1xm} * \frac{d}{dx} J_{1xn} \right\rangle \right\} \\ &+ \sum_n I_{2n} \left\{ \left\langle G_{xx}^A, J_{1xm} * J_{2xn} \right\rangle - \frac{1}{\omega^2} \left\langle G_q, \frac{d}{dx} J_{1xm} * \frac{d}{dx} J_{2xn} \right\rangle \right\} = \\ &\quad - \left\langle G_{xx}^A, J_{1xm} * J_s \right\rangle + \frac{1}{\omega^2} \left\langle G_q, \frac{d}{dx} J_{1xm} * \frac{d}{dx} J_s \right\rangle \end{aligned} \qquad \text{(IV.3.a)}$$

$$\sum_n I_{1n}\left\{\left\langle G_{xx}^A, J_{2xm} * J_{1xn}\right\rangle - \frac{1}{\omega^2}\left\langle G_q, \frac{d}{dx}J_{2xm} * \frac{d}{dx}J_{1xn}\right\rangle\right\}$$
$$+\sum_n I_{2n}\left\{\left\langle G_{xx}^A, J_{2xm} * J_{2xn}\right\rangle - \frac{1}{\omega^2}\left\langle G_q, \frac{d}{dx}J_{2xm} * \frac{d}{dx}J_{2xn}\right\rangle\right\} = \qquad \text{(IV.3.b)}$$
$$-\left\langle G_{xx}^A, J_{2xm} * J_s\right\rangle + \frac{1}{\omega^2}\left\langle G_q, \frac{d}{dx}J_{2xm} * \frac{d}{dx}J_s\right\rangle$$

The details of the evaluation of the convolution integrals over testing and basis functions are given in appendix A.2.

4.3 Software Implementation

The current distribution of coupled microstrip lines can be determined by solving (IV.3.a) and (IV.3.b). To solve these equations for I_{1n}'s and I_{2n}'s, the MoM matrix is constructed. The number of basis functions determines the matrix size, which can be changed to any value during the calculations. Moreover, the source can be at any arbitrary point on the active microstrip line. The entries of the MoM matrix require double integration which can be numerically approximated using Gaussian Quadrature which performs double integration of a complex function of two variables. In this application, the MoM matrix is symmetric; hence it is enough to calculate one of the row or column entries of MoM matrix to determine the actual MoM matrix. When the matrix elements are found, the load equations can also be added to the solution and the unknown current coefficients can be calculated by taking the inverse of the MoM matrix. The effects of the loads are related to the other basis functions by applying the load equations. The detailed analysis of the load equations are given in appendix B.2. In the program, the length of the lines, l_1 and l_2, and the widths of the lines, w_1, w_2 and the distance between the lines, s are set as variables. According to the different values of these variables, the current distributions on active and passive lines are determined. The results are given in the next section.

4.4 Results

In this section, the studies are performed for the coupled microstrip lines with open circuited terminations. First, the effect of changing spacing s, between the lines, on the current distributions is analyzed. Figure 31 is used as a reference

in this chapter for the analysis. It is given below the parameters of the coupled lines for this application as:

$$f = 1\,GHz$$
$$\varepsilon_r = 4$$
$$d = 0.02032\,cm$$
$$w_1 = w_2 = 0.08128\,cm$$
$$l_1 = l_2 = 10\,cm$$
$$\Delta x = 0$$

Source is located 0.75 cm away from the left end of the line-1. The number of the basis functions used for this application is 40. The amplitude of the current distributions on line-1 and line-2 are plotted in figure 32 and figure 33, respectively, for different values of spacing s.

Next, the effect of changing width of passive line, w_2 on the current distributions is analyzed. The parameters of the coupled lines for this application are as:

$$f = 1\,GHz$$
$$\varepsilon_r = 4$$
$$d = 0.02032\,cm$$
$$w_1 = 0.08128\,cm$$
$$l_1 = l_2 = 10\,cm$$
$$s = 0.135\,cm$$
$$\Delta x = 0$$

Source is located 0.75 cm away from the left end of the line-1. The number of the basis functions used for this application is also 40. The amplitude of the current distributions on line-1 and line-2 are plotted in figure 34 and figure 35, respectively, for different values of w_2.

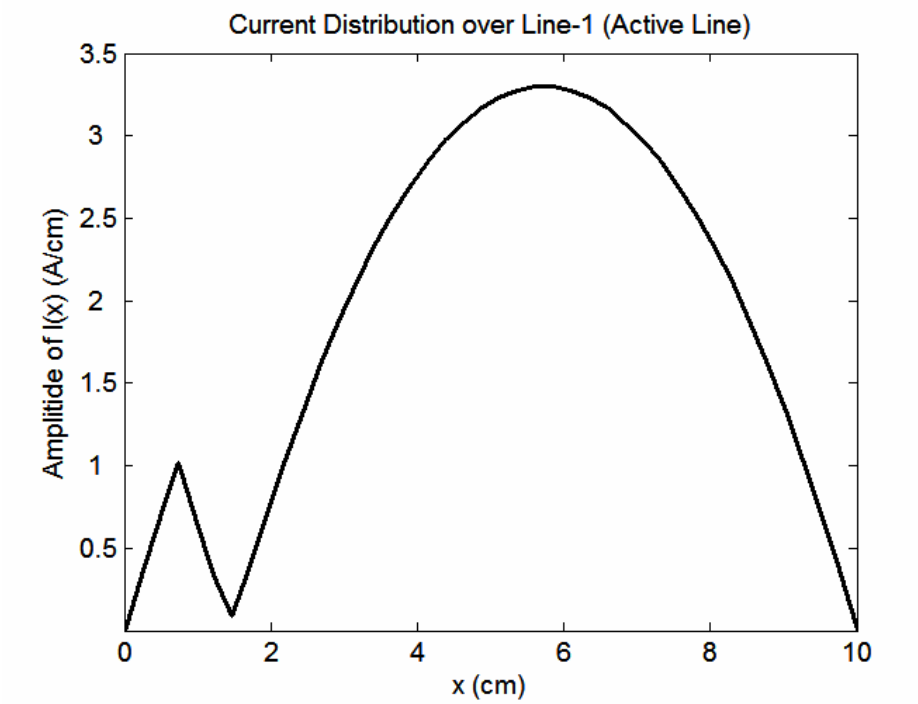

Figure 32 Amplitude of Current Distribution on Active Line, Excited at x=0.75 cm.

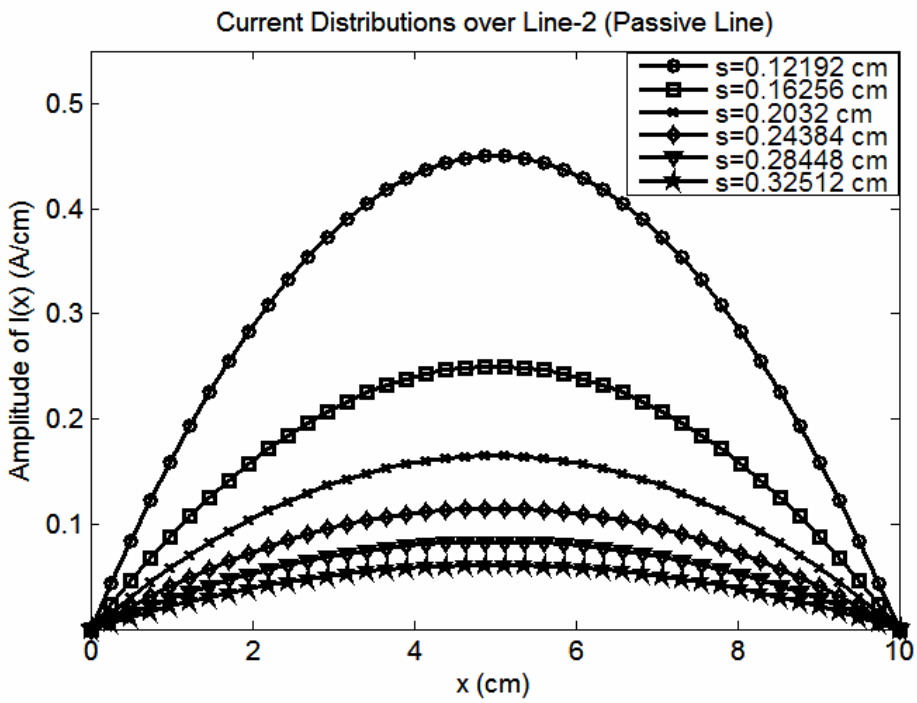

Figure 33 Amplitude of Current Distributions on Passive Line for Changing s.

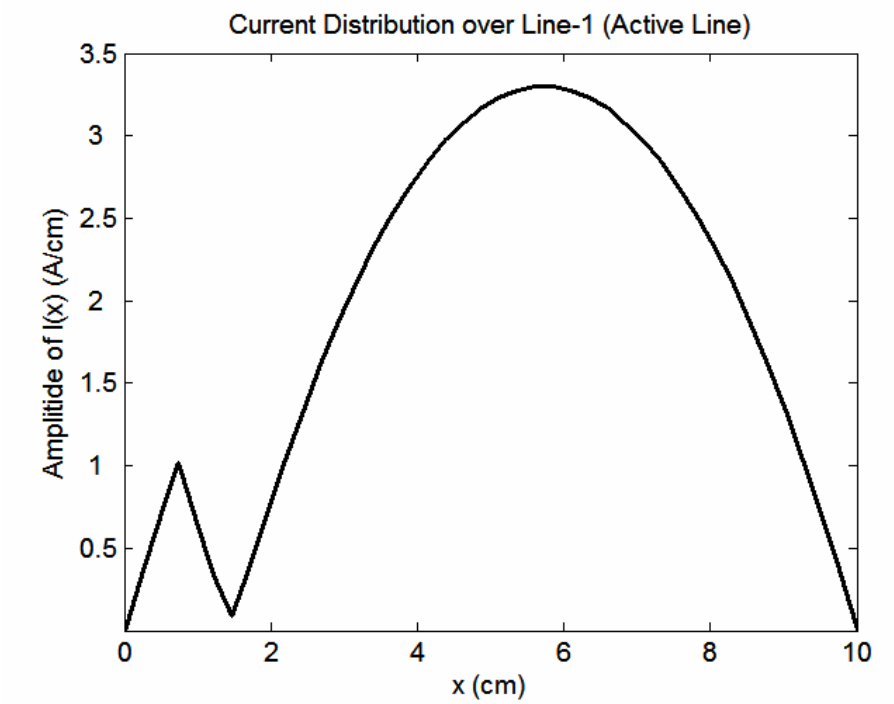

Figure 34 Amplitude of Current Distribution on Active Line, Excited at x=0.75 cm.

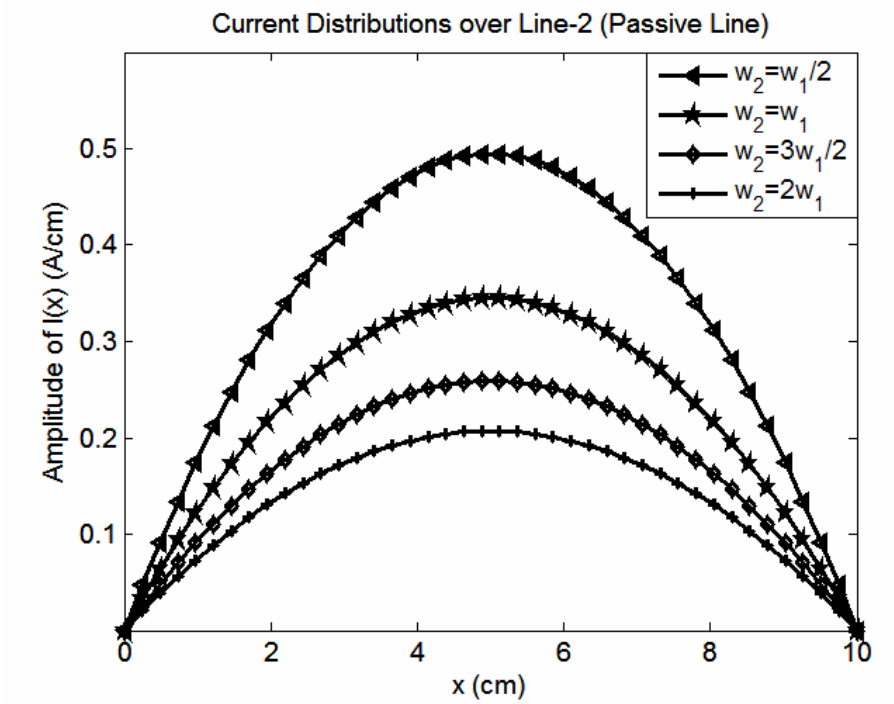

Figure 35 Amplitude of Current Distributions on Passive Line for Changing w_2.

Then, the effect of horizontal shift of line-2 compared to line-1, Δx, on the current distributions is analyzed. The parameters of the coupled lines for this application are as:

$$f = 1\,GHz$$
$$\varepsilon_r = 4$$
$$d = 0.02032\,cm$$
$$w_1 = w_2 = 0.08128\,cm$$
$$l_1 = l_2 = 10\,cm$$
$$s = 0.16256\,cm$$

Source is located 0.75 cm away from the left end of the line-1. The number of the basis functions used for this application is also 40. The amplitude of the current distributions on line-1 and line-2 are plotted in figure 36 and figure 37, respectively, for different values of Δx.

Next, current distributions on coupled microstrip lines whose lengths are close to resonant length, $\lambda/4$ are analyzed. To achieve this, two structures are examined. The parameters for the first one are given below. In this application, the effect of change of spacing, s is observed. Source is located 0.75 cm away from the left end of the line-1. The number of the basis functions used for this application is 40. The amplitude of the current distributions on line-1 and line-2 are plotted in figure 38 and figure 39, respectively, for different values of s.

$$f = 1\,GHz$$
$$\varepsilon_r = 4$$
$$d = 0.02032\,cm$$
$$w_1 = w_2 = 0.08128\,cm$$
$$l_1 = l_2 = 9\,cm$$
$$\Delta x = 0$$

The parameters for the second one are given below. In this application, the effect of horizontal shift of line-2 compared to line-1, Δx, on the current distributions is observed. Source is located 0.5 cm away from the left end of the line-1. The number of the basis functions used for this application is 40. The amplitude of the current distributions on line-1 and line-2 are plotted in figure 40 and figure 41, respectively, for different values of Δx.

$$f = 1\,GHz$$
$$\varepsilon_r = 4$$
$$d = 0.02032\ cm$$
$$w_1 = w_2 = 0.08128\ cm$$
$$l_1 = l_2 = 8\ cm$$
$$s = 0.08128\ cm$$

From the last two applications it is concluded that when the lengths of the lines are close to resonant length, the current distributions on the active line are maximized.

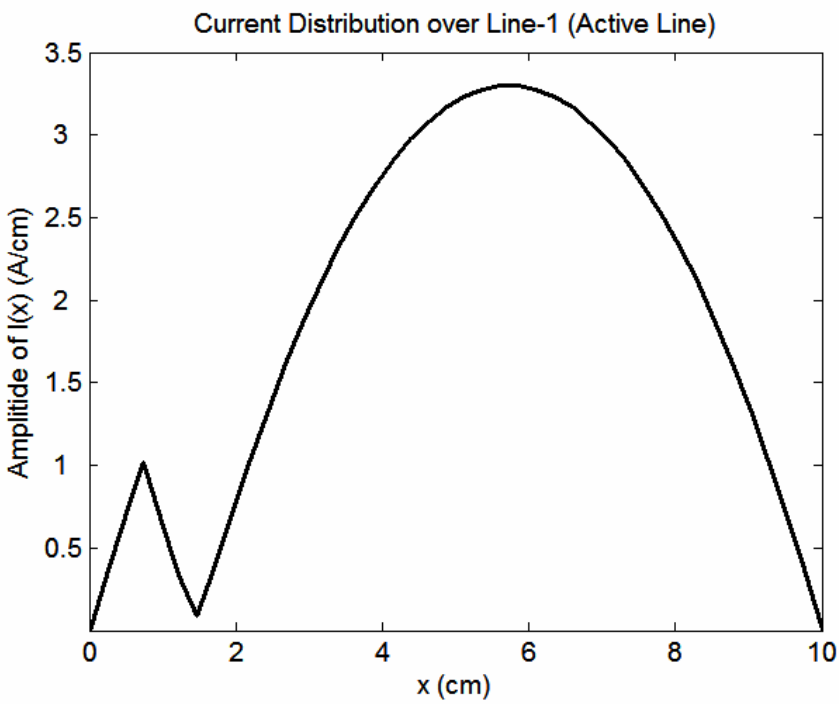

Figure 36 Amplitude of Current Distribution on Active Line, Excited at x=0.75 cm.

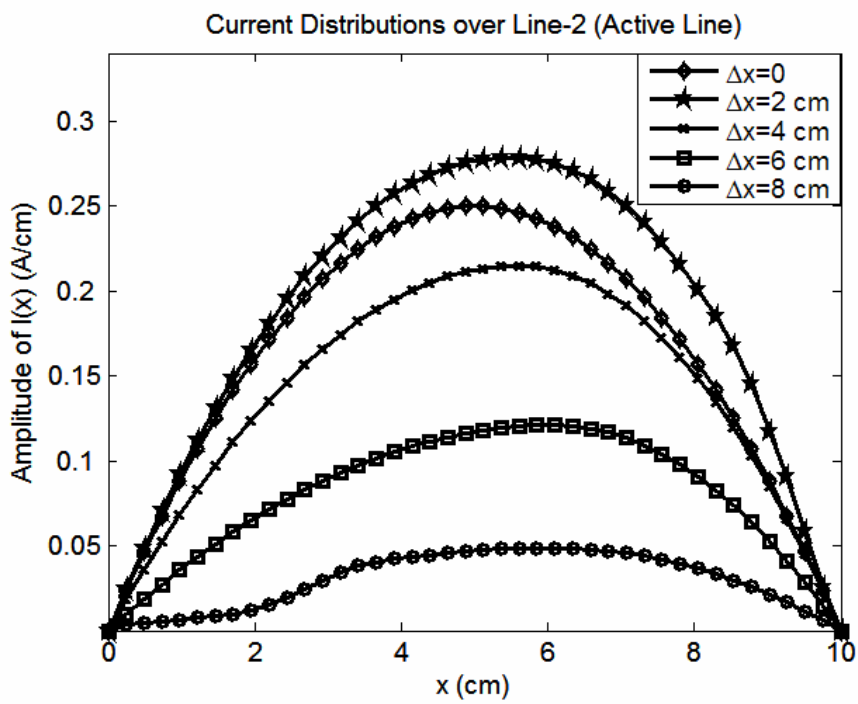

Figure 37 Amplitude of Current Distributions on Passive Line for Changing Δx.

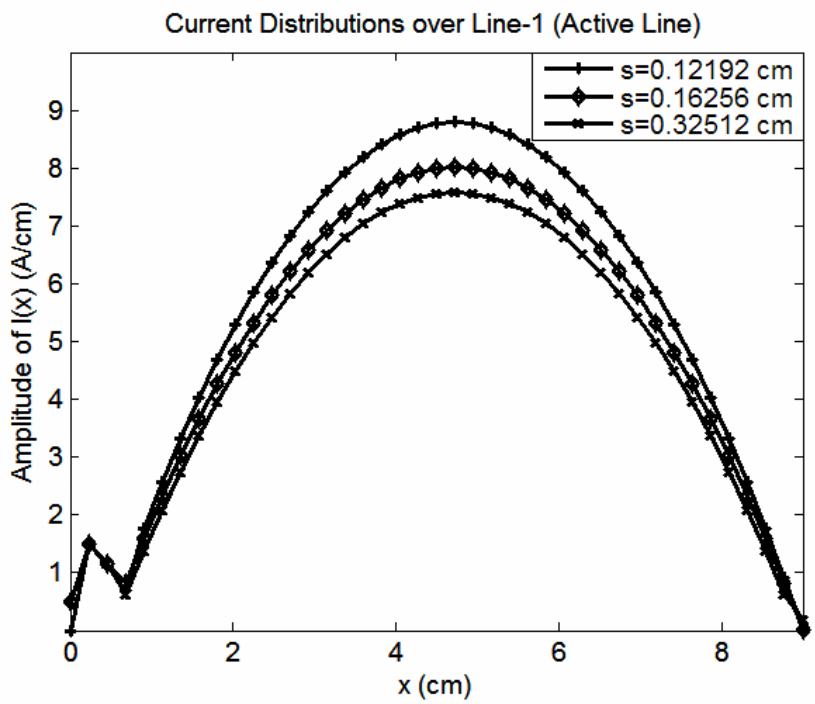

Figure 38 Amplitude of Current Distributions on Active Line, for Changing s.

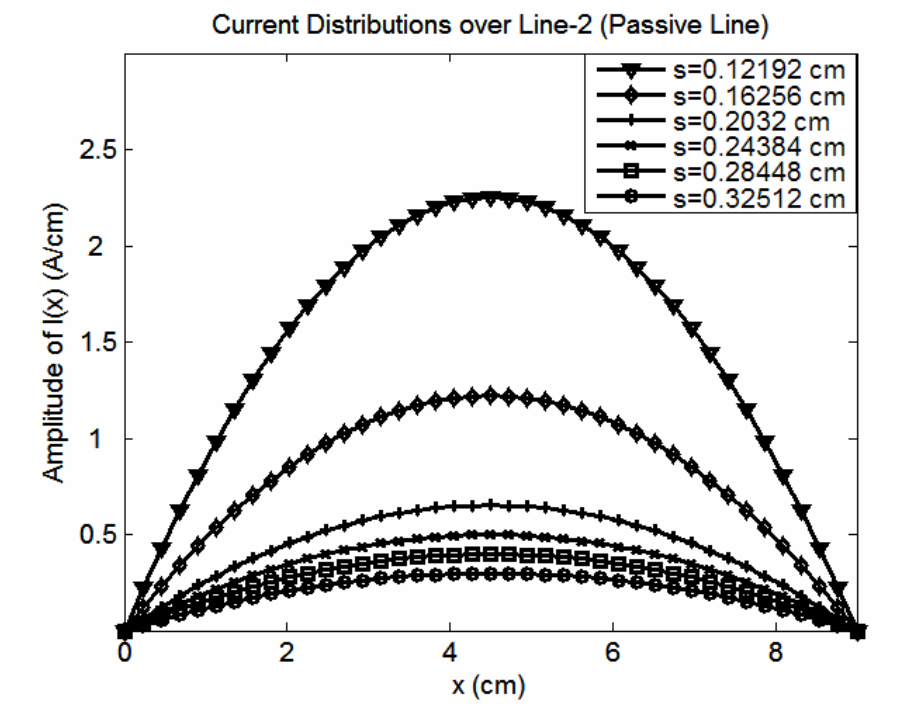

Figure 39 Amplitude of Current Distributions on Passive Line, for Changing s.

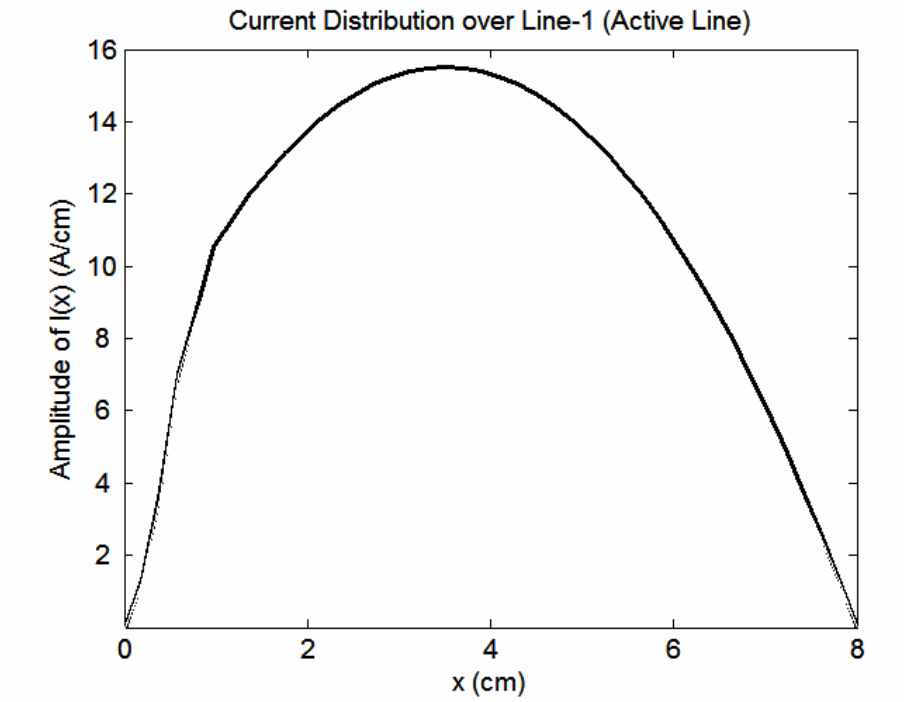

Figure 40 Amplitude of Current Distribution on Active Line, Excited at x=0.5 cm.

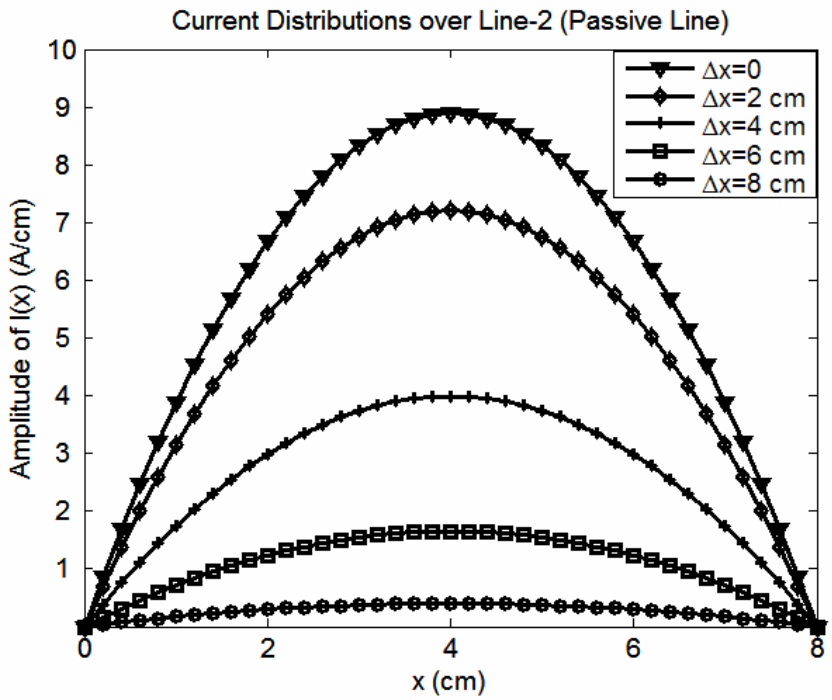

Figure 41 Amplitude of Current Distributions on Passive Line for Changing Δx .

4.5 Directional Coupler Application

In this section, the implementation of parallel coupled microstrip lines as directional couplers is described. Because it is possible to analyze the coupled parallel lines using MoM in conjunction with the closed form Green's functions, using the same procedure, the structures of parallel coupled lines are designed as directional couplers and the current distribution over the coupled lines are gathered. In this implementation, since the lines are terminated with matched loads, the load equations detailed in the appendix B.2 are used and the load terminations are related to the current distributions over the lines adopting the procedures described in chapter 3 for a single microstrip line structure analysis. Finally, the s-parameters of the directional couplers are found. The steps described here are carried out for 7dB, 10dB, 15dB and 20dB directional couplers.

Directional couplers are 4-port devices which can be constructed by two transmission lines passing close enough to each other for energy propagating on one line to couple to the other line. The power flow convention of the directional couplers examined in this study is set as below:

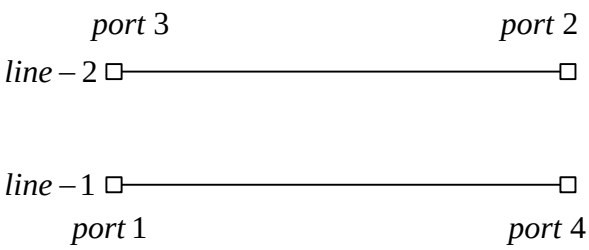

Figure 42 Power Flow Convention of the Directional Coupler.

where port 1 is the input port, the power supplied to port 1 is coupled to port 3 (the coupled port) and the remainder of the power is delivered to port 4 (the through port). Port 2 (the isolated port) delivers no power in ideal directional couplers [23]. Once the coupling coefficient of the directional couplers is defined, then it is possible to find the even and odd mode characteristic impedances of the directional couplers. Using the even and odd mode characteristics of the directional couplers, one can design the physical structure of the couplers. To do this, a software program is used in this study. This software tool is TXLINE 2003™. As an example, the design of 10dB directional coupler is achieved below as:

Coupling factor in dB is 10, hence coupling factor k is 0.31623. The characteristic impedance of each line, Z_o, is $50\ \Omega$. Using the below equations the even and odd mode characteristic impedances are found. Z_{oe} is $69.4762\ \Omega$ and Z_{oo} is $36.0186\ \Omega$.

$$Z_{oe} = Z_o \frac{\sqrt{1+k}}{\sqrt{1-k}} \qquad \text{(IV.4.a)}$$

$$Z_{oo} = Z_o \frac{\sqrt{1-k}}{\sqrt{1+k}} \qquad \text{(IV.4.b)}$$

The parameters of the physical structure of the directional couplers obtained using the software program TXLINE 2003™ are given as below:

$$f = 1\,GHz$$
$$\varepsilon_r = 4$$
$$d = 0.2032\ cm$$
$$w_1 = w_2 = 0.337\ cm$$
$$s = 0.0345\ cm$$
$$l_1 = l_2 = 4.35\ cm$$
$$\Delta x = 0$$
$$t = 1e-7\ cm$$

In appendix E, the notation information about the directional couplers and the physical structure information of the directional couplers are given in detail.

Once the physical structures of the directional couplers are determined, then it is possible to evaluate the current distributions over the microstrip lines. The number of the basis functions is chosen as 25 in this implementation. The active line is excited by the source at 0.174 cm from the left end of the line. Since both of the lines have matched load terminations at the end of each line Z_l is $50\,\Omega$. To analyze the effects of the load terminations, one should obtain the Maxwellian inductance and capacitance values for coupled line case. Using a software program, "RLGC - 2D Quasi-static Modeling Tool™", created by K. S. Oh, L_{ij}'s and C_{ij}'s per unit length of the coupled lines are found. In appendix E, for each directional coupler structure, those values are given. The resultant plots of the current distributions over the lines are demonstrated below as:

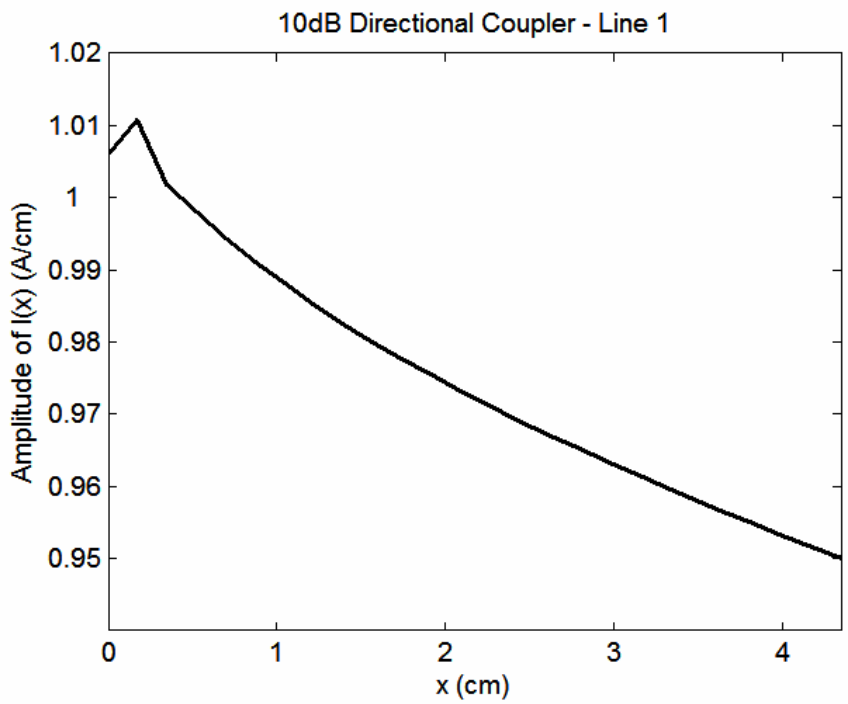

Figure 43 Amplitude of Current Distribution for 10dB Directional Coupler.

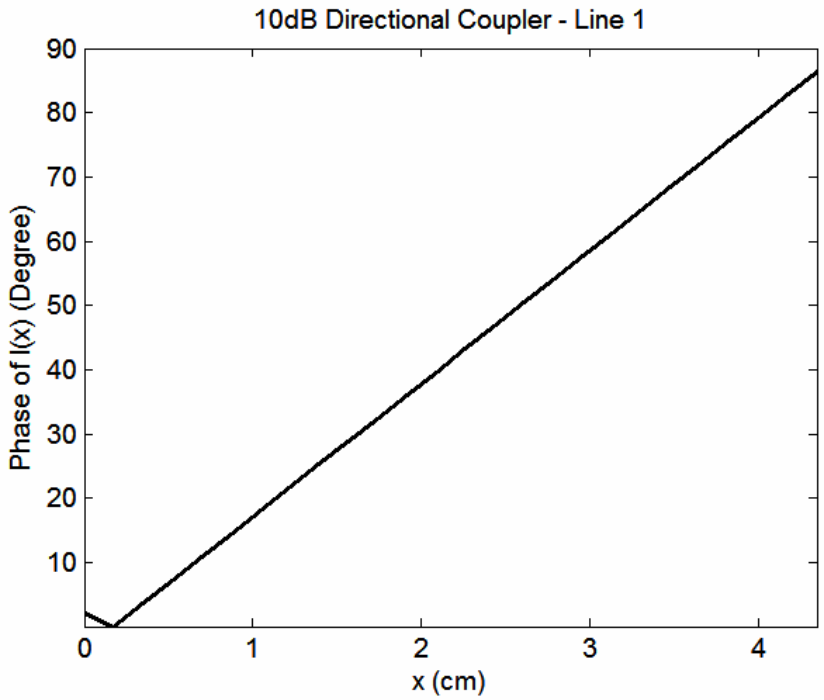

Figure 44 Phase of Current Distribution for 10dB Directional Coupler.

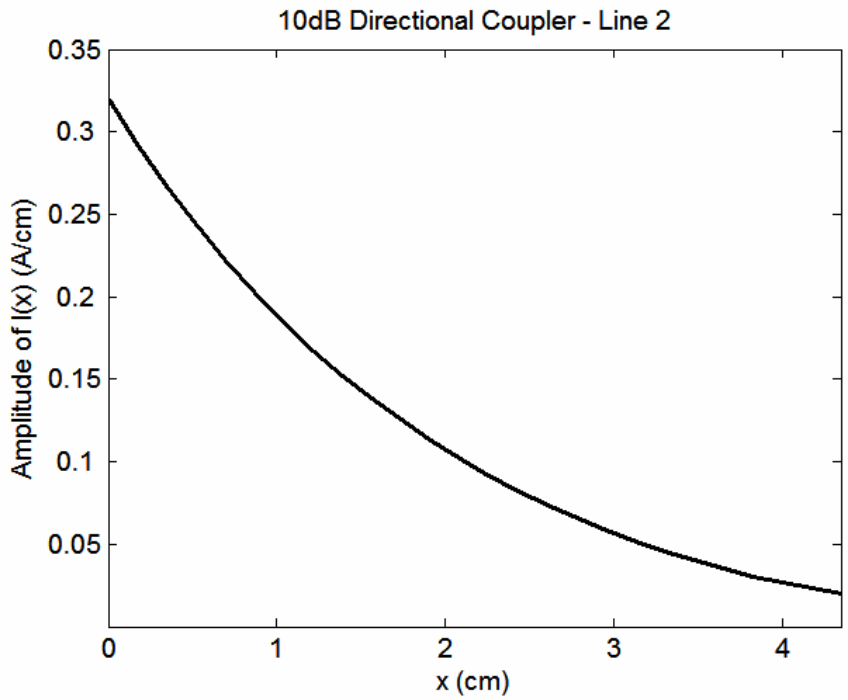

Figure 45 Amplitude of Current Distribution for 10dB Directional Coupler.

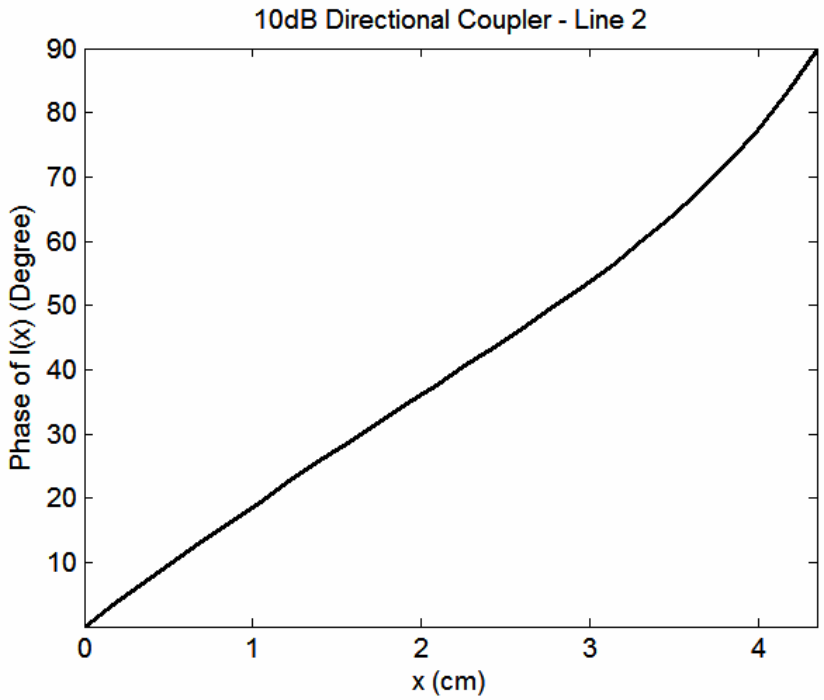

Figure 46 Phase of Current Distribution for 10dB Directional Coupler.

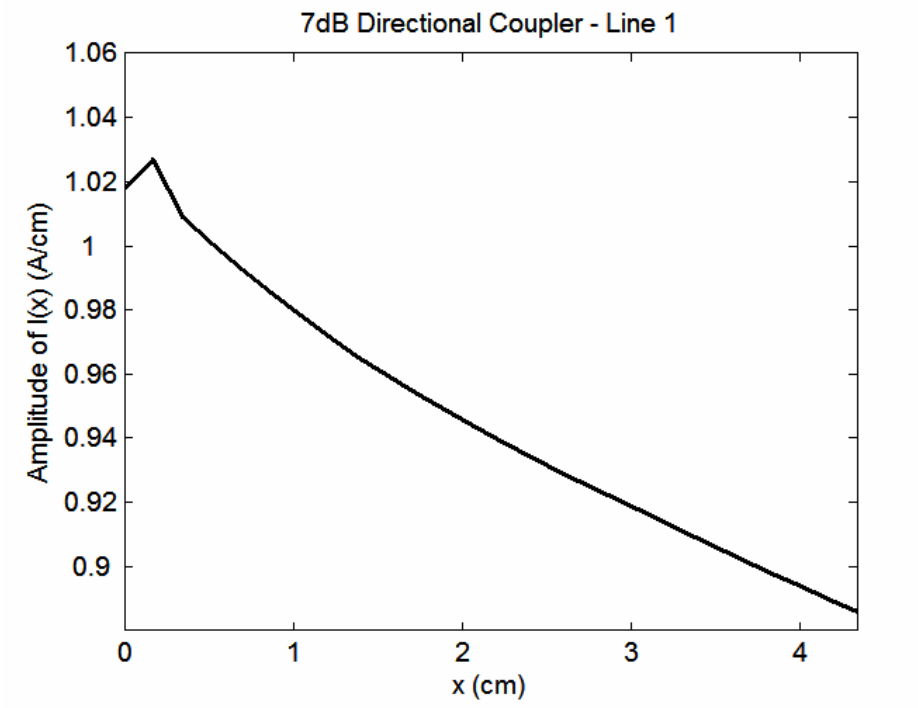

Figure 47 Amplitude of Current Distribution for 7dB Directional Coupler.

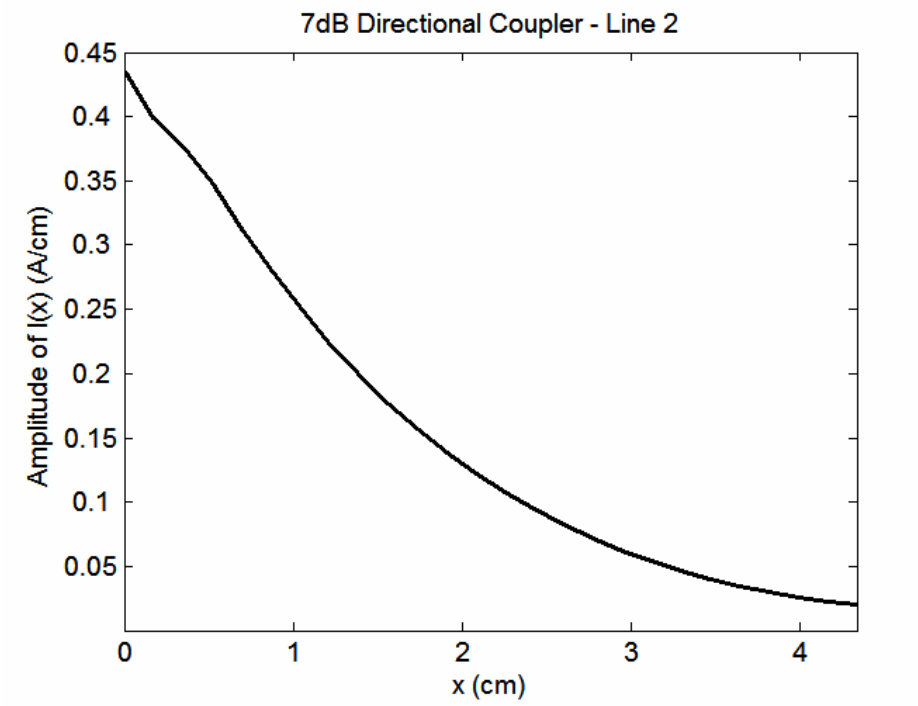

Figure 48 Amplitude of Current Distribution for 7dB Directional Coupler.

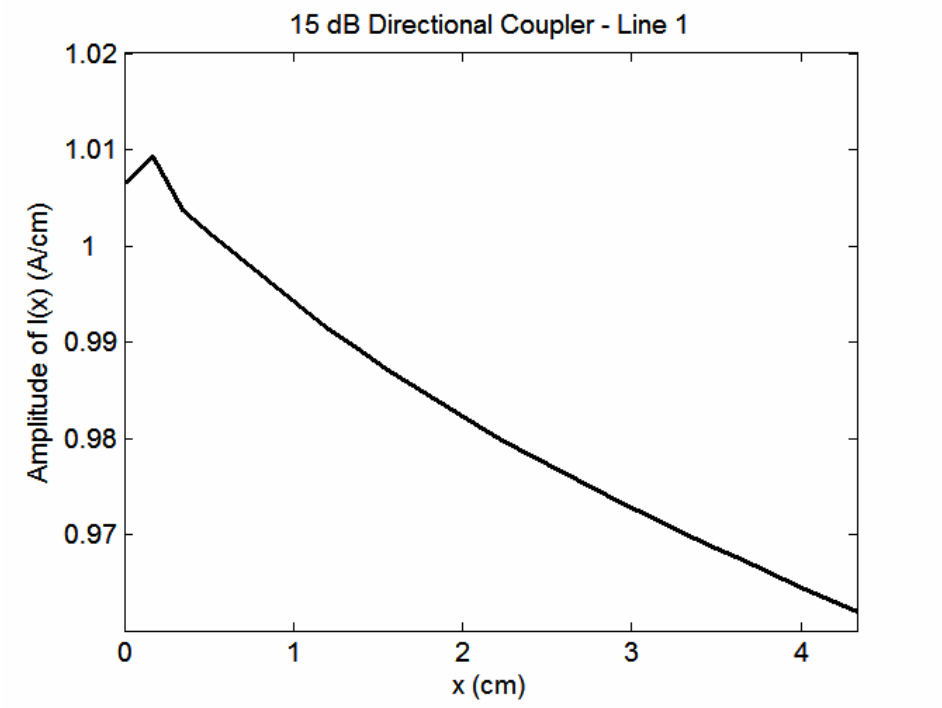

Figure 49 Amplitude of Current Distribution for 15dB Directional Coupler.

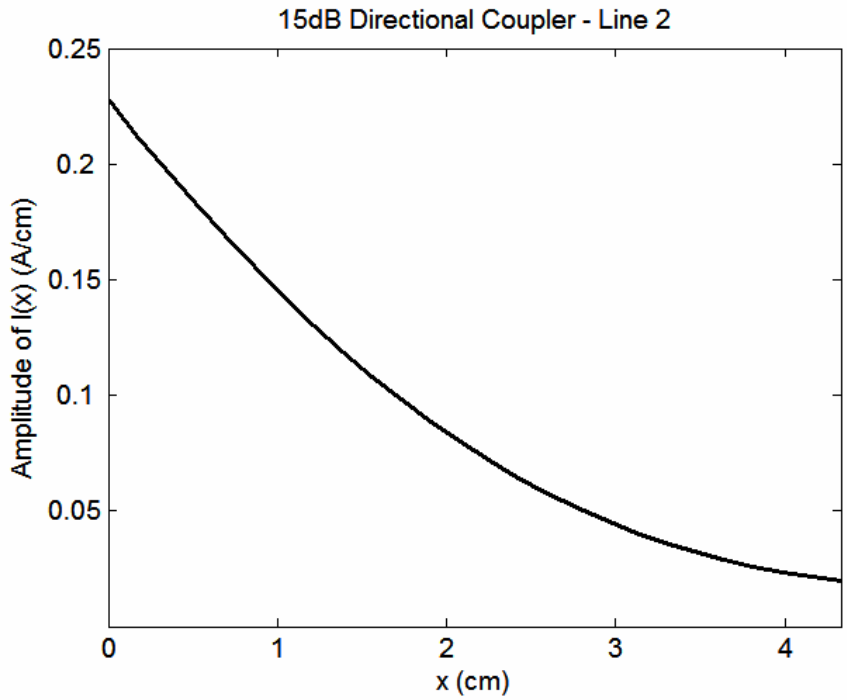

Figure 50 Amplitude of Current Distribution for 15dB Directional Coupler.

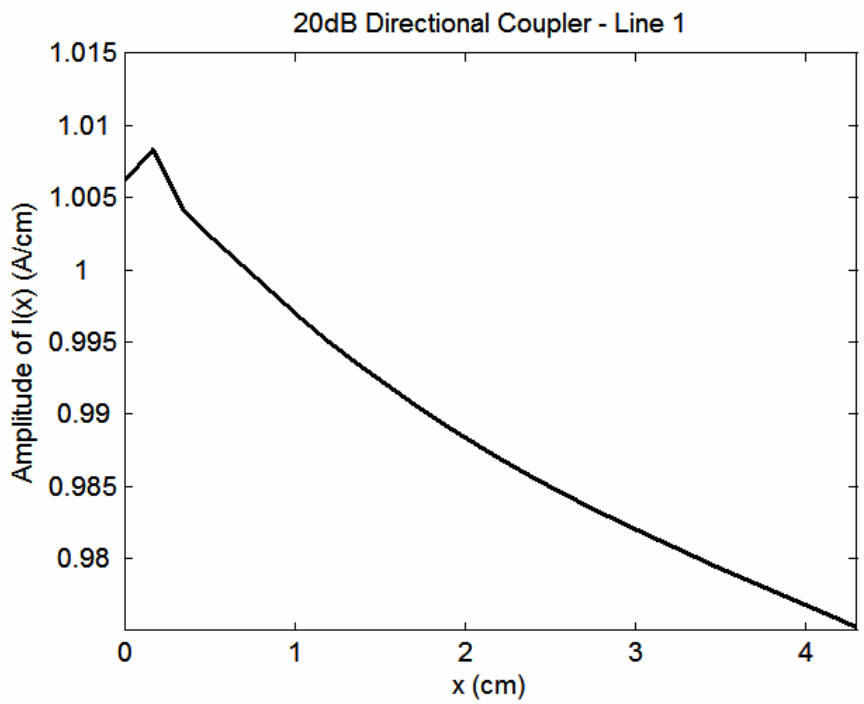

Figure 51 Amplitude of Current Distribution for 20dB Directional Coupler.

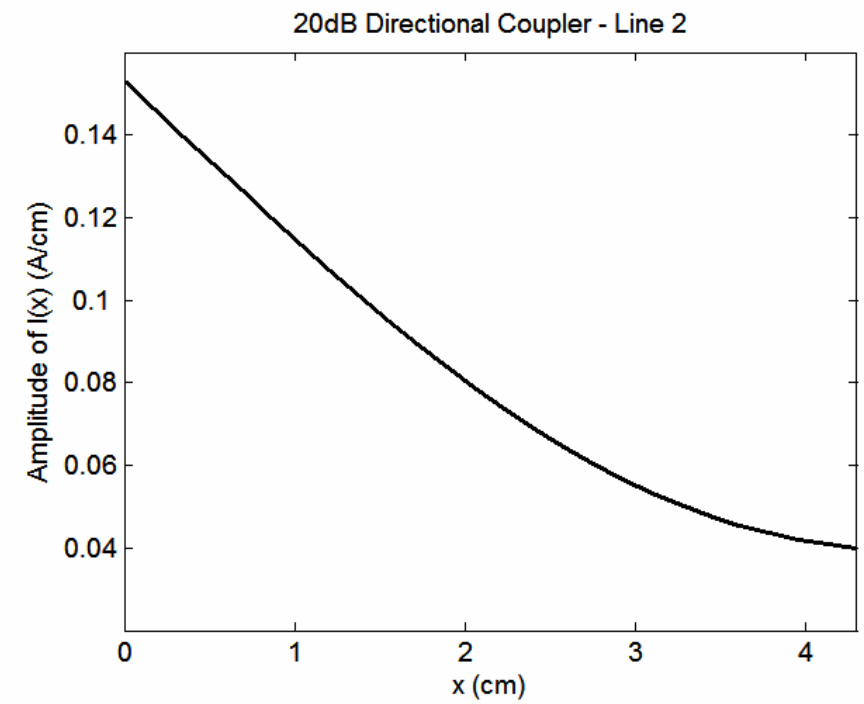

Figure 52 Amplitude of Current Distribution for 20dB Directional Coupler.

Once the current distributions over the lines are obtained, using Prony's method, it is possible to evaluate the incident and reflected wave coefficients and it is also possible to find the s-parameters. Using software programs CNL/2™ and Agilent Advanced Design System - ADS™, s-parameters analysis can also be gathered.

In this study, the s-parameters found by MoM in conjunction with closed-form Green's functions and s-parameters obtained by the software programs CNL/2™ and Agilent Advanced Design System - ADS™ are given in table 1 for the same directional coupler structures. The software program CNL/2™ finds the s-parameters using the network analysis approach for specific parallel line structures. However, the module Momentum of the software program Agilent Advanced Design System - ADS™ finds the s-parameters using MoM with 10GHz meshing. From the analyses, it is observed that the resultant s-parameters for defined structures obtained by the software programs and by this study are in good agreement although their solution methods are different.

s_{31} can be found using the formula below:

$$s_{31} = 20\log\left|\frac{I_3}{I_1}\right| \qquad \text{(IV.5)}$$

where the current flow of directional coupler is shown in figure 53.

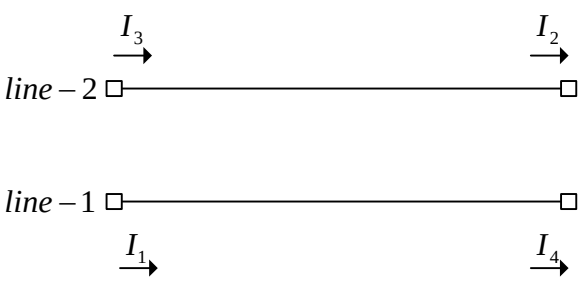

Figure 53 Current Flow over Directional Coupler.

Table 1 Comparison of S-parameters.

S-parameters of Directional Couplers (DC)	MoM, dB	CNL/2™, dB	ADS™, dB
s_{11} $(7dB)$	-31.1053	-29.62292	-29.069
s_{21} $(7dB)$	-25.2298	-24.14181	-23.530
s_{31} $(7dB)$	-7.50474	-6.97333	-7.522
s_{41} $(7dB)$	-1.04562	-1.00015	-0.876
s_{11} $(10dB)$	-31.0696	-32.65494	-29.877
s_{21} $(10dB)$	-23.1108	-23.13111	-22.765
s_{31} $(10dB)$	-10.3157	-10.04294	-10.304
s_{41} $(10dB)$	-0.45813	-0.47896	-0.455
s_{11} $(15dB)$	-39.8033	-38.21268	-31.529
s_{21} $(15dB)$	-25.2031	-23.43110	-23.075
s_{31} $(15dB)$	-15.2329	-15.10056	-15.173
s_{41} $(15dB)$	-0.32871	-0.15737	-0.159
s_{11} $(20dB)$	-40.6679	-44.71387	-33.338
s_{21} $(20dB)$	-27.3925	-24.81367	-24.526
s_{31} $(20dB)$	-20.8734	-19.97616	-19.965
s_{41} $(20dB)$	-0.20891	-0.05854	-0.062

CHAPTER 5

CONCLUSIONS

In this study, using spatial domain closed form Green's functions in conjunction with MoM, the analysis of single microstrip lines and coupled microstrip lines are achieved. As an application, different directional coupler structures whose physical parameters are determined by using a software program, TXLINE 2003™, examined. The results of the analysis described in this study are evaluated using a software program.

The current distributions over single microstrip lines with different load terminations are obtained and the results are plotted to show the change of the amplitude and the phase of the current distribution along the line with changing load terminations. The incident and reflected wave coefficients of the structures are also determined.

The current distributions over open circuited parallel coupled microstrip lines are obtained and the results are plotted to show the change of the amplitude of the current distribution along the line. The effects of the spacing between the lines, the lengths of the lines, the widths of the lines and the horizontal shift are also presented. As the lengths of the lines are chosen as be close to resonant lengths, current distributions on active lines are maximized.

The current distributions over different structured directional couplers are obtained and the results are plotted to show the change of the amplitude and the phase of the current distribution along the line. In this part of the analysis, to relate the load equations to the other basis functions, Maxwellian inductance and capacitance values are obtained by using a software program RLGC - 2D Quasi-static Modeling Tool™. The s-parameters of the directional couplers are determined and compared with the ones gathered by using simulation programs, CNL/2™ and Agilent Advanced Design System - ADS™.

The technique described in this study is a computationally efficient technique. First, the use of the closed-form Green's functions in the analysis of microstrip geometry by MoM improves the computational efficiency significantly. The conventional spatial domain Green's functions and spectral domain Green' functions include slowly convergent integrals.

Next, in the analysis, the Galerkin's Method of Moments is used in which the basis and testing functions are chosen to be same. Using same testing and basis functions results in a symmetric matrix. Then, it is enough to proceed to the analysis by determining only one of the rows or only one of the columns of the matrix. This also helps to reduce the computation time.

Finally, the use of rooftop functions as basis and testing function is very advantageous. Each final equation is an inner product term which is a 4-dimensional integral. Two of the integrals are from the definition of the inner product and two of them are from the closed-form Green's functions. Choosing the basis functions as rooftops, the two of the integrals which are called as convolution integral over testing and basis functions can be carried out analytically. Then the final equation becomes a 2-dimensional integral equation.

Since printed circuit board technology have found widespread areas of applications such as microstrip line-based filters, impedance transformers, hybrids, couplers, power dividers/combiners, delay lines, etc. and antennas, using spatial domain closed form Green's functions in conjunction with MoM, different types of microstrip line structures can also be achieved. Using software programs as developed in this study, before manufacturing the structures their parameters such as current distributions, input impedances etc. can be found easily. New structures can also be analyzed for specific parameters using software programs and then can be manufactured for the use of human beings.

REFERENCES

[1] R. F. Harrington, “Matrix methods for Field Problems,” *Proc. IEEE*, vol. 55, pp. 136-49, Feb. 1967.

[2] R. F. Harrington, *Field Computation by Moment Methods*, New York: MacMillan; Toronto, Ontario; Collier-MacMillan Publishing, 1968.

[3] N. K. Saydam, “Analysis of Microstrip Lines Using Closed-form Green’s Functions,” M. Sc. Thesis, Middle East Technical University, Ankara, Turkey, 1996.

[4] W. C. Chew, *Waves and Fields in Inhomogeneous Media*, New York: IEEE Press, 1995.

[5] M. I. Aksun and R. Mittra, “Derivation of Closed-form Green’s Functions for a General Microstrip Geometry,” *IEEE Trans. Microwave Theory Tech*., vol. 40, pp. 2055-2062, Nov. 1992.

[6] F. Arslan, “Analysis of Slot Geometries Using Closed-form Green’s Functions,” M. Sc. Thesis, Middle East Technical University, Ankara, Turkey, 1997.

[7] L. A. Hayırlıoğlu, “Use of Computationally Efficient MoM in the Analysis and Design of Printed Structures,” Ph.D. Thesis, Middle East Technical University, Ankara, Turkey, 1997.

[8] S. L. Sobolev, *Partial Differential Equations of Mathematical Physics*, New York: Pergamon Press, 1964.

[9] M. I. Aksun and R. Mittra, “Choices of Expansion and Testing Functions for The Method of Moments Applied to A Class of Electromagnetic Problems,” *IEEE Trans. Microwave Theory Tech*., vol. MTT-41, pp. 503-509, March, 1993.

[10] T. Utoh. “Spectral Domain Immitance Approach for Dispersion Characteristics of Generalized Printed Transmission Lines,” *IEEE Trans. Microwave Theory Tech.,* vol. MTT-28, pp. 733-736, July 1980.

[11] A. Sommerfeld, *Partial Differential Equations in Physics*, New York: Academic, 1949.

[12] Y. L. Chow, J. J. Yang, and D. F. Fang, and G. E. Howard, "Closed-Form Spatial Green's Function for the Thick Substrate," *IEEE Trans. Microwave Theory Tech.,* vol. 39, pp. 588-592, Mar. 1991.

[13] M. I. Aksun and R. Mittra, "Derivation of Closed-form Green's Functions for A General Microstrip Geometry," *IEEE Trans. Microwave Theory Tech.,* vol. 40, pp. 2055-2062, Nov. 1992.

[14] G. Dural and M. I. Aksun, "Closed-form Green's Functions for General Sources and Stratified Media," *IEEE Trans. Microwave Theory Tech.*, vol. 43, no. 7, pp. 1545–1552, Jul. 1995.

[15] Y. Hua and T. K. Sarkar, "Generalized Pencil-of-function Method for Extracting Poles of An EM System from Its Transient Response," *IEEE Trans. Antennas Propag.*, vol. AP-37, no. 2, pp. 229–234, Feb. 1989.

[16] M. I. Aksun, "A Robust Approach for the Derivation of Closed-form Green's Functions," *IEEE Trans. Microwave Theory Tech.*, vol. 44, no. 5, pp. 651–658, May. 1996.

[17] M. I. Aksun and G. Dural, "Clarification of Issues on the Closed-form Green's Functions in Stratified Media," *IEEE Trans. Antennas Propagation,* Vol. AP-53, 3644–3653, Nov. 2005.

[18] M. I. Aksun and R. Mittra, "Spurious Radiation from Microstrip Interconnects," *IEEE Trans. Electromagnetic Compatibility,* vol. 35, pp. 148-158, May, 1993.

[19] K. S. Oh, J. E. Schutt-Aine and R. Mittra, "Conductance and Resistance Matrices of Multiconductor Transmission Lines in a Multilayer Dielectric Medium," University of Illinois at Urbana-Champaign.

[20] R. E. Collin, *Foundations for Microwave Engineering*, McGraw-Hill, 1992.

[21] S. L. Marple, Jr., *Digital Spectral Analysis with Applications*, Prentice Hall, New Jersey, 1987.

[22] K. S. Oh, D. B. Kuznetsov and J. E. Schutt-Aine, "Capacitance Computations in Multilayered Dielectric Medium Using the Closed-form Spatial

Green's Functions," *IEEE Trans. Microwave Theory Tech.,* vol. MTT-42, pp. 1443-1453, August, 1994.

[23] D. M. Pozar, *Microwave Engineering*, Prentice Hall, John Wiley and Sons, Inc., 2005.

APPENDIX A

EVALUATION OF THE CONVOLUTION INTEGRALS OVER BASIS AND TESTING FUNCTIONS

The final integration formulas for the analysis of microstrip lines with MoM in conjunction with closed-form Green's functions are briefly given in chapter 3 and in chapter 4. These formulas consist of inner products of Green's functions and convolution of current distributions or inner products of Green's functions and convolution of derivatives of current distributions. The inner product terms are four-dimensional integral equations. However, the convolution of current distributions and convolution of derivatives of current distributions can be performed analytically. Then, the analytic solutions of the convolution integrals can be substituted into the inner product terms which results in double integral equations. This procedure simplifies the evaluation of inner product terms.

As mentioned before, current distribution over microstrip lines is represented by using basis functions and load basis functions. Likewise, the source over the microstrip line is represented by using source basis function. In this study, basis and testing functions are chosen to be rooftop functions. Hence, the convolution integrals over basis functions and shifted testing functions can be listed as below:

1.) Basis function with shifted testing function,

2.) Load basis function with shifted testing function,

3.) Source basis function with shifted testing function.

Similarly, the convolution integrals over the derivatives of the basis functions and the derivatives of the shifted testing functions can be listed as below:

4.) Derivative of basis function with derivative of shifted testing function,

5.) Derivative of load basis function with derivative of shifted testing function,

6.) Derivative of source basis function with derivative of shifted testing function.

In this appendix, the evaluation of convolution integrals for a single microstrip line and coupled microstrip lines are studied in two different subsections:

A.1 Evaluation of Convolution Integrals for a Single Microstrip Line

Basis Function:

$$J_{xn}(x,y)=\begin{cases}\dfrac{1}{wh_x}[(1-n)h_x+x] & (n-1)h_x\le x\le nh_x \quad , \quad |y|\le\dfrac{w}{2}\\ \dfrac{1}{wh_x}[(1+n)h_x-x] & nh_x\le x\le (n+1)h_x \quad , \quad |y|\le\dfrac{w}{2}\\ 0 & elsewhere\end{cases} \tag{A.1.1}$$

Shifted Testing Function:

$$J_{1xm}(x-u,y-v)=\begin{cases}\dfrac{1}{wh_x}[(1-m)h_x+x-u] & (m-1)h_x+u\le x\le mh_x+u\,,\ |y-v|\le\dfrac{w}{2}\\ \dfrac{1}{wh_x}[(1+m)h_x-x+u] & mh_x+u\le x\le (m+1)h_x+u\,,\ |y-v|\le\dfrac{w}{2}\\ 0 & elsewhere\end{cases} \tag{A.1.2}$$

Source Basis Function:

$$J_s(x,y)=\begin{cases}\dfrac{1}{wh_x}[(a-1)h_x-x] & (a-1)h_x\le x\le ah_x \quad , \quad |y|\le\dfrac{w}{2}\\ \dfrac{1}{wh_x}[(a+1)h_x-x] & ah_x\le x\le (a+1)h_x \quad , \quad |y|\le\dfrac{w}{2}\\ 0 & elsewhere\end{cases} \tag{A.1.3}$$

Load Basis Function:

$$J_{lL}(x,y)=\begin{cases}-\dfrac{1}{wh_x}[x-h_x] & 0\le x\le h_x \quad , \quad |y|\le \dfrac{w}{2}\\ 0 & elsewhere\end{cases} \tag{A.1.4.a}$$

$$J_{lR}(x,y)=\begin{cases}\dfrac{1}{wh_x}[x-Nh_x] & Nh_x\le x\le (N+1)h_x \quad , \quad |y|\le \dfrac{w}{2}\\ 0 & elsewhere\end{cases} \tag{A.1.4.b}$$

Derivative of Basis Function:

$$\frac{d}{dx}J_{xn}(x,y)=\begin{cases}\dfrac{1}{wh_x} & (n-1)h_x\le x\le nh_x \quad , \quad |y|\le \dfrac{w}{2}\\ -\dfrac{1}{wh_x} & nh_x\le x\le (n+1)h_x \quad , \quad |y|\le \dfrac{w}{2}\\ 0 & elsewhere\end{cases} \tag{A.1.5}$$

Derivative of Shifted Testing Function:

$$\frac{d}{dx}J_{xm}(x-u,y-v)=\begin{cases}\dfrac{1}{wh_x} & (m-1)h_x+u\le x\le mh_x+u\,,|y-v|\le \dfrac{w}{2}\\ -\dfrac{1}{wh_x} & mh_x+u\le x\le (m+1)h_x+u\,,|y-v|\le \dfrac{w}{2}\\ 0 & elsewhere\end{cases}$$

(A.1.6)

Derivative of Source Basis Function:

$$\frac{d}{dx}J_s(x,y)=\begin{cases}-\dfrac{1}{wh_x} & (a-1)h_x\le x\le ah_x \quad , \quad |y|\le \dfrac{w}{2}\\ -\dfrac{1}{wh_x} & ah_x\le x\le (a+1)h_x \quad , \quad |y|\le \dfrac{w}{2}\\ 0 & elsewhere\end{cases} \tag{A.1.7}$$

Derivative of Load Basis Function:

$$\frac{d}{dx}J_{lL}(x,y)=\begin{cases}-\dfrac{1}{wh_x} & 0\le x\le h_x \quad , \quad |y|\le \dfrac{w}{2}\\ 0 & elsewhere\end{cases} \tag{A.1.8.a}$$

$$\frac{d}{dx}J_{lR}(x,y)=\begin{cases}\dfrac{1}{wh_x} & Nh_x\le x\le (N+1)h_x\,,|y|\le \dfrac{w}{2}\\ 0 & elsewhere\end{cases} \tag{A.1.8.b}$$

Using these representations of basis functions, the convolution integrals can be calculated analytically. To show the details of the calculation, the convolution over load basis functions and testing functions are given in detail; other required convolution integrals are detailed in [3].

A.1.1 Convolution over Left Load Basis Functions and Shifted Testing Functions

(A.1.9.a) describes the convolution integral for the left side load basis function and shifted testing functions whereas (A.1.9.b) describes the convolution integral for the right side load basis function and shifted testing functions:

$$\int_{x_1}^{x_2}dx\int_{y_1}^{y_2}dyJ_{lL}(x.y)J_{xm}(x-u,y-v) \tag{A.1.9.a}$$

$$\int_{x_1}^{x_2}dx\int_{y_1}^{y_2}dyJ_{lR}(x.y)J_{xm}(x-u,y-v) \tag{A.1.9.b}$$

These integral equations are solved in two regions as the load basis functions and testing functions are piecewise differentiable. Below, the integral equations for each region are detailed. First, the notations simplifying the calculations are introduced.

$LELL=0$ ($LELL$: Left End of Left Load Basis Function),

$RELL=h_x$ ($RELL$: Right End of Left Load Basis Function),

$LERL=Nh_x$ ($LERL$: Left End of Right Load Basis Function),

$RERL=(N+1)h_x$ ($RERL$: Right End of Right Load Basis Function),

$LEST = (m-2)h_x + u$ ($LEST$: Left End of Shifted Testing Function),

$CST = (m-1)h_x + u$ (CST: Center of Shifted Testing Function),

$REST = mh_x + u$ ($REST$: Right End of Shifted Testing Function),

STF is used for shifted testing function and LBF is used for load basis function. N is the number of basis functions, with load basis functions, the total basis functions become $N+2$.

The number of shifted testing functions is also N, where $m = 2,3,...,N+1$.

Case 1: $(REST \geq LELL) \wedge (REST < RELL)$

The scheme for the case 1 is shown in the figure 54.

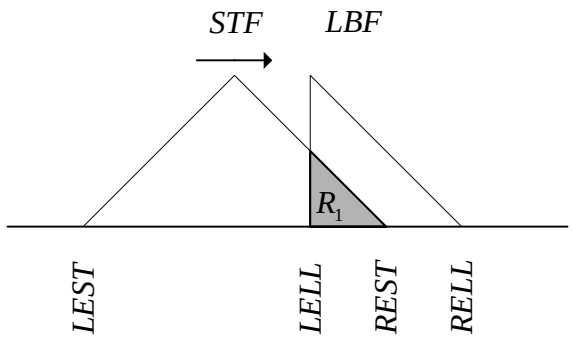

Figure 54 Convolution over Left Load Basis Function and Shifted Testing Function, Region 1.

Using the representations of the left load basis function and the shifted testing function, the convolution integral given in (A.1.9.a) can be rewritten for region 1 as below:

$$\int_{x_1}^{x_2} dx \int_{y_1}^{y_2} dy J_{IL}(x.y) J_{xm}(x-u, y-v) = -w \int_{x_1}^{x_2} \left(\frac{1}{wh_x} \right)^2 [(1+m)h_x - x + u][x - h_x] dx$$

(A.1.10)

Once the integration is performed then the result is gathered as below:

$$\int_{x_1}^{x_2} dx \int_{y_1}^{y_2} dy J_{IL}(x.y) J_{xm}(x-u, y-v) =$$

$$-\frac{1}{wh_x^2}\left[-\frac{x_2^3 - x_1^3}{2} + \frac{x_2^2 - x_1^2}{2}((2+m)h_x + u) - (x_2 - x_1)((1+m)h_x^2 + uh_x)\right]$$

(A.1.11)

For case 1, (A.1.11) is used to find the result of convolution integral.

Case 2: $(CST \geq LELL) \wedge (CST < RELL)$

The scheme for case 2 is shown in the figure 55.

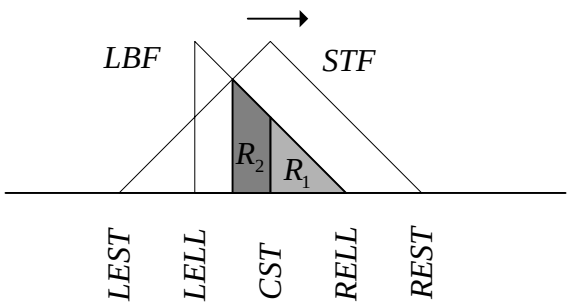

Figure 55 Convolution over Left Load Basis Function and Shifted Testing Function, Region 1 and Region 2.

Using the representations of the left load basis function and the shifted testing function, the convolution integral given in (A.1.9.a) can be rewritten for region 2 as below:

$$\int_{x_1}^{x_2} dx \int_{y_1}^{y_2} dy J_{IL}(x.y) J_{xm}(x-u, y-v) = -w\int_{x_1}^{x_2}\left(\frac{1}{wh_x}\right)^2 [(1-m)h_x + x - u][x - h_x]dx$$

(A.1.12)

Once the integration is performed then the result is gathered as below:

$$\int_{x_1}^{x_2} dx \int_{y_1}^{y_2} dy J_{IL}(x.y) J_{xm}(x-u, y-v) =$$

$$-\frac{1}{wh_x^2}\left[\frac{x_2^3 - x_1^3}{2} + \frac{x_2^2 - x_1^2}{2}(-mh_x - u) - (x_2 - x_1)((1-m)h_x^2 - uh_x)\right]$$

(A.1.13)

For case 2, for region 1 and region 2, (A.1.11) and (A.1.13) are used to find the result of convolution integral.

Case 3: $(LEST \geq LELL) \wedge (LEST \leq RELL)$

The scheme of the case 3 is shown in the figure 56.

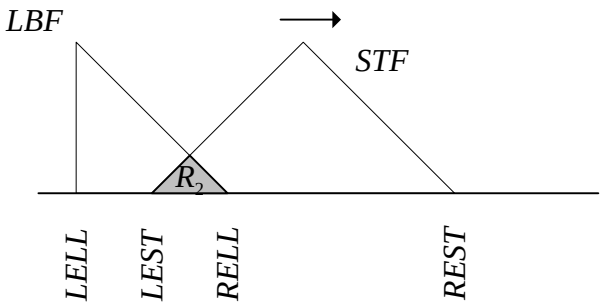

Figure 56 Convolution over Left Load Basis Function and Shifted Testing Function, Region 2.

For case 3, for the region 2, (A.1.13) is used to find the result of convolution integral.

As mentioned before, (A.1.9.b) describes the convolution integral for the right side load basis function and shifted testing. This integration is also solved in two regions as detailed below:

Case 1: $(REST \geq LELL) \wedge (REST < RELL)$

The scheme for the case 1 is shown in the figure 57.

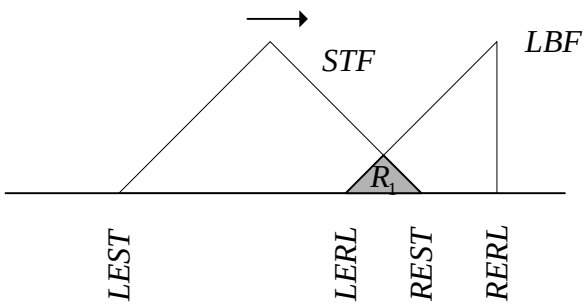

Figure 57 Convolution over Right Load Basis Function and Shifted Testing Function, Region 1.

Using the representations of the right load basis function and the shifted testing function, the convolution integral given in (A.1.9.b) can be rewritten for region 1 as below:

$$\int_{x_1}^{x_2} dx \int_{y_1}^{y_2} dy J_{IR}(x.y) J_{xm}(x-u, y-v) = w \int_{x_1}^{x_2} \left(\frac{1}{wh_x} \right)^2 [(1+m)h_x - x + u][x - Nh_x] dx \tag{A.1.14}$$

Once the integration is performed then the result is gathered as below:

$$\int_{x_1}^{x_2} dx \int_{y_1}^{y_2} dy J_{IR}(x.y) J_{xm}(x-u, y-v) =$$
$$\frac{1}{wh_x^2} \left[-\frac{x_2^3 - x_1^3}{2} + \frac{x_2^2 - x_1^2}{2} ((1+m+N)h_x + u) - (x_2 - x_1)((1+m)Nh_x^2 + uNh_x) \right] \tag{A.1.15}$$

For case 1, for region 1, (A.1.15) is used to find the result of convolution integral.

Case 2: $(CST \geq LELL) \wedge (CST < RELL)$

The scheme for case 2 is shown in the figure 58.

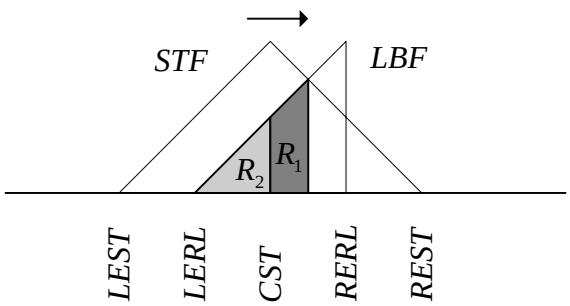

Figure 58 Convolution over Right Load Basis Function and Shifted Testing Function, Region 1 and Region 2.

Using the representations of the right load basis function and the shifted testing function, the convolution integral given in (A.1.9.b) can be rewritten for region 2 as below:

$$\int_{x_1}^{x_2} dx \int_{y_1}^{y_2} dy J_{IR}(x.y) J_{xm}(x-u, y-v) = w \int_{x_1}^{x_2} \left(\frac{1}{wh_x} \right)^2 [(1-m)h_x + x - u][x - Nh_x] dx$$

(A.1.16)

Once the integration is performed then the result is gathered as below:

$$\int_{x_1}^{x_2} dx \int_{y_1}^{y_2} dy J_{IR}(x.y) J_{xm}(x-u, y-v) =$$

$$\frac{1}{wh_x^2} \left[\frac{x_2^3 - x_1^3}{2} + \frac{x_2^2 - x_1^2}{2} ((1-m-N)h_x - u) - (x_2 - x_1)((1-m)Nh_x^2 - uNh_x) \right]$$

(A.1.17)

For case 2, for region 1 and region 2, (A.1.15) and (A.1.17) are used to find the result of convolution integral.

Case 3: $(LEST \geq LELL) \wedge (LEST \leq RELL)$

The scheme of the case 3 is shown in the figure 59.

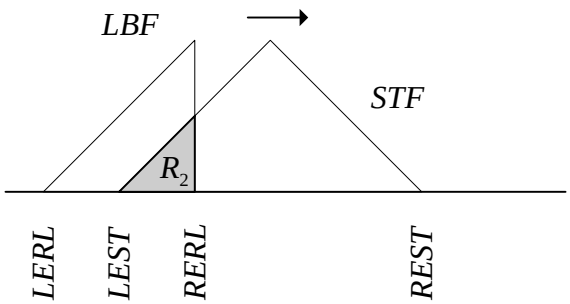

Figure 59 Convolution over Right Load Basis Function and Shifted Testing Function, Region 2.

For case 3, the region 2, (A.1.17) is used to find the result of convolution integral.

A.1.2 Convolution of Derivative of Load Basis Functions and Derivative of Shifted Testing Functions

(A.1.18.a) describes the convolution integral for derivatives of the left side load basis function and shifted testing functions whereas (A.1.18.b) describes the convolution integral for the derivatives of the right side load basis function and shifted testing functions:

$$\int_{x_1}^{x_2} dx \int_{y_1}^{y_2} \frac{d}{dx} J_{IL}(x.y) \frac{d}{dx} J_{xm}(x-u, y-v) dy \qquad \text{(A.1.18.a)}$$

$$\int_{x_1}^{x_2} dx \int_{y_1}^{y_2} \frac{d}{dx} J_{IR}(x.y) \frac{d}{dx} J_{xm}(x-u, y-v) dy \qquad \text{(A.1.18.b)}$$

These integral equations are solved in two regions as the derivatives of the load basis functions and testing functions are also piecewise differentiable. Below, the integral equations for each region are detailed. $DSTF$ is used for derivative of the shifted testing function and $DLBF$ is used for derivative of the load basis function.

Case 1: $(REST \geq LELL) \wedge (REST < RELL)$

The scheme for the case 1 is shown in the figure 60.

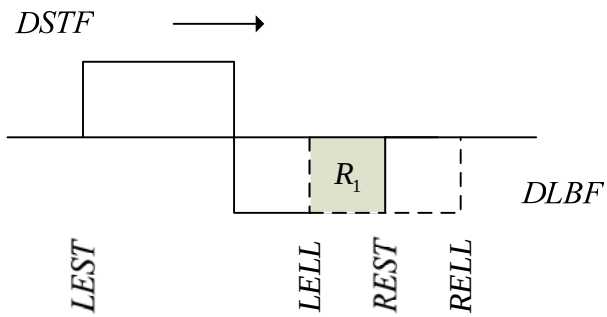

Figure 60 Convolution over Derivatives of Left Load Basis Function and Shifted Testing Function, Region 1.

Using the representations of the derivatives of left load basis function and the shifted testing function, the convolution integral given in (A.1.18.a) can be rewritten for region 1 as below:

$$\int_{x_1}^{x_2} dx \int_{y_1}^{y_2} \frac{d}{dx} J_{IL}(x.y) \frac{d}{dx} J_{xm}(x-u, y-v) = w \int_{x_1}^{x_2} \left(\frac{1}{wh_x} \right)^2 dx \qquad \text{(A.1.19)}$$

Once the integration is performed then the result is gathered as below:

$$\int_{x_1}^{x_2} dx \int_{y_1}^{y_2} \frac{d}{dx} J_{IL}(x.y) \frac{d}{dx} J_{xm}(x-u, y-v) = \frac{1}{wh_x^2} (x_2 - x_1) \qquad \text{(A.1.20)}$$

For case 1, for region 1, (A.1.20) is used to find the result of convolution integral.

Case 2: $(CST \geq LELL) \wedge (CST < RELL)$

The scheme for case 2 is shown in the figure 61.

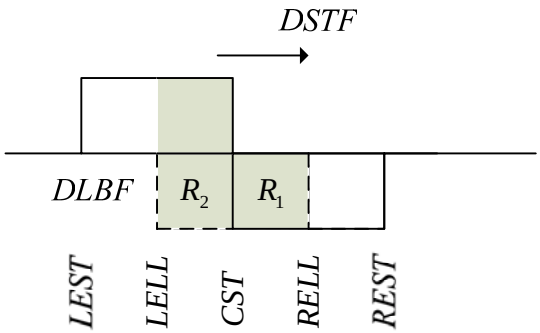

Figure 61 Convolution over Derivatives of Left Load Basis Function and Shifted Testing Function, Region 1 and Region 2.

Using the representations of the derivatives of left load basis function and the shifted testing function, the convolution integral given in (A.1.18.a) can be rewritten for region 2 as below:

$$\int_{x_1}^{x_2} dx \int_{y_1}^{y_2} \frac{d}{dx} J_{IL}(x.y) \frac{d}{dx} J_{xm}(x-u, y-v) = -w \int_{x_1}^{x_2} \left(\frac{1}{wh_x} \right)^2 dx \qquad \text{(A.1.21)}$$

Once the integration is performed then the result is gathered as below:

$$\int_{x_1}^{x_2} dx \int_{y_1}^{y_2} \frac{d}{dx} J_{IL}(x.y) \frac{d}{dx} J_{xm}(x-u, y-v) = -\frac{1}{wh_x^2} \left(x_2 - x_1 \right) \qquad \text{(A.1.22)}$$

For case 2, for region 1 and region 2, (A.1.20) and (A.1.22) are used to find the result of convolution integral.

Case 3: $(LEST \geq LELL) \wedge (LEST \leq RELL)$

The scheme of the case 3 is shown in the figure 62.

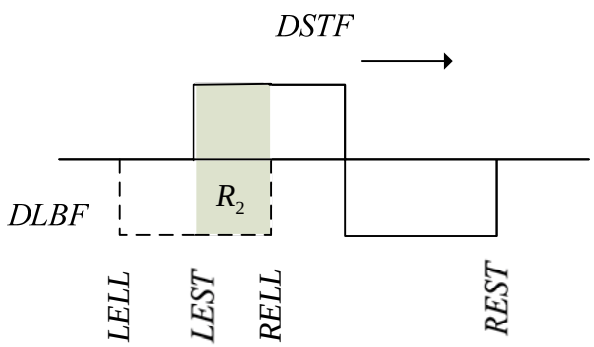

Figure 62 Convolution over Derivatives of Left Load Basis Function and Shifted Testing Function, Region 2.

For case 3, for the region 2, (A.1.22) is used to find the result of convolution integral.

As mentioned before, (A.1.18.b) describes the convolution integral for derivatives of the right side load basis function and shifted testing. This integration is also solved in two regions as detailed below:

Case 1: $(REST \geq LELL) \wedge (REST < RELL)$

The scheme for the case 1 is shown in the figure 63.

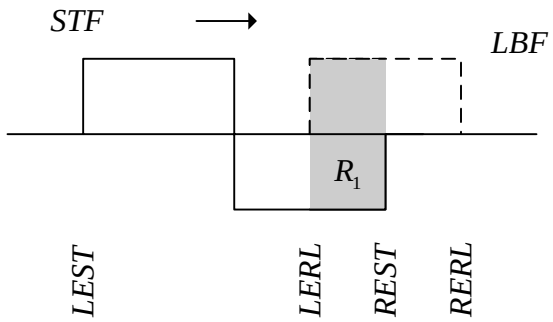

Figure 63 Convolution over Derivatives of Right Load Basis Function and Shifted Testing Function, Region 1.

Using the representations of the derivatives of right load basis function and the shifted testing function, the convolution integral given in (A.1.18.b) can be rewritten for region 1 as below:

$$\int_{x_1}^{x_2} dx \int_{y_1}^{y_2} \frac{d}{dx} J_{IR}(x.y) \frac{d}{dx} J_{xm}(x-u, y-v) = -w \int_{x_1}^{x_2} \left(\frac{1}{wh_x} \right)^2 dx \qquad \text{(A.1.23)}$$

Once the integration is performed then the result is gathered as below:

$$\int_{x_1}^{x_2} dx \int_{y_1}^{y_2} \frac{d}{dx} J_{IR}(x.y) \frac{d}{dx} J_{xm}(x-u, y-v) = -\frac{1}{wh_x^2}(x_2 - x_1) \qquad \text{(A.1.24)}$$

For case 1, for region 1, (A.1.24) is used to find the result of convolution integral.

Case 2: $(CST \geq LELL) \wedge (CST < RELL)$

The scheme for case 2 is shown in the figure 64.

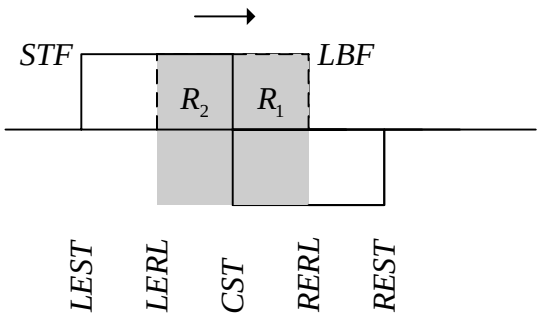

Figure 64 Convolution over Derivatives of Right Load Basis Function and Shifted Testing Function, Region 1 and Region 2.

Using the representations of the derivatives of right load basis function and the shifted testing function, the convolution integral given in (A.1.18.b) can be rewritten for region 2 as below:

$$\int_{x_1}^{x_2} dx \int_{y_1}^{y_2} \frac{d}{dx} J_{IR}(x.y) \frac{d}{dx} J_{xm}(x-u, y-v) = w \int_{x_1}^{x_2} \left(\frac{1}{wh_x} \right)^2 dx \qquad \text{(A.1.25)}$$

Once the integration is performed then the result is gathered as below:

$$\int_{x_1}^{x_2} dx \int_{y_1}^{y_2} \frac{d}{dx} J_{IR}(x.y) \frac{d}{dx} J_{xm}(x-u, y-v) = \frac{1}{wh_x^2}(x_2 - x_1) \qquad \text{(A.1.26)}$$

For case 2, for region 1 and region 2, (A.1.24) and (A.1.26) are used to find the result of convolution integral.

Case 3: $(LEST \geq LELL) \wedge (LEST \leq RELL)$

The scheme of the case 3 is shown in the figure 65.

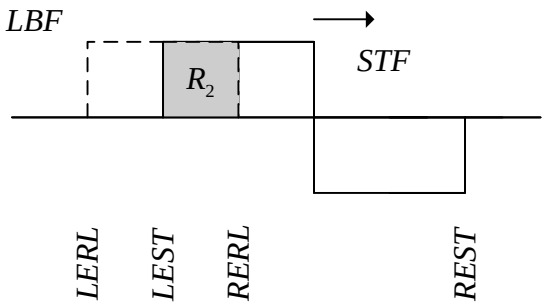

Figure 65 Convolution over Derivatives of Right Load Basis Function and Shifted Testing Function, Region 2.

For case 3, for the region 2, (A.1.26) is used to find the result of convolution integral.

A.2 Evaluation of Convolution Integrals for Coupled Lines

The representations of the basis and shifted testing functions of coupled microstrip lines are given as below:

Basis Function of Line 1:

$$J_{1xn}(x,y) = \begin{cases} \dfrac{1}{w_1 h_x}[(1-n)h_x + x] & (n-1)h_x \leq x \leq nh_x \quad , \quad |y| \leq \dfrac{w_1}{2} \\ \dfrac{1}{w_1 h_x}[(1+n)h_x - x] & nh_x \leq x \leq (n+1)h_x \quad , \quad |y| \leq \dfrac{w_1}{2} \\ 0 & elsewhere \end{cases} \qquad \text{(A.2.1)}$$

Basis Function of Line 2:

$$J_{2xn}(x,y)=\begin{cases}\frac{1}{w_2h_x}[(1-n)h_x+x-\Delta x] & (n-1)h_x+\Delta x\le x\le nh_x+\Delta x, |y-\Delta y|\le\frac{w_2}{2}\\ \frac{1}{w_2h_x}[(1+n)h_x-x+\Delta x] & nh_x+\Delta x\le x\le (n+1)h_x+\Delta x, |y-\Delta y|\le\frac{w_2}{2}\\ 0 & elsewhere\end{cases}$$

(A.2.2)

Shifted Testing Function of Line 1:

$$J_{1xm}(x-u,y-v)=\begin{cases}\frac{1}{w_1h_x}[(1-m)h_x+x-u] & (m-1)h_x+u\le x\le mh_x+u,\ |y-v|\le\frac{w_1}{2}\\ \frac{1}{w_1h_x}[(1+m)h_x-x+u] & mh_x+u\le x\le (m+1)h_x+u,\ |y-v|\le\frac{w_1}{2}\\ 0 & elsewhere\end{cases}$$

(A.2.3)

Shifted Testing Function of Line 2:

$$J_{2xm}(x-u,y-v)=\begin{cases}\frac{1}{w_2h_x}[(1-m)h_x+x-u-\Delta x] & \\ & (m-1)h_x+u+\Delta x\le x\le mh_x+u+\Delta x, |y-v-\Delta y|\le\frac{w_2}{2}\\ \frac{1}{w_2h_x}[(1+m)h_x-x+u+\Delta x] & \\ & mh_x+u+\Delta x\le x\le (m+1)h_x+u+\Delta x, |y-v-\Delta y|\le\frac{w_2}{2}\\ 0 & \\ & elsewhere\end{cases}$$

(A.2.4)

Source Basis Function:

$$J_s(x,y)=\begin{cases}\frac{1}{w_1h_x}[(a-1)h_x-x] & (a-1)h_x\le x\le ah_x\quad,\quad |y|\le\frac{w_1}{2}\\ \frac{1}{w_1h_x}[(a+1)h_x-x] & ah_x\le x\le (a+1)h_x\quad,\quad |y|\le\frac{w_1}{2}\\ 0 & elsewhere\end{cases}\qquad (A.2.5)$$

Load Basis Function of Line 1:

$$J_{1lL}(x,y)=\begin{cases}-\dfrac{1}{w_1h_x}[x-h_x] & 0\le x\le h_x \quad , \quad |y|\le \dfrac{w_1}{2}\\ 0 & elsewhere\end{cases} \tag{A.2.6.a}$$

$$J_{1lR}(x,y)=\begin{cases}\dfrac{1}{w_1h_x}[x-Nh_x] & Nh_x\le x\le (N+1)h_x \quad , \quad |y|\le \dfrac{w_1}{2}\\ 0 & elsewhere\end{cases} \tag{A.2.6.b}$$

Load Basis Function of Line 2:

$$J_{2lL}(x,y)=\begin{cases}-\dfrac{1}{w_2h_x}[x-h_x-\Delta x] & \Delta x\le x\le h_x+\Delta x, |y-\Delta y|\le \dfrac{w_2}{2}\\ 0 & elsewhere\end{cases}$$

(A.2.7.a)

$$J_{2lR}(x,y)=\begin{cases}\dfrac{1}{w_2h_x}[x-Nh_x-\Delta x] & Nh_x+\Delta x\le x\le (N+1)h_x+\Delta x, |y-\Delta y|\le \dfrac{w_2}{2}\\ 0 & elsewhere\end{cases}$$

(A.2.7.b)

Derivative of Basis Function of Line 1:

$$\frac{d}{dx}J_{1xn}(x,y)=\begin{cases}\dfrac{1}{w_1h_x} & (n-1)h_x\le x\le nh_x \quad , \quad |y|\le \dfrac{w_1}{2}\\ -\dfrac{1}{w_1h_x} & nh_x\le x\le (n+1)h_x \quad , \quad |y|\le \dfrac{w_1}{2}\\ 0 & elsewhere\end{cases} \tag{A.2.8}$$

Derivative of Basis Function of Line 2:

$$\frac{d}{dx}J_{2xn}(x,y)=\begin{cases}\dfrac{1}{w_2h_x} & (n-1)h_x+\Delta x\le x\le nh_x+\Delta x \quad , \quad |y-\Delta y|\le \dfrac{w_2}{2}\\ -\dfrac{1}{w_2h_x} & nh_x+\Delta x\le x\le (n+1)h_x+\Delta x \quad , \quad |y-\Delta y|\le \dfrac{w_2}{2}\\ 0 & elsewhere\end{cases}$$

(A.2.9)

Derivative of Shifted Testing Function of Line 1:

$$\frac{d}{dx} J_{1xm}(x-u, y-v) = \begin{cases} \dfrac{1}{w_1 h_x} & (m-1)h_x + u \le x \le mh_x + u\,,\ |y-v| \le \dfrac{w_1}{2} \\ -\dfrac{1}{w_1 h_x} & mh_x + u \le x \le (m+1)h_x + u\,,\ |y-v| \le \dfrac{w_1}{2} \\ 0 & elsewhere \end{cases}$$

(A.2.10)

Derivative of Shifted Testing Function of Line 2:

$$\frac{d}{dx} J_{2xm}(x-u, y-v) = \begin{cases} \dfrac{1}{w_2 h_x} & (m-1)h_x + u + \Delta x \le x \le mh_x + u + \Delta x,\ |y-v-\Delta y| \le \dfrac{w_2}{2} \\ -\dfrac{1}{w_2 h_x} & mh_x + u + \Delta x \le x \le (m+1)h_x + u + \Delta x,\ |y-v-\Delta y| \le \dfrac{w_2}{2} \\ 0 & elsewhere \end{cases}$$

(A.2.11)

Derivative of Source Basis Function:

$$\frac{d}{dx} J_s(x, y) = \begin{cases} -\dfrac{1}{w_1 h_x} & (a-1)h_x \le x \le ah_x \quad , \quad |y| \le \dfrac{w_1}{2} \\ -\dfrac{1}{w_1 h_x} & ah_x \le x \le (a+1)h_x \quad , \quad |y| \le \dfrac{w_1}{2} \\ 0 & elsewhere \end{cases} \qquad \text{(A.2.12)}$$

Derivative of Load Basis Function of Line 1:

$$\frac{d}{dx} J_{1lL}(x, y) = \begin{cases} -\dfrac{1}{w_1 h_x} & 0 \le x \le h_x \quad , \quad |y| \le \dfrac{w_1}{2} \\ 0 & elsewhere \end{cases} \qquad \text{(A.2.13.a)}$$

$$\frac{d}{dx} J_{1lR}(x, y) = \begin{cases} \dfrac{1}{w_1 h_x} & Nh_x \le x \le (N+1)h_x\,,\ |y| \le \dfrac{w_1}{2} \\ 0 & elsewhere \end{cases} \qquad \text{(A.2.13.b)}$$

Derivative of Load Basis Function of Line 2:

$$\frac{d}{dx} J_{2IL}(x,y) = \begin{cases} -\dfrac{1}{w_2 h_x} & \Delta x \le x \le h_x + \Delta x \quad , \quad |y - \Delta y| \le \dfrac{w_2}{2} \\ 0 & elsewhere \end{cases} \tag{A.2.14.a}$$

$$\frac{d}{dx} J_{2IR}(x,y) = \begin{cases} \dfrac{1}{w_2 h_x} & Nh_x + \Delta x \le x \le (N+1)h_x + \Delta x, \ |y - \Delta y| \le \dfrac{w_2}{2} \\ 0 & elsewhere \end{cases}$$

(A.2.14.b)

Using these representations of basis functions and shifted testing functions and the procedure described in appendix A.1, the convolution integrals can be calculated analytically.

APPENDIX B

EQUATIONS FOR THE LOAD BASIS FUNCTIONS

As described in chapter 3 and chapter 4, the microstrip lines can be terminated by any loads at both ends. To add the effects of the load terminations to the current distribution over the microstip lines, one should relate the coefficients of the load basis functions to the rest of the basis functions by invoking additional boundary conditions at the load terminals [18]. This can be done by using transmission line analysis in conjunction with finite difference approximation. In this appendix, for a single microstrip line and for a coupled-line system, the derivation of the load equations is examined in two subsections:

B.1 Load Equations for a Single Microstrip Line

In the transmission line analysis, there are two basic formulas which give the relation between the total voltage $V(x)$ and total current $I(x)$ which are:

$$\frac{dI(x)}{dx} = -YV(x) \qquad \text{(B.1.1.a)}$$

$$\frac{dV(x)}{dx} = -ZI(x) \qquad \text{(B.1.1.b)}$$

where $Y = j\beta / Z_o$ and $Z = j\beta Z_o$ are the shunt admittance and series impedance per unit length of the line, respectively. Besides, Z_o is the characteristic impedance and β is the propagation constant of the line. To calculate the characteristic impedance and the propagation constant of the line, empirical formulas are used based on a quasi-static analysis [20]. To derivative the load equations which relate the coefficients of the load basis functions to the rest of the basis functions, finite difference approximation method is used as detailed below.

To obtain the load equation at the left end of the microstrip line:

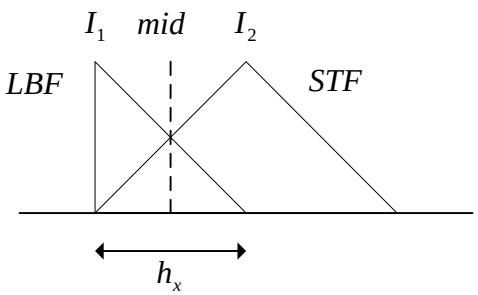

Figure 66 Representation of the Surface Currents as Basis Functions at the Left End of a Microstrip Line.

Step 1: Using central differencing between 0 and h_x, the relation between voltage V_{mid} at $h_x/2$ and basis function coefficients is gathered as:

$$\frac{I_1 - I_2}{h_x} = -\frac{j\beta}{Z_o} V_{mid} \tag{B.1.2}$$

Step 2: Using forward differencing between 0 and $h_x/2$, the following equation is obtained:

$$\frac{V_1 - V_{mid}}{h_x/2} = -j\beta Z_o I_1 \tag{B.1.3}$$

Step 3: Substituting the equation $V_1 = I_1 Z_{lL}$ into (B.1.3), V_{mid} can be expressed as:

$$V_{mid} = I_1 (Z_{lL} + j\beta Z_o \frac{h_x}{2}) \tag{B.1.4}$$

Step 4: Substituting (B.1.4) into (B.1.2), the left end load equations are obtained as:

$$I_1[1 + j\beta h_x \frac{Z_{lL}}{Z_o} - \frac{\beta^2 h_x^2}{2}] - I_2 = 0 \tag{B.1.5}$$

where Z_{lL} is the left end load impedance of the microstrip line.

Similarly, to obtain the load equation at the right end of the microstrip line:

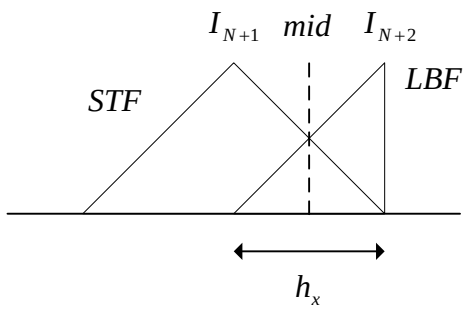

Figure 67 Representation of the Surface Currents as Basis Functions at the Right End of a Microstrip Line

Step 1: Using central differencing between Nh_x and $(N+1)h_x$, the relation between voltage V_{mid} at $(N+1/2)h_x$ and basis function coefficients is gathered as:

$$\frac{I_{N+2} - I_{N+1}}{h_x} = -\frac{j\beta}{Z_o} V_{mid} \tag{B.1.6}$$

Step 2: Using backward differencing between $(N+1)h_x$ and $(N+1/2)h_x$, the following equation is obtained:

$$\frac{V_{N+2} - V_{mid}}{h_x / 2} = -j\beta Z_o I_{N+2} \tag{B.1.7}$$

Step 3: Substituting the equation $V_{N+2} = I_{N+2} Z_{lR}$ into (B.1.7), V_{mid} can be expressed as:

$$V_{mid} = I_{N+2}(Z_{lR} + j\beta Z_o \frac{h_x}{2}) \tag{B.1.8}$$

Step 4: Substituting (B.1.8) into (B.1.6), the right end load equations are obtained as:

$$I_{N+2}[1 + j\beta h_x \frac{Z_{lR}}{Z_o} - \frac{\beta^2 h_x^2}{2}] - I_{N+1} = 0 \tag{B.1.9}$$

where Z_{lR} is the right end load impedance of the microstrip line.

B.2 Load Equations for Coupled Microstrip Lines

For the coupled line microstrip line systems, the given procedure in appendix B.1 is used which leads to four supplementary equations which relate the load basis functions to the remaining basis functions.

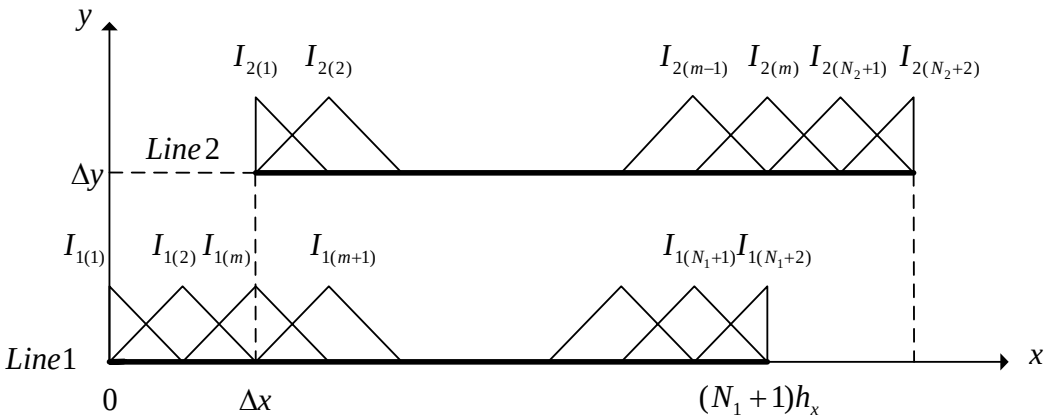

Figure 68 Representation of the Surface Currents as Basis Functions over Coupled Microstrip Lines.

According to the transmission line analysis, the differential equations defining the coupled line system are given below as:

$$-\frac{dV_1(x)}{dx} = j\omega L_{11} I_1(x) + j\omega L_{12} I_2(x) \qquad \text{(B.2.1.a)}$$

$$-\frac{dV_2(x)}{dx} = j\omega L_{21} I_1(x) + j\omega L_{22} I_2(x) \qquad \text{(B.2.1.b)}$$

$$-\frac{dI_1(x)}{dx} = j\omega C_{11} V_1(x) + j\omega C_{12} V_2(x) \qquad \text{(B.2.1.c)}$$

$$-\frac{dI_2(x)}{dx} = j\omega C_{21} V_1(x) + j\omega C_{22} V_2(x) \qquad \text{(B.2.1.d)}$$

where L_{ij} 's and C_{ij} 's are the Maxwellian inductances and capacitances per unit length of the coupled line. In this study, using a software program, "RLGC - 2D Quasi-static Modeling Tool™", created by K. S. Oh, L_{ij} 's and C_{ij} 's per unit length of the coupled lines can be found. The software program is an implementation of

the methods discussed in [19] and [22]. The values of L_{ij}'s and C_{ij}'s per unit length of the coupled lines analyzed in this study are given in appendix E.

From figure B.2.1, one can see that the left end of line 1 and right end of line 2 can be regarded as belonging to a single line system and the right end of line 1 and left end of line 2 can be regarded as belonging to a coupled line system. If the left end load of the line 1 is analyzed, the equations (B.2.1.a) and (B.2.1.c) return to the equations (B.1.1.a) and (B.1.1.b), respectively, because I_2 and V_2 are zero at $[0, \Delta x]$. Similarly, if the right end load of the line 2 is analyzed, the equations (B.2.1.b) and (B.2.1.d) return to the equations (B.1.1.a) and (B.1.1.b), respectively, because I_1 and V_1 are zero at $[(N_1+1)h_x, (N_1+1)h_x + \Delta x]$. Hence, using the procedure described in appendix B.1, two of the load equations are obtained as below:

Load Equation for the Left End of Line 1:

$$I_{1(1)}[1 + j\beta_1 h_x \frac{Z_{1lL}}{Z_{1o}} - \frac{\beta_1^{\,2} h_x^2}{2}] - I_{1(2)} = 0 \qquad \text{(B.2.2.a)}$$

Load Equation for the Right End of Line 2:

$$I_{2(N_2+2)}[1 + j\beta_2 h_x \frac{Z_{2lR}}{Z_{2o}} - \frac{\beta_2^{\,2} h_x^2}{2}] - I_{2(N_2+1)} = 0 \qquad \text{(B.2.2.b)}$$

To find the load equation for the right end of the line 1, the following procedure should be followed:

Step 1: By central differencing, (B.2.1.c) can be rewritten as:

$$\frac{I_{1(N_1+2)} - I_{1(N_1+1)}}{h_x} = -j\omega C_{11} V_1(mid_{N_1+2,N_1+1}) - j\omega C_{12} V_2(mid_{m,m-1}) \qquad \text{(B.2.3)}$$

Step 2: Using backward differencing, (B.2.1.a) can be written as:

$$\frac{V_{1(N_1+2)} - V_1(mid_{N_1+2,N_1+1})}{h_x / 2} = -j\omega L_{11} I_{1(N_1+2)} - j\omega L_{12} I_{2(m)} \qquad \text{(B.2.4)}$$

Step 3: It is also known that

$$V_{1(N_1+2)} = Z_{1lR} I_{1(N_1+2)} \qquad \text{(B.2.5)}$$

Step 4: $V_1(mid_{N_1+2,N_1+1})$ can be written as below if (B.2.5) is substituted into (B.2.4):

$$V_1(mid_{N_1+2,N_1+1}) = [Z_{1lR} + j\omega(h_x/2)L_{11}]I_{1(N_1+2)} + j\omega(h_x/2)L_{12}I_{2(m)} \quad \text{(B.2.6)}$$

Step 5: If (B.2.1.d) is rewritten by using central differencing, then it will be possible to relate $V_2(mid_{m+1,m})$ to current basis coefficients:

$$\frac{I_{2(m)} - I_{2(m-1)}}{h_x} = -j\omega C_{21}V_1(mid_{N_1+2,N_1+1}) - j\omega C_{22}V_2(mid_{m,m-1}) \quad \text{(B.2.7)}$$

Substituting (B.2.6) into (B.2.7), the following equation is obtained:

$$\begin{aligned} V_2(mid_{m,m-1}) = -\frac{1}{j\omega C_{22}h_x}\Bigg[& I_{1(N_1+2)}\left[j\omega C_{21}h_x Z_{1lR} - \frac{\omega^2 h_x^2}{2} C_{21}L_{11} \right] \\ & - I_{2(m-1)} + I_{2(m)}\left[1 - \frac{\omega^2 h_x^2}{2} C_{21}L_{12} \right]\Bigg] \end{aligned} \quad \text{(B.2.8)}$$

Step 6: Substituting (B.2.8) and (B.2.6) into (B.2.3), the final equation is obtained as:

$$\begin{aligned} & -I_{1(N_1+2)}\left[\frac{C_{22}}{j\omega h_x \Delta c} + Z_{1lR} + j\frac{\omega h_x}{2}L_{11} \right] + I_{1(N_1+1)}\frac{C_{22}}{j\omega h_x \Delta c} \\ & -I_{2(m)}\frac{C_{12}}{j\omega h_x \Delta c} + I_{2(m+1)}\left[\frac{C_{12}}{j\omega h_x \Delta c} - j\frac{\omega h_x}{2}L_{12} \right] = 0 \end{aligned} \quad \text{(B.2.9)}$$

Similiarly, load equations for the left end of the line 2 can also be driven using the same steps as:

$$\begin{aligned} & -I_{2(1)}\left[\frac{C_{11}}{j\omega h_x \Delta c} + Z_{2lL} + j\frac{\omega h_x}{2}L_{22} \right] + I_{2(2)}\frac{C_{11}}{j\omega h_x \Delta c} \\ & -I_{1(m+1)}\frac{C_{21}}{j\omega h_x \Delta c} + I_{1(m)}\left[\frac{C_{21}}{j\omega h_x \Delta c} - j\frac{\omega h_x}{2}L_{21} \right] = 0 \end{aligned} \quad \text{(B.2.10)}$$

The notations used in the derivations are listed as:

N_1: Number of basis functions for the line 1,

$N_1 + 2$: Total number of basis functions including the load basis functions over line 1,

$I_{1(m)}$: Each basis function coefficient over the line 1 and $m = 1,2,...,(N_1 + 2)$,

β_1: Propagation constant of line 1,

Z_{1o}: Characteristic impedance of the line 1,

Z_{1lL}: Left End Load impedance of the line 1,

Z_{1lR}: Right End Load impedance of the line 1,

N_2: Number of basis functions for the line 2,

$N_2 + 2$: Total number of basis functions including the load basis functions over line 2,

$I_{2(m)}$: Each basis function coefficient over the line 2 and $m = 1,2,...,(N_2 + 2)$,

β_2: Propagation constant of line 2,

Z_{2o}: Characteristic impedance of the line 2,

Z_{2lL}: Left End Load impedance of the line 2,

Z_{2lR}: Right End Load impedance of the line 2 and

$\Delta c = C_{11}C_{22} - C_{12}C_{21}$.

APPENDIX C

CALCULATION OF CHARACTERISTIC IMPEDANCE

In this study, approximate formulas are used to evaluate the characteristic impedance of the microstrip lines [20]. The accuracy of the approximate formulas is 1 percent or better.

Capacitance per length of a strip of width w at a height h above a ground plane and with a medium air filled is defined as below:

$$C_a = \frac{2\pi\varepsilon_0}{\ln(\frac{8h}{w} + \frac{w}{4h})} \qquad \frac{w}{h} \le 1$$
$$C_a = \varepsilon_0\left[\frac{w}{h} + 1.393 + 0.667\ln(\frac{w}{h} + 1.444)\right] \qquad \frac{w}{h} > 1 \tag{C.1}$$

Then, the effective width of the line is calculated as:

$$w_e = w + 0.398t(1 + \ln\frac{4\pi w}{t}) \qquad \frac{w}{h} \le \frac{1}{2\pi}$$
$$w_e = w + 0.398t(1 + \ln\frac{2h}{t}) \qquad \frac{w}{h} > \frac{1}{2\pi} \tag{C.2}$$

Although the effect of finite thickness t for the microstrip on the distributed capacitance is normally negligible, it is included in (C.2).

To calculate the characteristic impedance of the microstrip line, one should find the effective constant ε_e. This constant can be found using Schneider-Hammerstad formula:

$$\varepsilon_e = \frac{\varepsilon_r + 1}{2} + \frac{\varepsilon_r - 1}{2}(1 + \frac{12h}{2})^{-1/2} + F(\varepsilon_r, h) - 0.217(\varepsilon_r - 1)\frac{t}{\sqrt{wh}} \tag{C.3}$$

where

$$F(\varepsilon_r, h) = 0.02(\varepsilon_r - 1)(1 - \frac{w}{h})^2 \qquad \frac{w}{h} < 1$$

$$F(\varepsilon_r, h) = 0 \qquad \frac{w}{h} > 1 \tag{C.4}$$

Then, the characteristic impedance of the line can be found using the formula below and the expressions given above:

$$Z_c = \sqrt{\frac{\mu_0 \varepsilon_0}{\varepsilon_e}} \frac{1}{C_a} \tag{C.5}$$

APPENDIX D

PRONY'S METHOD

Prony's method is a technique which is used for modeling sampled data as linear combinations of exponentials [21]. In this study, using the current distributions over the lines as sampled data, the reflected wave coefficients and incident wave coefficients can be found and the sampled data can be formulated as given below:

$$I(x) \cong c_1 e^{\beta_1 x} + c_2 e^{\beta_2 x} \tag{D.1}$$

To do this, first, one should define a p-exponent discrete function as:

$$I[x] \cong \sum_{k=1}^{p} c_k e^{\beta_k x} \tag{D.2}$$

where c_k and β_k are the unknown complex parameters which will be found using the sampled data, $I[x]$. It should be noted that the sampled data is gathered at x equally spaced points over the line as

$$x = \frac{length\ of\ line}{N+1} n \qquad where \quad 0 \le n \le N+1 \quad (N\ is\ number\ of\ basis.) \tag{D.3}$$

and

$$z_k = e^{\beta_k \frac{length\ of\ line}{N+1}} \tag{D.4}$$

When (D.3) and (D.4) are substituted into (D.2), the following equation is obtained:

$$I[n] \cong \sum_{k=1}^{p} c_k z_k^n \tag{D.5}$$

(D.5) can be represented in the matrix form as:

$$\begin{bmatrix} z_1^0 & z_2^0 & . & . & z_{p-1}^0 & z_p^0 \\ z_1^1 & z_2^1 & . & . & z_{p-1}^1 & z_p^1 \\ & & & & & \\ & & & & & \\ z_1^{N+1} & z_2^{N+1} & . & . & z_{p-1}^{N+1} & z_p^{N+1} \end{bmatrix} \begin{bmatrix} c_1 \\ c_2 \\ \\ \\ c_p \end{bmatrix} = \begin{bmatrix} I[0] \\ I[1] \\ \\ I[N] \\ I[N+1] \end{bmatrix} \tag{D.6}$$

(D.5) can be recognized as the solution to some homogenous linear constant-coefficient difference equation. In order to find the form of this difference equation, the polynomial, $\phi(z)$ should be defined as:

$$\phi(z) = \prod_{k=1}^{p} (z - z_k) \tag{D.7}$$

where z_k 's are its roots. This polynomial can also be represented as:

$$\phi(z) = \sum_{m=0}^{p} a[m] z^{p-m} \tag{D.8}$$

where $a[m]$'s are complex coefficients to be found and $a[0] = 1$. To determine these coefficients, $(p+1)$ equations are multiplied by $a[p], a[p-1], ..., a[1], 1$, respectively, and the results are added. This process is repeated $(N+1-p)$ times and the following $(N+2-p)$ linear equations are obtained:

$$\begin{bmatrix} I[0] & I[1] & I[p-2] & I[p-1] \\ I[1] & I[2] & I[p-1] & I[p] \\ & & & \\ & & & \\ I[N+1-p] & I[N+2-p] & I[N-1] & I[N] \end{bmatrix} \begin{bmatrix} a[p] \\ a[p-1] \\ \\ \\ a[1] \end{bmatrix} = \begin{bmatrix} -I[p] \\ -I[p+1] \\ \\ \\ -I[N+1] \end{bmatrix} \tag{D.9}$$

In general $N > 2p$, hence, using the method of least squares, $a[m]$'s are found. Then the roots of (D.8) can be gathered by substituting $a[m]$'s in that equation. If z_k 'a are known, β_k 's can be obtained as described in (D.4). Using the equation (D.6), c_k 's can also be found.

APPENDIX E

RLGC – 2D QUASI-STATIC MODELING TOOL™

Using “RLGC - 2D Quasi-Static Modeling Tool™” which was developed by K. S. Oh, it is possible to compute the four transmission line parameters, the capacitance matrix C, the inductance matrix L, the conductance matrix G and the resistance matrix R. The tool uses MoM in conjunction with the closed-form Green’s functions which is one of the most efficient and accurate methods for static solutions. This tool is an implementation of the methods discussed in [19] and [22] which can handle an arbitrary number of dielectric layers as well as an arbitrary number of conductors. Moreover, the cross section of a conductor can be arbitrary or even be infinitely thin.

In this study, coupled lines are modeled as directional couplers and the matched load terminations at the end of the microstrip lines are included in the analysis. At this step, as described in chapter 4 and appendix B.2, the capacitance matrix C per unit length and the inductance matrix L per unit length are used for the load equations.

In chapter 4, 7dB, 10dB, 15dB and 20dB directional couplers are analyzed. For each application, the capacitance matrix C per unit length and the inductance matrix L per unit length are found using “RLGC - 2D Quasi-Static Modeling Tool™”. In table 2, required parameters defining the directional couplers and their capacitance matrix C per unit length and the inductance matrix L per unit length are listed:

Table 2 Parameters of Directional Couplers Required for MoM Analysis.

	7dB Directional Coupler	10dB Directional Coupler	15dB Directional Coupler	20dB Directional Coupler
z_{oe} (Ω)	80.0150	69.4762	59.8070	55.2771
z_{oo} (Ω)	30.6410	36.0186	41.8690	45.2267
f (GHz)	1	1	1	1
ε_r	4	4	4	4
d (cm)	0.2032	0.2032	0.2032	0.2032
$w_1(=w_2)$ (cm)	0.29	0.337	0.379	0.39464
s (cm)	0.008	0.0345	0.12	0.245
$l_1(=l_2)$ (cm)	4.34	4.35	4.33	4.3
t (cm)	1e-7	1e-7	1e-7	1e-7
$l_{11}(=l_{22})$ (nH/m)	3.2223e+2	3.1173e+2	3.0349e+2	3.0105e+2
$l_{12}(=l_{21})$ (nH/m)	1.5444e+2	1.1161e+2	6.6981e+1	4.1685e+1
$c_{11}(=c_{22})$ (pF/m)	1.2248e+2	1.1553e+2	1.1317e+2	1.1317e+2
$c_{12}(=c_{21})$ (pF/m)	-4.8548e+1	-3.0911e+1	-1.5147e+1	-7.3727

where z_{oe} is the even mode characteristic impedance, z_{oo} is the odd mode characteristic impedance, t is the thickness of the conductors and l_1 and l_2 are the length of the microstrip lines. The structure of the directional couplers is demonstrated in figure 69.

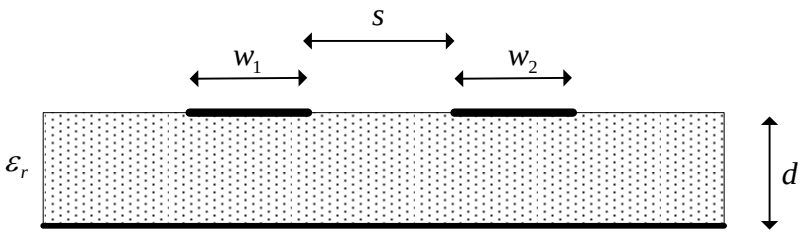

Figure 69 Directional Coupler Structure